LATE HOLOCENE PALEOCLIMATE RECONSTRUCTION OF THE NORTHERN GULF OF AQABA USING FORAMINIFERA AS A PROXY

A THESIS IN
Environmental and Urban Geosciences

Presented to the Faculty of the University
of Missouri-Kansas City in partial fulfillment of
the requirements for the degree

Master of Science

By
Julie Louise Galloway

B.S. Geology, University of Missouri-Kansas City, 2009

Kansas City, Missouri
2011

LATE HOLOCENE PALEOCLIMATE RECONSTRUCTION OF THE NORTHERN GULF OF AQABA USING FORAMINIFERA AS A PROXY

Julie Louise Galloway, Candidate for the Master of Science Degree

University of Missouri-Kansas City, 2011

ABSTRACT

A multiproxy analyses of sediment from a 4.3 m core extracted from 25 m water depth on the shelf of the northern Gulf of Aqaba suggest shifts in depositional environments over the past 4000 yrs. Foraminifera assemblages, grain-size distribution, sediment characterization, and radiocarbon age dating indicate several eco-stratigraphic zones including two periods of aridity from ~3900 to 2900 yr BP and ~1130 yr BP to present, a transitional period from ~2900 to 2500 yr BP, and an abrupt shift to wetter conditions between ~2500 to 1130 yr BP. Furthermore, this study records two foraminifera-barren horizons at 170 and 190 cm that correlate to grain size anomalies at that depth. A tsunami wave generated sometime during 2200-1800 yr BP is one possible explanation for this occurrence. Seismic stratigraphy indicates a reflector at approximately 3 m below the seafloor that delineates the boundary between a relict, coral fringing reef horizon, U8, and the overlying U9 strata. Sedimentation rates that adjust for sediment compaction suggest the sequence lies near the foraminifera-barren horizons at ~200 cm in the core. These data signify a dramatic environmental event possibly corresponding to reef termination on the Northern Gulf of Aqaba shelf.

The faculty listed below, appointed by the Dean of the College of Arts and Sciences have examined a thesis titled "Late Holocene Paleoclimate Reconstruction of the Northern Gulf of Aqaba Using Foraminifera as a Proxy," presented by Julie Louise Galloway, a candidate for the Master of Science degree, and certify that in their opinion it is worthy of acceptance.

Supervisory Committee

Tina M. Niemi, Ph.D., Committee Chair
Professor
Department of Geosciences

Caroline P. Davies, Ph.D.
Associate Professor
Department of Geosciences

James B. Murowchick, Ph.D.
Associate Professor
Department of Geosciences

TABLE OF CONTENTS

List of Illustrations

Tables

AKNOWLEDGMENTS

It is impossible to express fully the gratitude I feel towards the people in my life who have contributed time, effort, thought, support, and humor to me during the course of this project. As those before me already know, and those after me will learn, the experiences, knowledge, opportunities, and friendships that develop with a project of this nature are immeasurable. In reaching this goal, I have inadvertently become engulfed in world politics, absorbed multiple religions, been immersed in unfamiliar cultures, and witnessed science on an international level. Beyond the charts and graphs, this project has helped me broaden my small scope on this very large world.

For this, I would like to sincerely thank Dr. Tina Niemi. I would like to thank her for making this project and many other academic endeavors a positive experience. She has far exceeded ordinary responsibilities of a mentor. Dr. Niemi has given me space to be self-motivated, yet has maintained much appreciated continual guidance. I am truly grateful for our friendship both on an academic and personal level.

I also want to thank my committee members, Dr. James Murowchick and Dr. Molly Davies, for their availability and support. Throughout my studies at the University of Missouri-Kansas City, they have always put students' needs at the top of their priorities. Though they are overwhelmingly busy, they have always taken time to assist me in any way possible. They have shown patience when I am confused and offer advice when I have questions.

I would like to thank Dr. Beverly Goodman for her guidance and expertise. Foraminifera analysis of any kind would not be possible without the initiative and knowledge of Dr. Goodman. Her assistance and scientific insight are the foundation of this study.

I owe a very special thank you to the entire Geophysical Imaging of the Gulf of Aqaba/Eilat (GAE) team funded by the U.S. Agency for International Development in the Middle East Regional Cooperation Program for letting me join this exceptional project. I want to thank the GAE team of Dr. Zvi Ben-Avraham, Dr. Abdallah Al-Zoubl, Dr. Gideon Tibor, and Dr. Tina Niemi for leading this study.

I also want to thank the 2010 Jordanian research team of John Rucker, Jeremy Haynes, Alivia Allison, and Linda Moore who made me laugh daily during our time in Jordan.

My travels abroad were greatly enhanced by the welcoming nature and unabated hospitality of Mor Kanari. His kindness is truly appreciated. I would also like to thank Dr. Rivital Bookman and her wonderful family for opening their home to me while in Israel. Of course, I cannot forget all the laboratory assistance and conversations graciously offered by Nairooz Qupty.

Now, a little closer to home, words cannot express the gratitude I have for my family. They have shown nothing but love and encouragement throughout my entire life as well as my academic career. I am truly grateful to have such an amazing family. I want especially to thank my sister, friend, and roommate, Carrie, for providing daily support.

Finally yet importantly, I want to thank my partner in crime, my scholastic soul mate, the other half of the JuliAmy Monster, and my dear friend, Amy Ameis.

CHAPTER 1

INTRODUCTION

Due to increasing awareness and concern for global climate change, understanding paleoclimate regimes in order to predict future trends is crucial. Because modern instrumental records operate on a timescale not adequate for observing long-term trends, environmental changes must be observed through paleoenvironment reconstruction. Marine sediments, as collected in this study, provide such a record. Documenting late-Holocene environmental shifts is essential when considering the interaction between humans and their environment. Even mild climatic changes are capable of producing significant effects on ancient civilizations. A high-resolution investigation on the rate and amplitude of these changes is paramount in correlating anthropogenic influences with environmental fluctuations. The purpose of this study is to reconstruct the paleoclimate and paleoenvironment of the Northern Red Sea in the Gulf of Aqaba based on microfossil foraminiferal assemblages, grain size analysis, and composition from a 4.3-meter long sediment core recovered from the shelf at a water depth of 25 m.

The Northern Red Sea (Gulf of Aqaba) is a restricted basin surrounded by a modern desert, making it a prime location to investigate changing climate regimes. Arid regions, like the Gulf of Aqaba, adequately preserve small environmental shifts, which often have a direct signal in marine core proxies. The majority of Red Sea studies examine long temporal, low-resolution Quaternary records, which do not investigate late-Holocene climatological shifts (during the past 4,000 years). Several foraminiferal studies present long records in deep-water cores (Reiss *et al.*, 1980; Almogi-Labin, 2010), in short (<1 m) shallow-water cores (Al-Rousan *et al.*, 2004), and in modern surface samples (Khalil *et al.*, 1997). However, due

to the difficult nature of retrieving long cores from the sandy shelf substrate, few studies examine shelf sediment to a depth great than 1 m. Red Sea studies that do investigate late-Holocene sediment document considerable climatological and hydrological anomalies in the marine records (e.g. Edelman-Furstenberg *et al.*, 2009; Arz *et al*., 2006). However, these studies are restricted to deeper waters (~900-1500 m) of both the Gulf of Aqaba and the Red Sea basin. To date, few studies examine paleoclimate shifts recorded on the shallow continental shelf. The purpose of this study is to provide a previously undocumented chronology of environmental changes in the northern Gulf of Aqaba during the late Holocene.

Foraminifera are single-celled organisms that inhabit all marine and freshwater ecosystems. They are an excellent paleoenvironmental indicator due to their abundance, diversity, small size, high capacity for preservation, and in the ability to associate environmental preferences to a particular species or collection of species. Microfossil analysis as a paleoenvironment proxy is a reliable and widely used technique. Modern micropaleontology is responsible for reconstructing global glacial-eustatic sea-level curves, is a primary tool in biostratigraphy and paleoecology, and offers immeasurable insight to palaeoceanography and palaeoclimatology. A wide range of environmental factors including depth, substrate texture, temperature, slope, nutrient availability, sediment size, system inputs, and light penetration can alter the character of the foraminiferal assemblages. Reiss *et al.* (1980), Almago-Labin (1982), Arz *et al.* (2006), Edelman-Furstenberg *et al.* (2009), and others have demonstrated how foraminifera can serve as useful paleoclimate indicators in this region. Quantitative analyses of shell chemistry, oxygen isotope composition, and Mg/Ca ratios are used to determine ocean chemistry, sea surface salinity (SSS), and sea surface

temperature (SST). For Holocene-age (<10,000 years before present, yr BP) records, modern analogs are a reasonable basis for interpreting paleorecords.

The following sections will describe the Northern Gulf of Aqaba site location, including the local hydrography, geology, tectonic setting, and modern geomorphology. They will provide coring techniques, laboratory methodology, and descriptions of the analyses used in this study. A central objective is to employ the use of foraminifera as a paleoenvironment proxy and infer climatic and hydrologic shifts on a local and possibly regional scale. The results of foraminifera data coupled with grain-size distribution, matrix composition, and radiocarbon dates define five climatic boundaries along with a dramatic sediment supply anomaly manifested by foraminifera-barren zones at 170 and 190 cm core depth. Finally, a discussion will synthesize previously published sedimentological and climatological reports from this region with newly acquired data obtained by this study.

CHAPTER 2

STUDY AREA

Location

The Gulf of Aqaba and the Gulf of Suez are the northern most extensions of the Red Sea. The Gulf of Aqaba is a deep, semi-enclosed basin at the northeastern end of the Red Sea. It is 160 km long, 24 km wide, and reaches a maximum depth of 1850 m in the central basin. It lies within the Arabian Desert belt and is surrounded by Egypt to the west, Israel and Jordan to the north, and Saudi Arabia to the east (Figures 2.1 & 2.2). The region is characterized by extensive onshore and offshore faulting. The core analyzed in this study was collected approximately 500 m from the present-day northern shoreline east of the Evrona Fault.

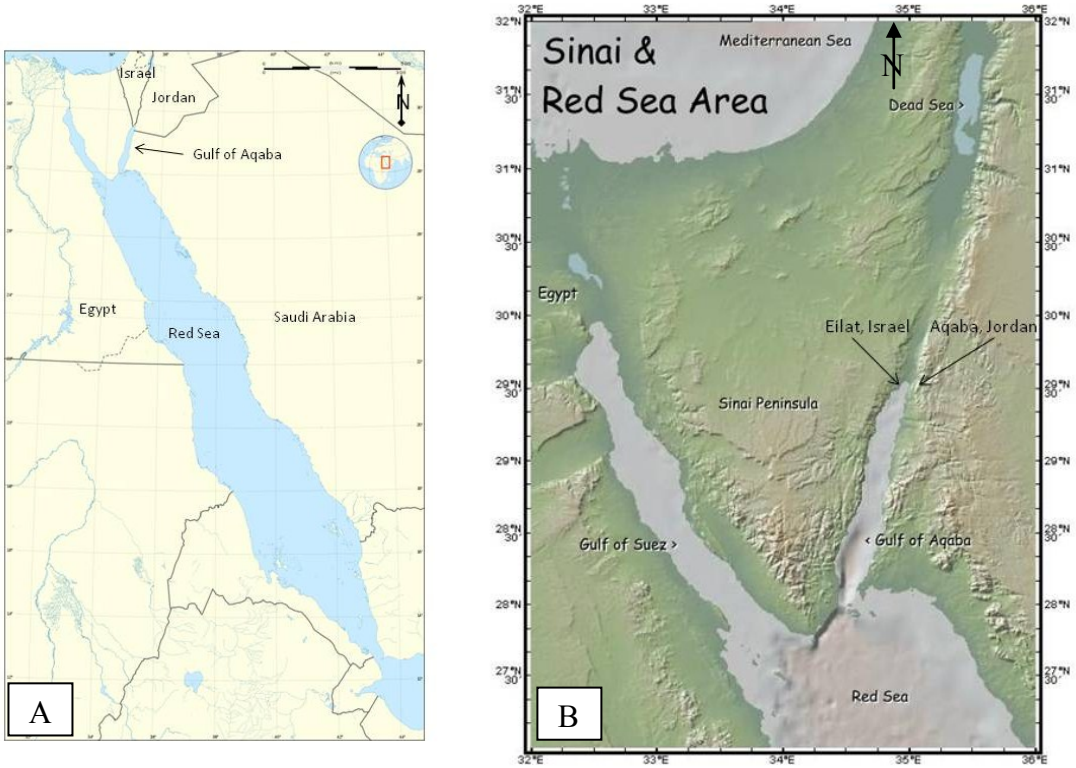

Figure 2.1 Study area (A) Red Sea and adjacent region (Googlemaps, 2011). (B) Northern Red Sea and Gulf of Aqaba (BiblicalZionist, 2011)

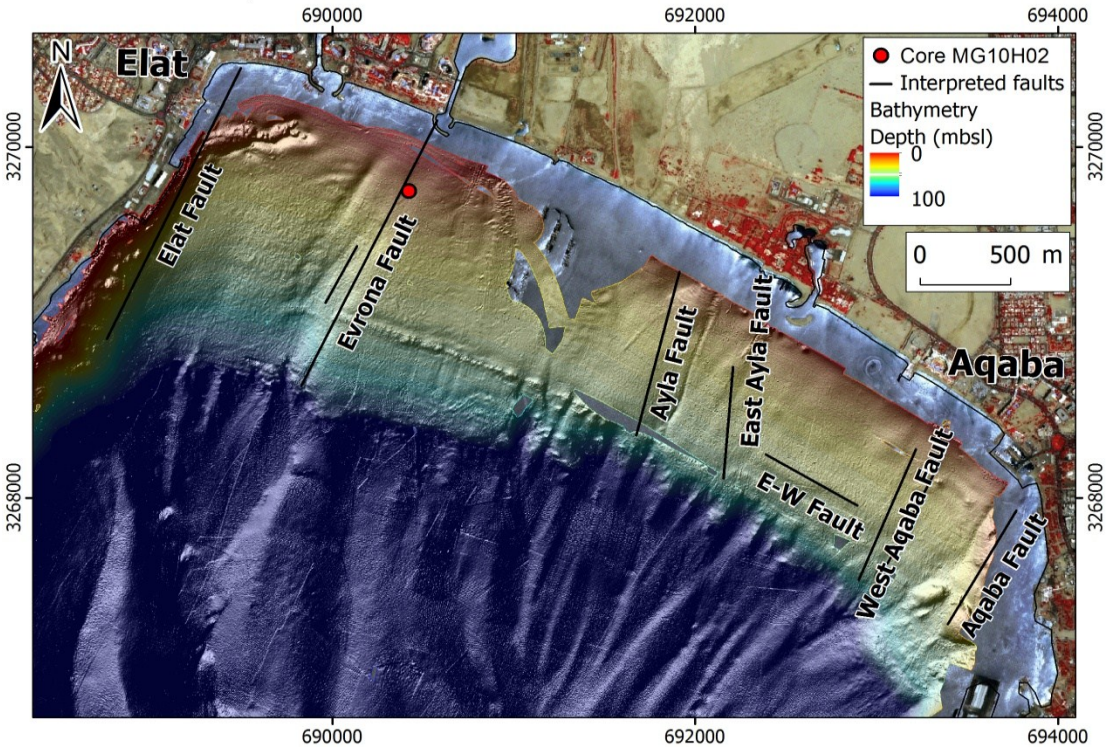

Figure 2.2 Northern Gulf of Aqaba including offshore faults interpreted from seismic reflection data and the location of core MG10H02 (Ben-Avraham *et al.*, 2009; Hartman, 2011).

Hydrography

Present seasonal sea surface temperatures (SST) recorded offshore Eilat range from 21 to 26° C for winter and summer, respectively (Moustafa, 2000). Modern average salinity is approximately $40.5^{0}/_{00}$. The Gulf exhibits a thermohaline-driven circulation pattern (Figure 2.3). An upper layer of inflowing warm water from the Red Sea drives this overturning cell. The Straits of Tiran restrict the Gulf of Aqaba from otherwise cooler influences, which cause relatively weak vertical stratification, from the central Red Sea (Lamy *et al.*, 2006). In addition, the Straits allow relatively low saline, highly oxygenated, and nutrient depleted waters to enter the Gulf. Flowing northward, the waters increase in salinity due to evaporation, sink, then produce a subsurface nutrient-rich outflow (Paytan, 2011).

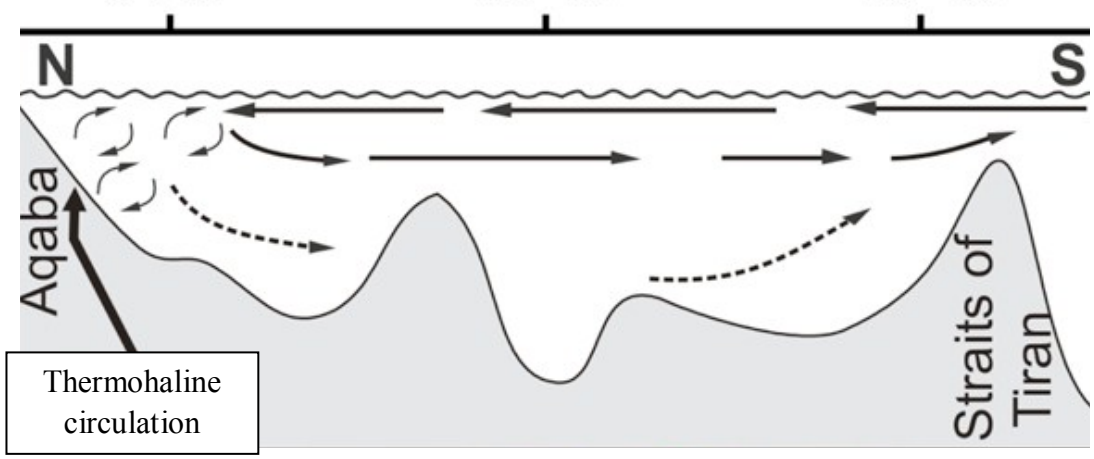

Figure 2.3 Gulf of Aqaba profile illustrating thermohaline-driven ocean circulation pattern (Lamy *et al*., 2006).

Geologic Setting

Burdon (1959) initially described the geology of this region and provided interpretations of geologic maps generated by Quennell (1959). Bender (1974) expanded the geologic interpretation based on a series of geologic maps at a 1:100,000 scale in Jordan. Garfunkel (1970) mapped the Eilat region and the Arava Valley and presented a map of active faults (Garfunkel *et al.,* 1981).

The geologic history of the region can be divided into three tectonic phases: plutonic, carbonate platform, and continental break-up (Garfunkel, 1988). The first phase (plutonic) occurred during the Pan-African Orogeny in the late Precambrian with continental convergence and pluton emplacement. High temperature/low pressure metamorphisms characterize this tectonic event that culminated in regional uplift during the early Cambrian. The second phase was an extensive period of marine sedimentation punctuated by periods of non-deposition or erosion during the Cambrian to mid-Cenozoic. This platform phase resulted in the deposition of the four geologic sequences: Ram, Kurnub, Ajlun (or Judean in Israel), and Belqa (or Mt. Scopus in Israel). Lastly, the third (continental break-up) phase occurred during the Oligocene-Miocene. Continental rifting along the African-Arabian plate

boundary in the Red Sea defines this phase. In addition to producing the Dead Sea transform fault zone system, this phase is associated with uplift, faulting, folding, and pulses of volcanism.

The 107 km of accumulated offset on the Dead Sea transform system results in vastly different geology adjacent to the Wadi ‘Arabah (Arava) valley floor. The Jordanian mountains east of the Gulf of Aqaba are some of Jordan’s old rocks dating to 640-560 million years ago (Jarrar *et al.*, 2003). The Aqaba Complex comprises the base of these mountains and consists of igneous and metamorphic units. Igneous rocks of this complex are mainly granite, monzogranite, granodiorite, and diorite (Ibrahim and McCourt, 1995). The metavolcanic and metasedimentary greenschists and amphibolite rock facies experienced low-pressure metamorphism 750-800 Ma (Jarrar *et al.*, 2003). Intrusive igneous dikes formed from regional tensional stress cross this crystalline series. An unconformity overlies the Aqaba Complex, which separates it from the younger Araba Complex (Ibrahim and McCourt, 1995). Alkaline rhyolitic volcanics and lesser amounts of contemporaneous granites comprise the Araba Complex, which dates to approximately 550-540 Ma (Ibrahim and McCourt, 1995). The igneous, metamorphic and cross-cutting dikes are all part of the Pan-African tectonic phase.

An unconformity overlying the Aqaba Complex distinguishes the earlier Pan-African phase from the carbonate platform phase. The lower units (Ram Group) are Cambrian in age and consist of fluvial and marine arkosic sandstone and quartzose sandstone.

An unconformity separates the Ram Group from the Kurnub Sandstone. This unconformity, however, represents an extensive period of non-deposition or erosion. Upper Paleozoic and lower Mesozoic strata are missing. The Kurnub sandstone is capped by the

Cretaceous marine deposits of the Ajlun and Belqa Group limestones in Jordan. Deposition of these units took place as eustatic sea level rose flooding the continent and precipitating hundreds of meters of carbonate sediment.

The Eilat Mountains west of the Gulf of Aqaba are comprised of the marine Ajlun and Belqa units described above. However, across the Israeli border, they are named the Judaen and Mt. Scopus units, respectively. Here, the Cretaceous limestones overlie Ram or Kurnub sandstones. Underlying the sandstone are grey and red granite and metamorphic rocks cut by acid and basic dikes (Harpez, 1960). Precambrian basement rock in the mountains of southern Israel extent is limited, but outcrop across much of the Sinai Peninsula in Egypt.

Dead Sea Transform System

Reconstruction of past environments must always take into consideration the role of tectonics. Tectonic subsidence, uplift, and faulting have the potential to alter relative sea level and sediment depositional patterns. Therefore, this study must address the mechanisms and extent of tectonics in the region. The study area lies along the Dead Sea Transform fault system (DST). Extending over 1000 km from the Red Sea rift north into eastern Turkey, it is the boundary between the Arabian and African tectonic plates (Freund *et al.*, 1970). Accumulating sinistral (left-lateral), strike-slip fault displacement of 107 km is documented on the DST (Burdon, 1959, p. 60). Large pull-apart basins developed along the strike of the DST by a component of extension (Garfunkel *et al.*, 1981; Ben-Avraham *et al.,* 1979). The Earth's lowest topographic depression, the Dead Sea (bottom depth of 725 m below sea level), is located along the DST and expresses the magnitude of this crustal extension. Red Sea rifting and the formation of the DST initiated in the Miocene and continues today.

Klinger *et al*. (2000), Niemi *et al.* (2001), and Le Béon *et al.* (2010) estimated Dead Sea fault Quaternary slip rates in Wadi 'Arabah at 4 ± 2, 4.3 ± 1.7, and 5.4 ± 2.7 (Le Béon also gives slip rates of 4.5 ± 0.9 and 8.1 ± 2.9 for two other sites) mm/yr, respectively. Makovsky *et al.* (2008) using Chirp seismic reflection data estimated a rate of 2.7 ± 1.7 mm/yr for the offshore Evrona fault based on an offset coral reef on the shelf of the northern Gulf of Aqaba.

Strike-Slip Faults

Strike-slip faults are the physical expression of large-scale plate motion along transform boundaries. Strike-slip faults can occur in continental and oceanic plate boundaries, intraplate areas (perhaps in response to plate collision), and transfer zones that connect normal faults or thrust faults in rift systems and fold-thrust belts, respectively (Cunningham and Mann, 2007). The Gulf of Aqaba along the DST is one place in the world where a mid-ocean ridge system runs into a continent and changes into a transform system (Ben-Avraham *et al.*, 1979; Ben-Avraham, 1985). Figure 2.4 illustrates this concept. As displacement increases along strike-slip faults, individual fault segments tend to link leading to localized zones of convergence and divergence. Cunningham and Mann (2007) define these areas of linkage, known as bends, as offset areas where bounding faults are continuously linked and continuously curved across the offset. Step-overs are zones of slip transfer between overstepping, but distinctly separate and subparallel strike-slip faults. However, because fault step-overs may connect leading to a fault bend, these terms are often interchangeable.

Depending on local compression or extension, either a restraining or releasing bend will result, respectively. The submarine pull-apart basins of the Gulf of Aqaba are an

example of the latter. Such pull-apart basins form in the areas between step-over faults (e.g. Sylvester, 1988). Releasing bends are sites of subsidence, crustal extension, and possible volcanism.

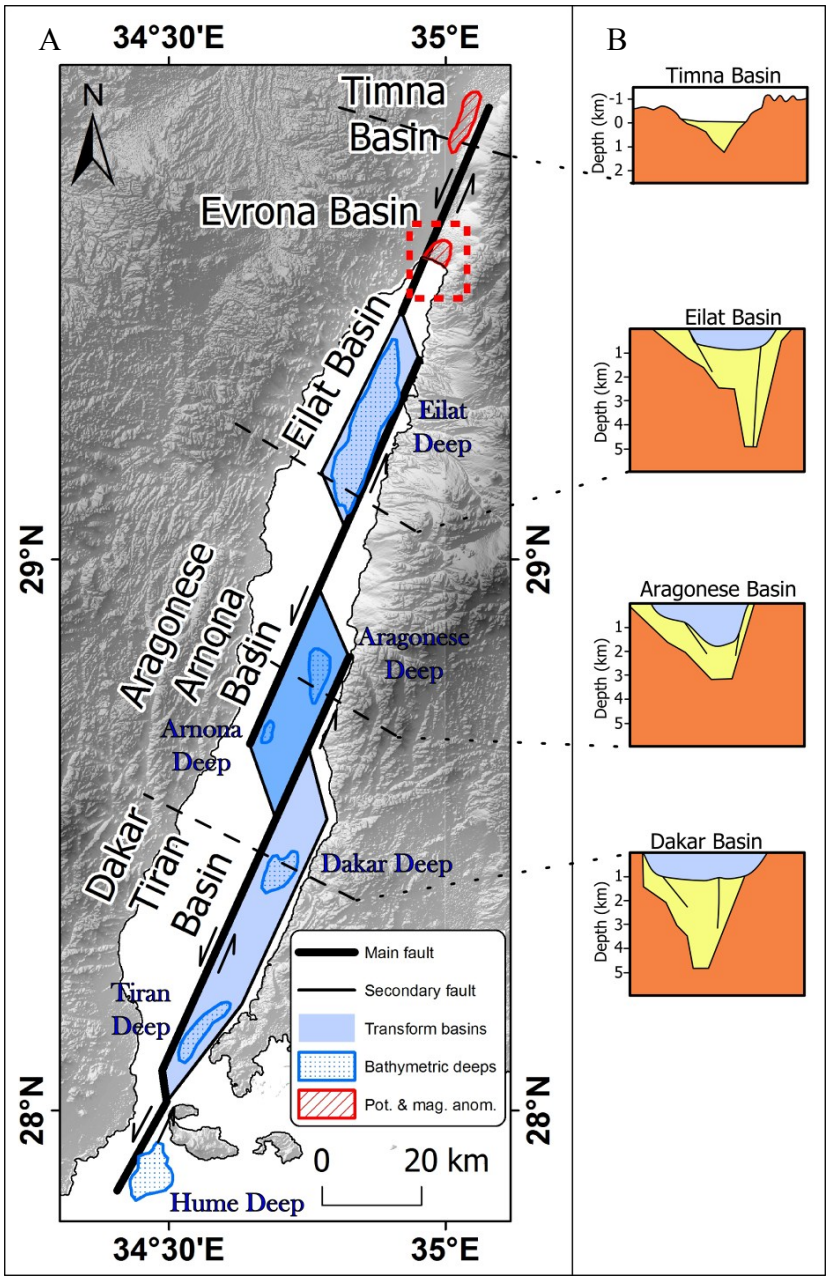

Figure 2.4 (A) Gulf of Aqaba fault system and (B) profiles of Timna, Eilat, Aragonese, and Dakar Basins (After Ben-Avraham, 1985; Hartman, 2011).

Modern Physiography

The Dead Sea-Jordan Rift valley is a geomorphic component of a larger system of rift tectonics that extend over 65° of latitude and separate Europe from Asia Minor (Burdon, 1959). The 375 km of the rift valley stretches from the Gulf of Aqaba north to the Sea of Galilee. The Wadi ‘Arabah (Arava Valley) drainage is the valley that extends northward to the Dead Sea roughly 170 km from the Gulf of Aqaba. Here, terrestrial deposits, alluvial fans, gravel outwash plains, and sand dunes dominate the landscape. This section is a flat broad valley whose width varies from 20 km in the north to 10 km in the south. Rugged north-south trending mountains flank the valley floor to the east and west. This region displays typical arid erosion and deposition features controlled by episodic flash floods.

Geomorphology

The severe lack of precipitation restricts fluvial runoff into the Gulf of Aqaba to ephemeral type drainage systems. The steep granitic mountains of southern Jordan flank the eastern margins of the Wadi ‘Arabah and rise nearly 1200 m from the valley floor. Adjacent to the Wadi ‘Arabah on the west, the sandstone and limestone mountains of southern Israel gain roughly half that elevation (600 m) to their summit. The Gulf of Aqaba drainage basin is constrained by these two mountain ranges to the east and west and by a topographical high 80 km north in the Wadi ‘Arabah. Jebel Ar-Risha located within the valley divides the drainage from flowing north into the Dead Sea and flowing south into the Gulf of Aqaba.

CHAPTER 3

FORAMINIFERA

Although detailed foraminifera morphology and taxonomy are beyond the scope of this study, a general background in the organism is presented here. Foraminifera exist in either a benthic (bottom dwelling) or planktonic (in the water column) variety. They can live in all aquatic environments, including freshwater lakes and a wide range of marine temperatures and salinities. Of those occupying oceans and seas, benthic-dwelling species commonly populate shallow shelf environments, while planktonic foraminiferan generally thrive in surface waters over bathyal depths.

The test (shell) surrounds the soft inside tissue of the organism and is the only remnant preserved in the fossil record. Because of this high preservation characteristic of foraminiferan tests, taxonomists classify them primarily by test composition. Tests can be either 1) secreted organically, tectin, 2) secreted mineralogically as calcite, aragonite, or silica, or 3) agglutinated from preexisting sediment particles. In addition to test composition, foraminifera are classified by chamber number and arrangement.

Life Cycle

Foraminifera have two reproductive generations termed the agamont and gamont, which reproduce asexually and sexually, respectively and may be complete in one year. During this cycle (Figure 3.1), cytoplasm of the agamont generation splits into multiple daughter haploid cells. These cells form chambers and are released into the water to become the gamont generation. Sexual reproduction is achieved when gametes, mitotically produced from the gamont, fuse together creating a full, diploid chromosome number. Variations in this cycle may occur in larger benthic foraminifera, where a schizont generation exists after

the agamont. This may delay the complete life cycle several years. Planktonic foraminifera are thought to reproduce sexually in concert with the lunar cycle (Armstrong and Brasier, 2005).

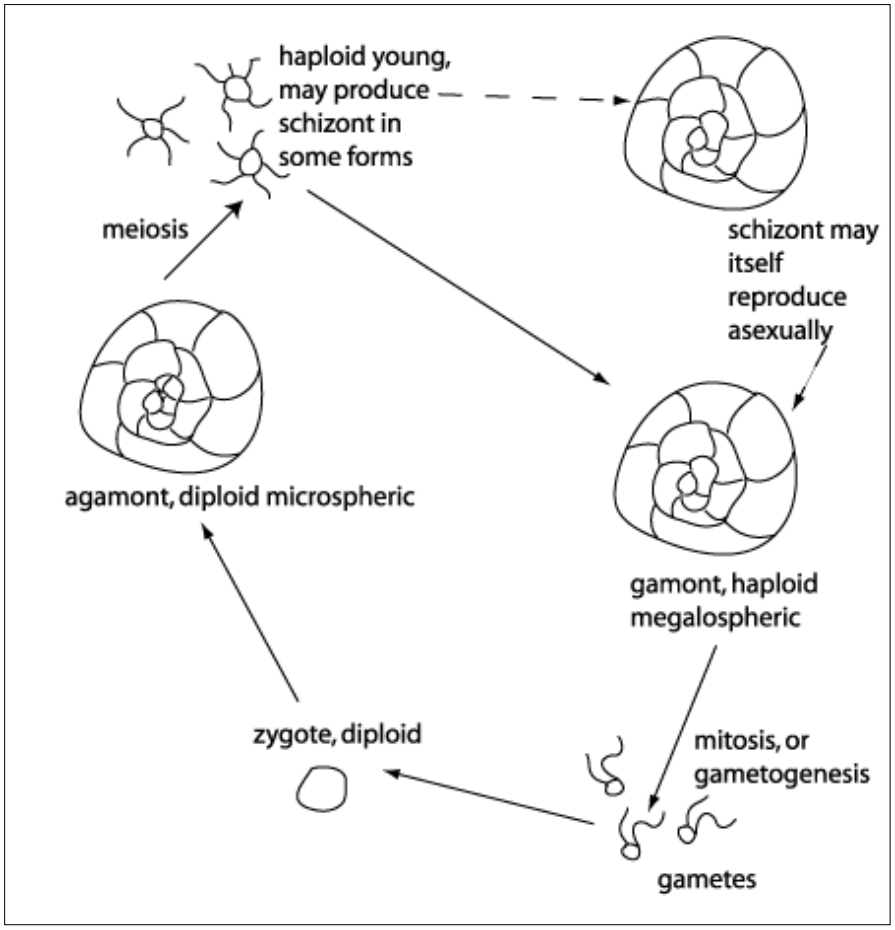

Figure 3.1 Foraminifera life cycle diagram. Note in smaller benthic foraminifera, the schizont generation may be absent (After Goldstein, 1999).

Classification

Foraminifera belong to the Domain Eukaryota and Kingdom Protozoa. Their class, subclass, and order are not entirely consistent in the scientific community. Cavalier-Smith (1993) considers foraminiferida an order in the class Reticulosa, then later (Cavalier-Smith, 1998), elevated them to their own phylum (Armstrong and Brasier, 2005). Prothero (2004)

classifies order Foraminiferida in the subclass Rhizopoda, which is in turn part of class Granuloreticulosa. Regardless of these upper level inconsistencies, micropalaeontologists generally agree upon divisions at the suborder level, which is the focus of, and consequently, more important to this study.

Micropalaeontologists base subsequent divisions on order of importance from 1) wall structure and composition, 2) chamber shape and arrangement, and 3) aperture and ornament. Textulariina, Miliolina, Rotaliina, and Globigerinina are some of the suborders of foraminiferida of reference to this study. The suborder Textlariina is an agglutinating benthic variety, typically displaying one cavity. Miliolina have an imperforate, porcelaneous-appearing calcareous test. They can be planispirally (coiling occurs in a single horizontal plain away from the axis of coiling), or streptospirally (addition of tabular chambers) coiled. They may also uncoil and grow uniserially (Armstrong and Brasier, 2005). Rotaliina have a perforate hyaline calcareous test and can grow uniserially, biserially, or triserially. They are commonly recognized by optically radial growth. Globigerinina are planktonic and achieve buoyancy through coarsely perforated inflated chambers made of low-magnesium calcite (Armstrong and Brasier, 2005).

Seasonality

When examining century- and millennia-scale climate variability through micropaleontology, it is important to consider seasonal changes in biologic assemblages. Though seasonal patterns of a stratified water column primarily affect planktonic foraminifera assemblages (largely absent in this study), benthic populations appear indirectly impacted by these fluctuations. The Gulf of Aqaba summer months (April-October) bring warm, relatively low salinity, highly oxygenated waters from the Red Sea northward through

the Straits of Tiran. As water flows north, salinity increases due to evaporation. Combined with the prevailing north wind stress, the northbound water sinks and initiates a southward migration of cooler denser water. This pattern creates a weak thermocline during summer months.

In comparison, winter months (January-March) again carry warm, relatively low salinity, highly oxygenated water northward. However, because inflowing water is cooled earlier in its northward migration, a more homothermal stage characterizes the winter months (Reiss and Hottinger, 1984).

The most striking seasonal pattern foraminifera display is their relationship to adjacent biotic communities. Juvenile foraminifera along the Sinai coast inhabit algal blooms loosely covering permanent vegetation. These algal clouds transport primarily amphisteginids, soritids, and textulariids during storm induced increased currents. This is perhaps the most significant transport mechanism and is closely associated with seasonal variation of foraminifera in this region (Reiss and Hottinger, 1984).

Paleoenvironmental Indicators

As mentioned above, foraminifera are an important paleoenvironmental tool because of their abundance, small size, and specific preferences for characteristic ecological zones. Benthic/planktonic ratios and agglutinated/porcelaneous/haline proportions play a vital role in reconstructing marine paleoenvironments. In general, benthic/planktonic ratios decrease with increasing distance from the continental shelf to the slope as does species diversity. Agglutinated/porcelaneous/haline proportions are indicative of specific offshore habitats (Armstrong and Brasier, 2005). Paleoenvironment and paleoclimate reconstruction relies on

modern analogs from foraminifera currently inhabiting various marine environments of today.

Modern Analog

Foraminiferan as paleoenvironmental proxies are especially useful due to the existence of their modern analog. Modern surface samples provide information useful for comparative analysis. For example, the subfamily Sortinae and Amphistigidae are associated with green algae (Reiss and Hottinger, 1984). *Amphistegina, Amphisorus hemprichii,* and *Sorities orbiculus* in particular display this characteristic, which links their habitat to the presence and distribution of green algae. *Amphisorus hemprichii* are largely epiphytic and found mainly on *Halophila* leaves (Reiss and Hottinger, 1984). Both *A. hemprichii* and *S. orbiculus* are restricted to less than 35 m water depth, where they and *Halophila* can survive. Modern analogs are also useful in morphological changes in response to changing environmental conditions. Reiss and Hottinger (1984) attribute morphological changes in *A. hemprichii* and *S. orbiculus* to places where temperature and salinity are temporarily elevated, such as a tidal pool. These deformations are expressed as an additional growth plane perpendicular to the original, twinning, or a change in growth direction. The genus *Amphistegina* present in the Gulf of Aqaba lives both on *Halophila* leaves and hard substrate. They can occupy high-energy environments or they may occur in quiet lagoons and channels (Reiss and Hottinger, 1984).

CHAPTER 4

METHODS

Coring

The 4.3-meter long core analyzed in this study was collected during the February 2010 field campaign as part of Phase II of the "High Resolution Marine Geophysical Imaging of Active Faults in the Aqaba-Eilat Region" (GAE) project. The goal of the GAE project led by Tel Aviv University, Israel Oceanographic and Limnological Research, and Al Balqaa' Applied University in Jordan is to assess earthquake hazards along the rapidly developing coastal cities of Eilat, Israel and Aqaba, Jordan. Phase I of the GAE project conducted during 2006-2009 mapped submerged active faults offshore in the Gulf of Aqaba using high-resolution seismic reflection data and multibeam sonar data (Tibor *et al*., 2010; Hartman, 2011). The GAE Phase II project, "Marine Coring and Onshore Correlations," seeks to date active fault motion by dating marine subsurface sediments retrieved from cores and to correlate the core stratigraphy to seismic reflection data and to the onshore faults.

The February 2010 coring campaign was conducted aboard the R/V *Mediterranean Explorer*. The ship is 20 meters in length and is equipped with specially designed coring devices including a hydraulic crane (7 ton/m) and a multipurpose winch. The team collected 35 cores during the three-week research cruise. They utilized piston, vibracore, and diver-assisted pneumatic hammer methods for core collection, retrieving 27, 6, and 3 cores using each method, respectively. These cores were collected in various water depths of 20-550 meters and range in length from ~0.4 meters to 4.5 meters. Figure 4.1 shows a map with the core locations and core recovery type.

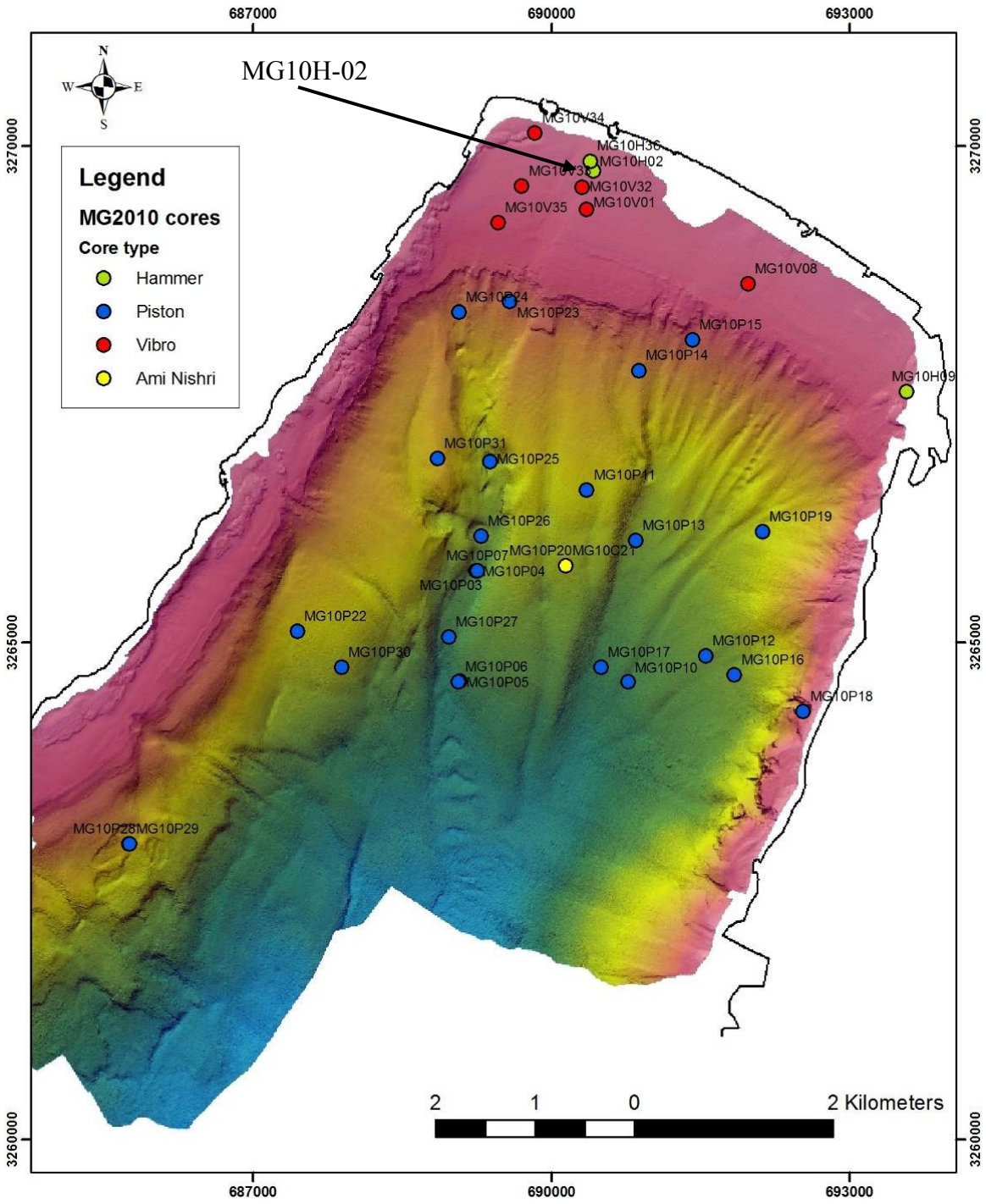

Figure 4.1 Core location and collection methods overlain on bathymetry of the Gulf of Aqaba (Tibor *et al*., 2010). Core MG10H-02 was retrieved at UTM coordinates 690420 E and 3269750 (Ben-Avraham *et al*., 2010).

The core analyzed in this study, number MG10H02, was retrieved using the newly developed, diver-assisted pneumatic hammer technique. Designed in part by Beverly Goodman (University of Haifa), this technique was developed specifically for collecting sediment from the sandy shallow (< 30 m) shelf. To minimize sediment loss within the core, a hand-made aluminum core catcher was attached to the bottom of the aluminum core pipe prior to coring (Figure 4.2C). The divers, Dr. Beverly Goodman and Dr. Timor Katz, operated an underwater pneumatic hammer connected to a tending compressor that was stationed on the research vessel by an air hose. An adapter attaches the hammer to the aluminum pipe. A weighted base (Figure 4.2D) stabilizes the lower section of the pipe, while lines attached to counter-floats balance the upper portion (Goodman, pers. comm., 2010). This method allows divers to extract and immediately cap the core under-water, minimizing potential water intake and the subsequent loss of sediment. Once reaching maximum penetration, the core was cut at the water-sediment interface, capped, and lifted to the surface by inflating air-lift bags. The components of the diver-assisted coring technique are depicted in Figure 4.2.

The MG10H02 core was collected on February 11, 2010, from 25.4 m water depth, at UTM coordinates: 690420 E and 3269750 N. Maximum penetration depth reached 5.5 m. The total recovered core length is 4.3 m indicating 1.2 m of compaction during collection. The core was cut into three sections for ease of transport and storage and labeled A, B, and C top to bottom. Upon docking the research vessel for the day, the core was refrigerated at the InterUniversity Institute in Eilat, Israel for the remainder of the coring campaign, then transported to the Israel Oceanographic and Limnological Research (IOLR) in Haifa, Israel where it was refrigerated.

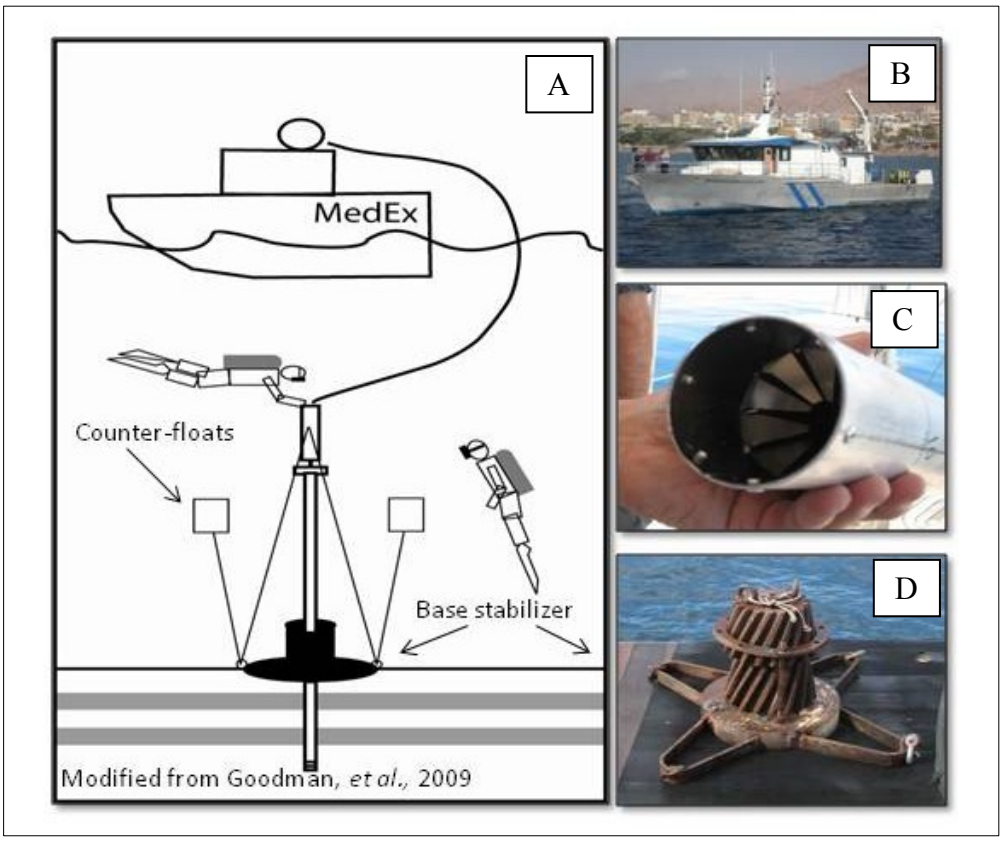

Figure 4.2 (A) Cartoon diagram illustrating the diver-assisted coring technique (After Goodman *et al.,* 2009). (B) R/V *Mediterranean Explorer*. (C) Hand-made core catcher at the base of the aluminum core barrel. (D) Weighted base stabilizer that is placed on the seafloor over the coring location.

Determination of the core retrieval locations were based on GAE project Sparker seismic reflection lines. Interpretation of the seismic stratigraphy revealed distinct lithological units in the subsurface depicted in Figures 4.3 and 4.4. Hartman (2011) provides detailed interpretations of these data including the description of two relict fringing fossil reefs at ~20 m and ~65 m water depth. A shallow buried reef is located between reflector units U8 and U9. This ancient reef grew sub-parallel to the northern coastline. A central objective of this study is to date reflectors identified in GAE Phase I project, to interpret paleoenvironment and paleoceanic conditions of the region, and to constrain the age of reflectors and associated depositional events such as the burial of the reef. Because reef

ecosystems thrive in a narrow range of tolerable conditions and are sensitive to changes in sunlight penetration, sediment input, salinity, water temperature, and other environmental factors, they are an excellent paleoenvironment indicator.

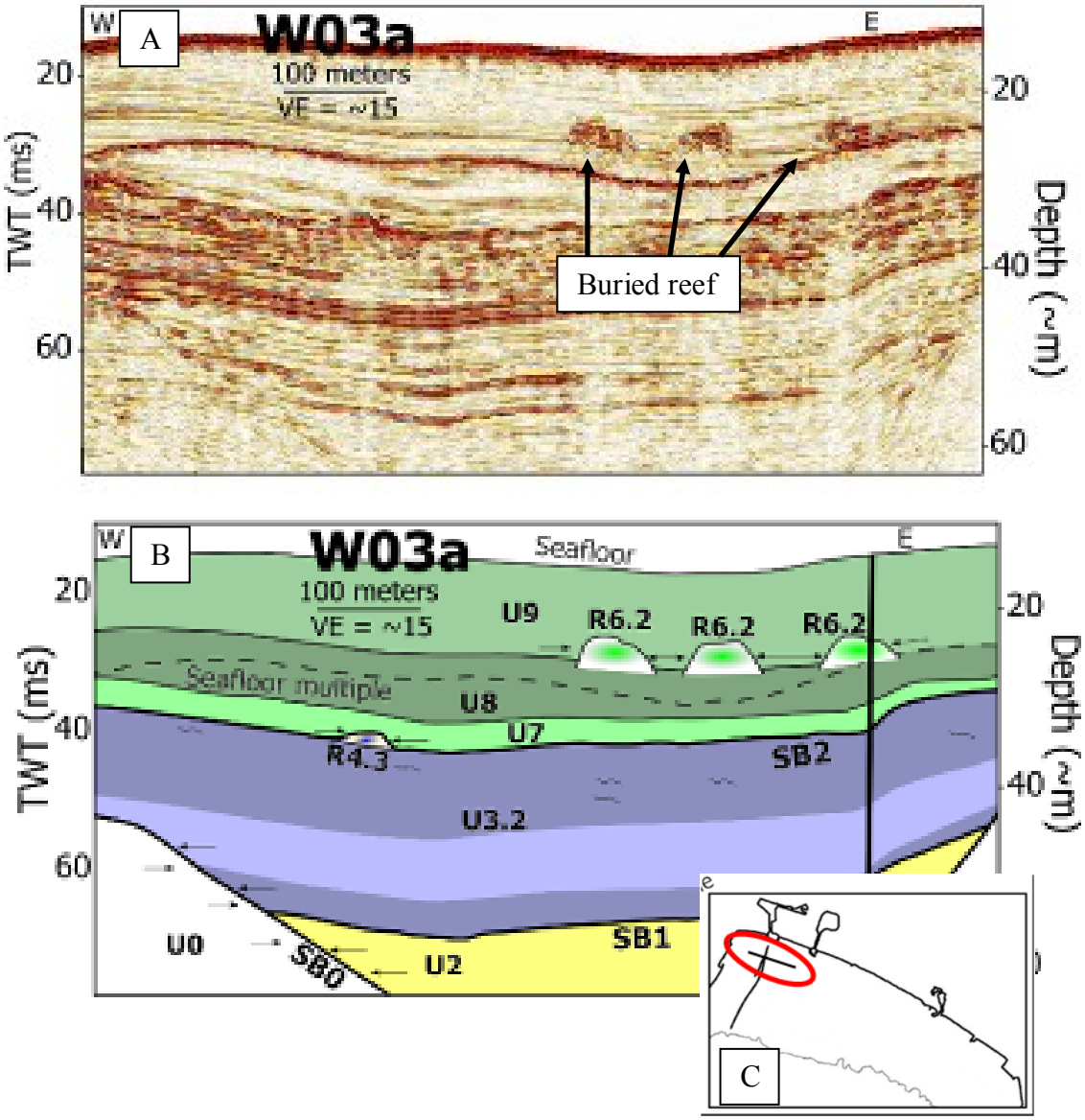

Figure 4.3 (A) W03a seismic profile with reef R6 reflector. (B) Stratigraphic interpretation and R6 location. (C) Sparker seismograph line W03a (Hartman, 2011).

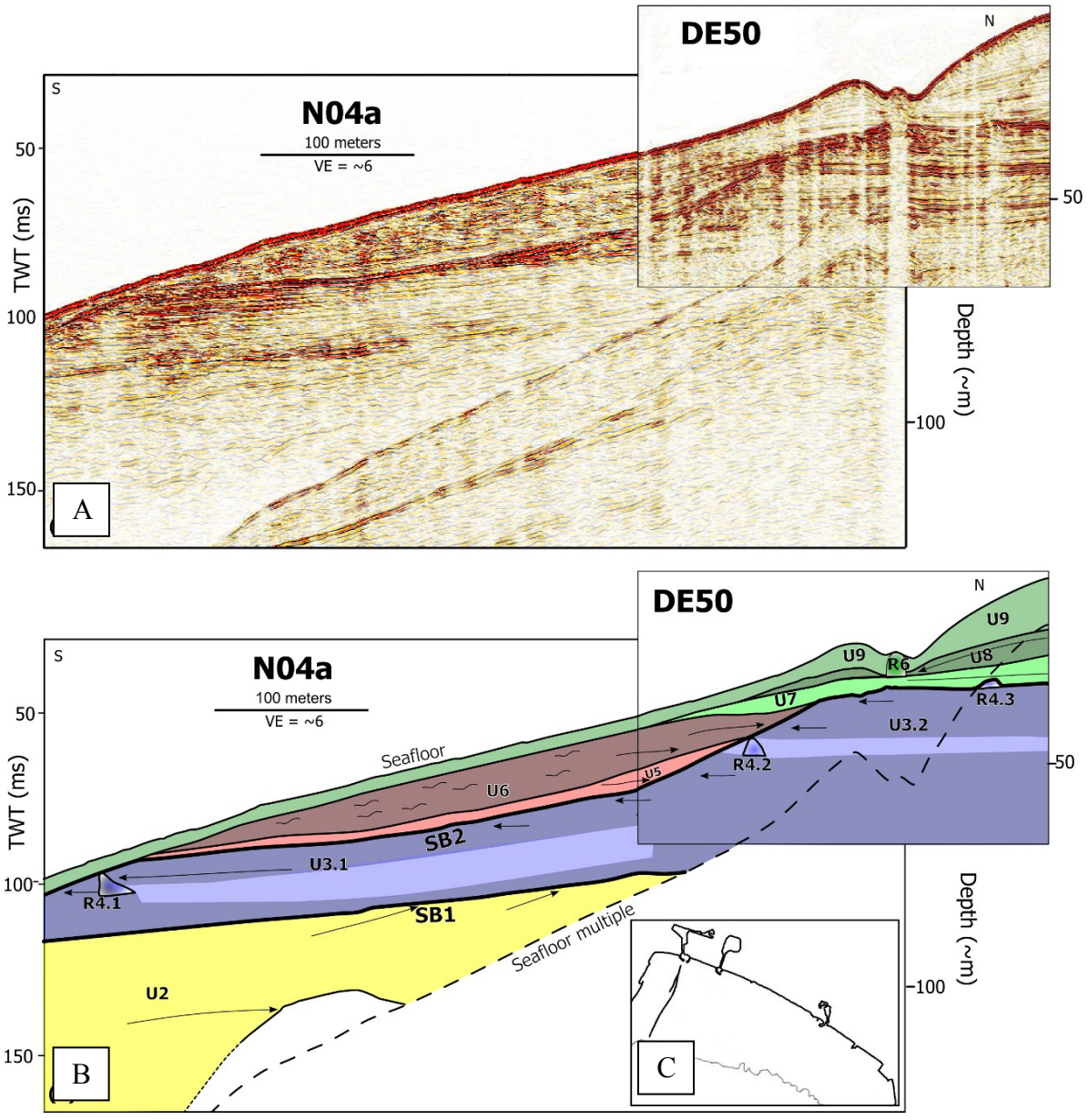

Figure 4.3 (A) Sparker seismic lines N06a, N04A and DE50 from the MERC Phase I geophysical data acquisition campaign. (B) Stratigraphic interpretation of seismic stratigraphy, approximate MG10H02 location is north off the map. (C) Location of N06a and DE50 seismic lines (Modified after Ben-Avraham *et al.,* 2010; Hartman, 2011).

Laboratory Procedures and Analyses

In July of 2010, core MG10H-02 was split at the IOLR in Haifa, Israel. The core was photographed immediately in order to most accurately document the original color and moisture content. Core lithology was described at this time. One half was wrapped in polyvinylidene chloride (plastic wrap) and refrigerated for archival purposes. The other half was sliced every centimeter and placed into plastic sample bags for grain size analysis. At every tenth centimeter, approximately one cubic centimeter was collected for foraminifera analysis.

Foraminifera Analysis

The ten centimeter subsample intervals were transported to the Interuniversity Institute for Marine Sciences (IUI) in Eilat, Israel and sieved to >150 micron portions. To achieve statistical validity, each sample was split to obtain a minimum of 300 specimens per aliquot following the methods of Goodman *et al*. (2008). Foraminifera were picked and identified from each sample using an American Optical binocular microscope at the University of Missouri-Kansas City. Fragmented or broken foraminifera were only counted if more than 75% of its original test remained intact. Fragments were also counted if a distinct single characteristic was present, such as the center of a radial specimen. Identifications were made using photographic resources from internet databases, books, along with the aid of personal identification from micropaleontologists at the IUI, Jerusalem University, and Haifa University. Each genus was photographed to create an excel spreadsheet containing all identified specimens from each sample. Species not immediately recognized were temporarily assigned the label JG1 (Julie Galloway 1), JG2, JG3 and so on for future identification. Aided by foraminifera identification references (e.g. web resources,

books), these species were identified to at least the genus level prior to the final count. In addition, foraminifera per gram of sediment were calculated using equation 1.

Equation 1. Foram/gram = (Wt of picked forams/Wt sample) * 100

Matrix Composition

In addition to foraminifera analysis, this study characterized the matrix composition based initially on siliciclastic or bioclastic dominated-sediment. Visual percent estimation further characterized the sediment within each siliciclastic or bioclastic category. The categories quartz, feldspar, mica, and heavy minerals each received an estimated percent of the matrix siliciclastic portion. Gastropods, ostracodes, bivalves, foraminifera fragments, plant matter, and trace fossils (i.e. worm tubes) comprised the bioclastic subdivisions. The majority of visual estimates were established in one sitting to maintain consistency and minimize subjective error. Each subdivided category summed or totaled to 100%. Although the siliciclastic portion of the sediment may only be 15% of the total sample, the quartz, feldspar, mica, and heavy minerals must add to 100%, thus describing only the siliciclastic particles in the sample. The gastropods, ostracodes, bivalves, foraminifera fragments, plant matter, and trace fossils also totaled 100% characterizing the bioclastic portion of the sample.

Lastly, each sample received a sorting and degree of roundness descriptive term. Again, assigned by visual estimation, these terms range from poorly sorted to well sorted and from subrounded to rounded. Supplementary notes (see Appendix D) on each sample explain any ambiguity or possible sources of error in the sediment characterization process. For example, some bioclastic particles were too fragmented to confidently identify even at a phylum level.

Grain Size

Grain size analysis was performed at the University of Haifa in Haifa, Israel on a Beckman-Coulter LS 230 laser particle size analyzer. A one-centimeter sample interval was used from 0 to 350 centimeters. All samples were digested with hydrogen peroxide to remove organics. Results from the particle size analyzer were compiled into a master spreadsheet in Excel, then exported to Ocean Data View 3.3.2-2007 software, which generated a contour grid plot. This X, Y, Z scatter plot represents grain size distribution (X) plotted against depth (Y) and percent volume of each particle size bin (Z). The z-range is limited to 10% for simplicity.

Statistics

Multivariate statistical analysis was performed on the foraminifera data collected from each sample using the micropaleontology software PAleontological Statistics (PAST) version 1.90 (Hammer and Harper, 2009). The cluster analysis included all foraminifera genus present and their corresponding sample depth. Statistical groups were generated from the cluster analysis function under the multivariate tool bar using the similarity measure option 'correlation.' Rows in the spreadsheet represent each 10 cm depth interval and columns contain foraminifera genus. Thus, incorporating all foraminifera present at each depth interval. This defines statistically similar foraminifera assemblages (StatSoft, Inc., 2001). This analysis examines five assemblages based on predetermined zones established from grain size, lithological, and mineralogical boundaries.

Radiocarbon Dating

Radiocarbon samples were prepared at the University of Missouri-Kansas City and shipped to Lawrence Livermore National Laboratory in Livermore, California.

Approximately 50 specimens of *Amphistegina lessonii* were collected from each of the five samples. Sample preparations required physically washing each foraminiferan in methanol, rinsing, sonicating, and drying the specimens at room temperature overnight. Samples were chosen based on distinct boundaries in the grain size distribution and foraminifera abundance anomalies.

Samples were collected from 50, 160, 200, 260, and 400 cm in the core. Sample one was collected from 50 cm depth and marks a bimodal grain size distribution boundary and a low foraminifera abundance zone. Samples two and three, collected at 160 cm and 200 cm, constrain the age of the foraminifera barren horizons located at 170 cm and 190 cm. Sample four at 260 cm marks the lower boundary of the homogenous fine-grained middle portion of the core. Lastly, sample five collected from 400 cm marks the upper boundary of bimodal, grain size distribution found in the lower portion of the core. Sample weights for the five sample intervals 50, 160, 200, 260, and 400 cm were 10.7, 8.4, 14.9, 13.7, and 12.5 mg, respectively.

Results were calibrated using CALIB Radiocarbon Calibration Execute Version 6.0 (Reimer *et al.*, 2009). Calibration utilized a two-sigma probability and included the Marine09 curve selection (See Table 5.1 for radiocarbon results).

CHAPTER 5

RESULTS

Lithology

Visual lithological descriptions reveal eighteen units (A-R) of varying grain textures (see Appendix E for complete lithology). Six broad lithological zones are shown in Figure 5.1. These zones range from 1) basal clayey silt in the lower ~400-435 cm, 2) laminated beds between 400-330 cm, 3) coarse-grained microfossil-rich central unit from ~330-230 cm, 4) fine-grained brown laminations from ~230-150 cm, 5) fine-grained gray slightly laminated unit from ~150-50 cm, 6) poorly-sorted coarse-grained upper unit from ~50-10 capped by a 10 cm thick organic rich surface horizon.

The lowest unit below 400 cm to the base of the core is not laminated and exhibits a ~5 cm thick dark brown unit at the base. From 400 to ~330 cm, alternating strata of clayey silt, silt, and silty clay persist (units K-Q). At approximately 330-230 cm (units H-J), grain size increases to a sandy silt and contains whole shells, shell fragments, and visible foraminifera. A particle size decrease from coarse- to fine-grain sediment coupled with a color change from gray to brown defines the laminated unit from ~230-150 cm (unit G). The two foraminifera-barren horizons lie within this division punctuating the surrounding brown sediment with grayer homogeneous deposit. The interval from ~150- 100 cm (unit D) is a non-stratified layer of coarse silt and fine sand. From ~100-50 cm (unit C) slightly laminated fine- to medium grain layers with interbedded clay lenses persists. A sharp contact at 50 cm marks the transition to units B. This interval is characterized by poorly sorted, bimodal particle distribution of fine- and coarse- to very coarse-grain size. A 10 cm medium-grained, dark gray, organic layer with abundant mottling and bioturbation caps the core.

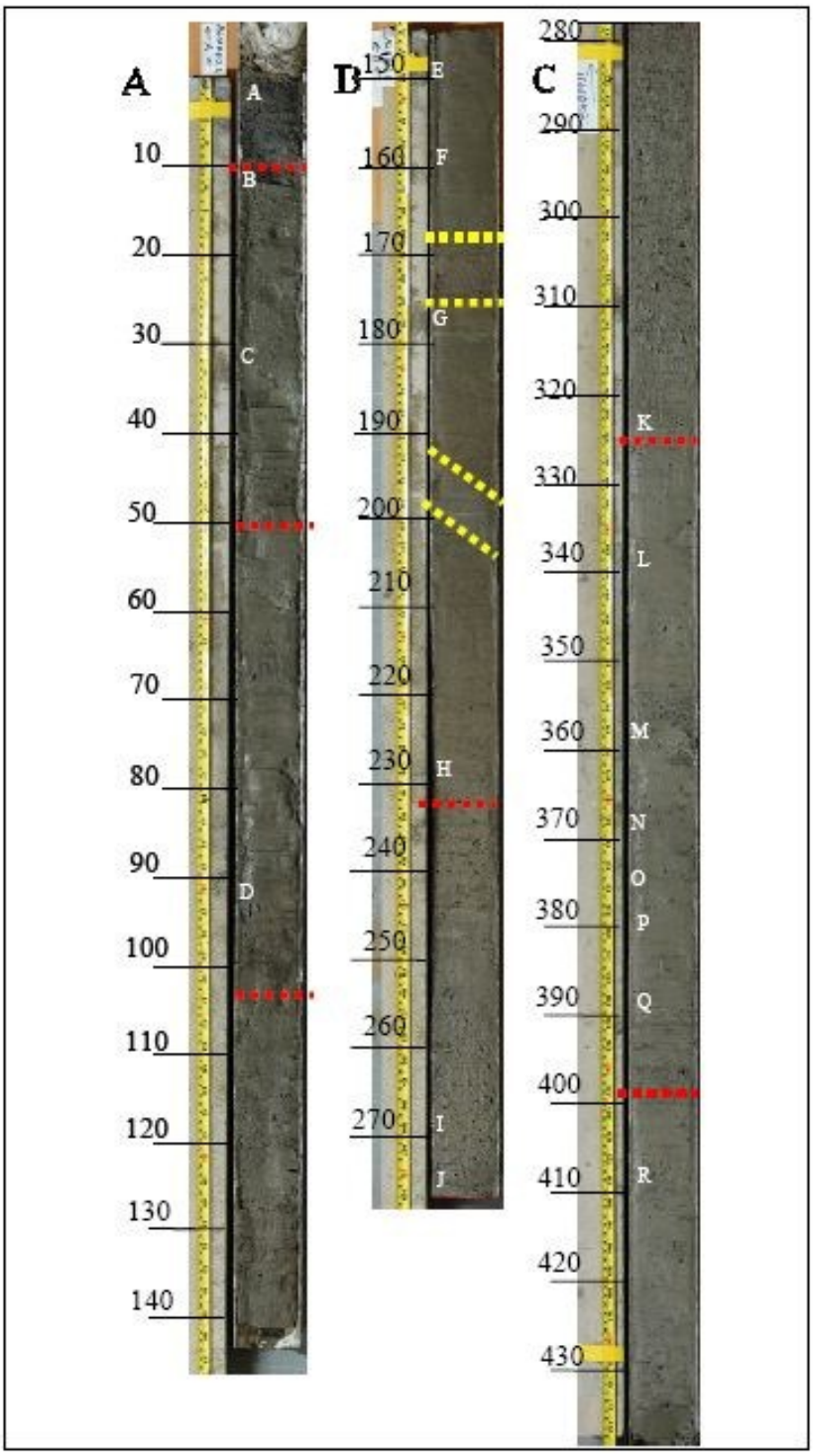

Figure 5.1 Photograph of core MG10-H02 segments A, B, and C with scale bar. Dashed red lines mark the lithologic zones, dashed yellow lines represent foraminifera-barren horizons

Figure 5.2 illustrates the distinct transition from the basal clayey silt, gray, foraminifera-poor unit to the overlying coarse-grained, gray, foraminifera-rich unit at ~330 cm (Figure 5.2C). This coarse-grained unit is overlain by a fine-grain, brown, foraminifera-poor, laminated unit at ~230 cm (Figure 5.2B).

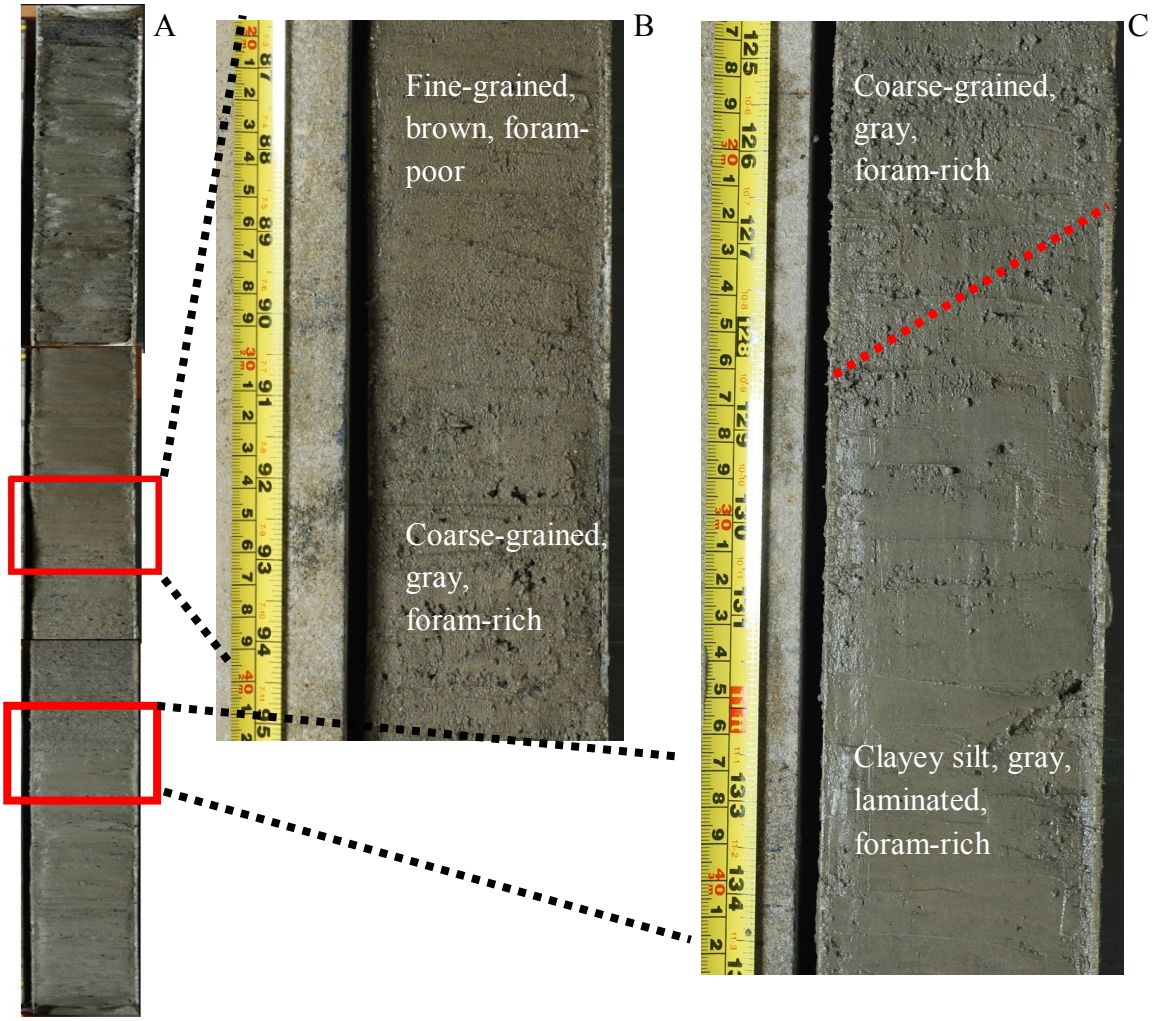

Figure 5.2 (A) MG10H-02 with highlighted areas of interest. (B) Transition from fine-grained, brown, foraminifera-poor unit to underlying coarse-grained sediment. (C) Boundary between coarse-grained unit and basal clayey silt (Ben-Avraham *et al.,* 2011)

Foraminifera Results

Foraminifera analysis reveals varying assemblages throughout the core. Appendix A contains a complete list of foraminifera collected. Foraminifera are most abundant in the upper 50 cm and at depths greater than 250 cm. This is, however, with the exception of two foraminifera barren zones at 170 and 190 cm. The sediment at these intervals is heavily siliciclastic and foraminifera content is negligible. Figure 5.3 illustrates foraminifera abundance per gram of sediment revealing that at depths less than 50 and greater than 250 cm are the most foraminifera-rich zones. Foraminifera abundance in the lower portion of the core (>250 cm) reaches a maximum at ~275 cm then declines in a stair step fashion until near the bottom of the core. In the middle portion (50-250 cm) of the core, foraminifera abundance remains relatively constant, fluctuating between 0 and ~2,500 specimens per gram. From 40 cm upward, foraminiferan abundance increases dramatically from ~2,500 to nearly 15,000 specimens per gram.

The three dominate suborders Rotaliina, Miliolina, and Textulariina were identified and compared by their relative abundance. The suborder Rotaliina dominate the upper 50 cm and from 340 to 400 cm. Miliolina prevail from 50-340 cm, while Textulariina only reach a

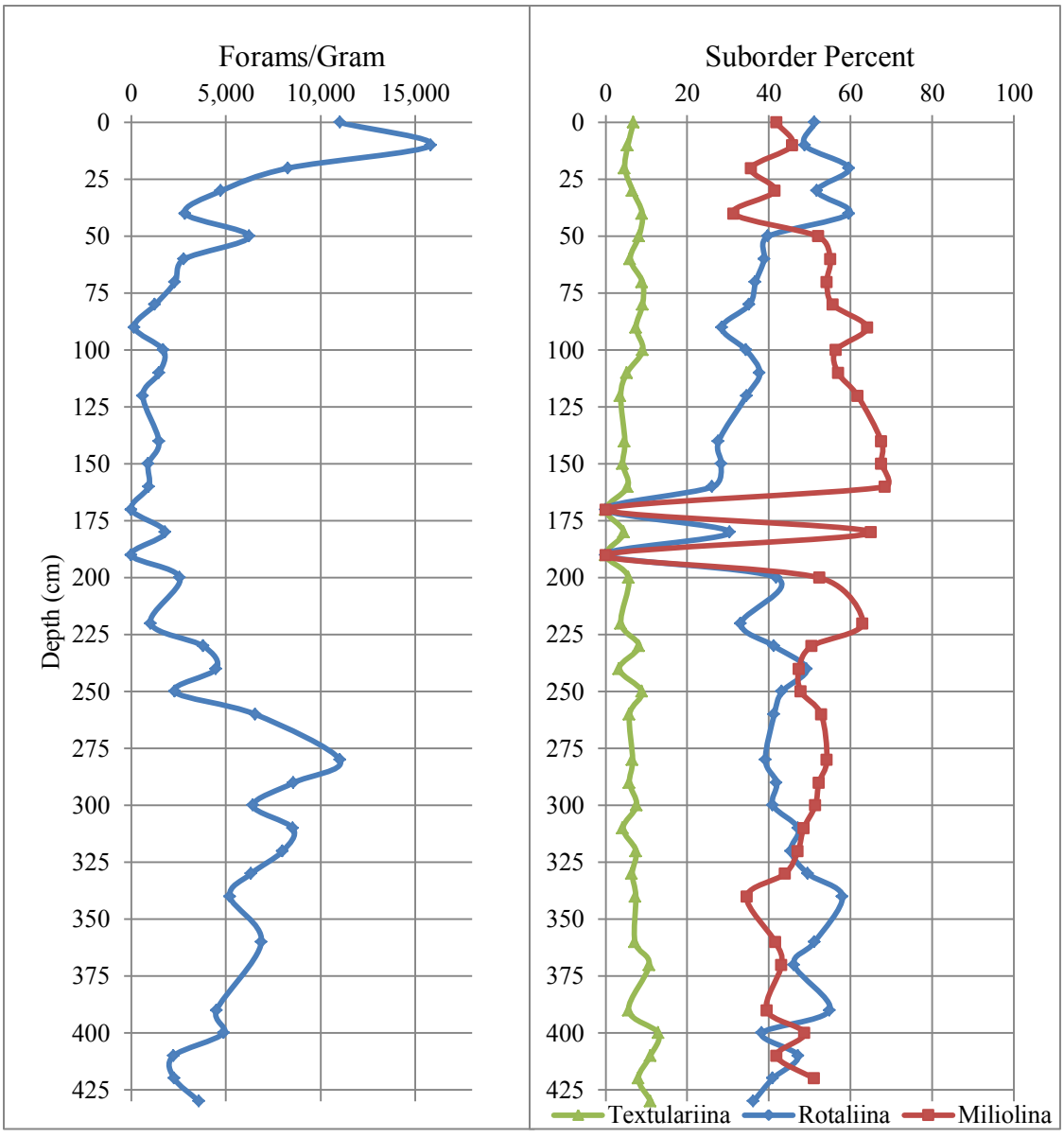

Figure 5.3 Number of foraminifera present per one gram of sample (left). The three suborders Rotaliina, Miliolina, and Textulariina and their relative abundance (right). Note the inverse relationship between Rotaliina and Miliolina.

maximum of ~10% relative abundance at depths greater than 390 cm.

Within the suborder Rotaliina, *Amphistegina, Assilina, Cibicides,* and *Elphidium* were most prevalent, with *Amphistegina* reaching 30% of the total forams picked at depth of 20

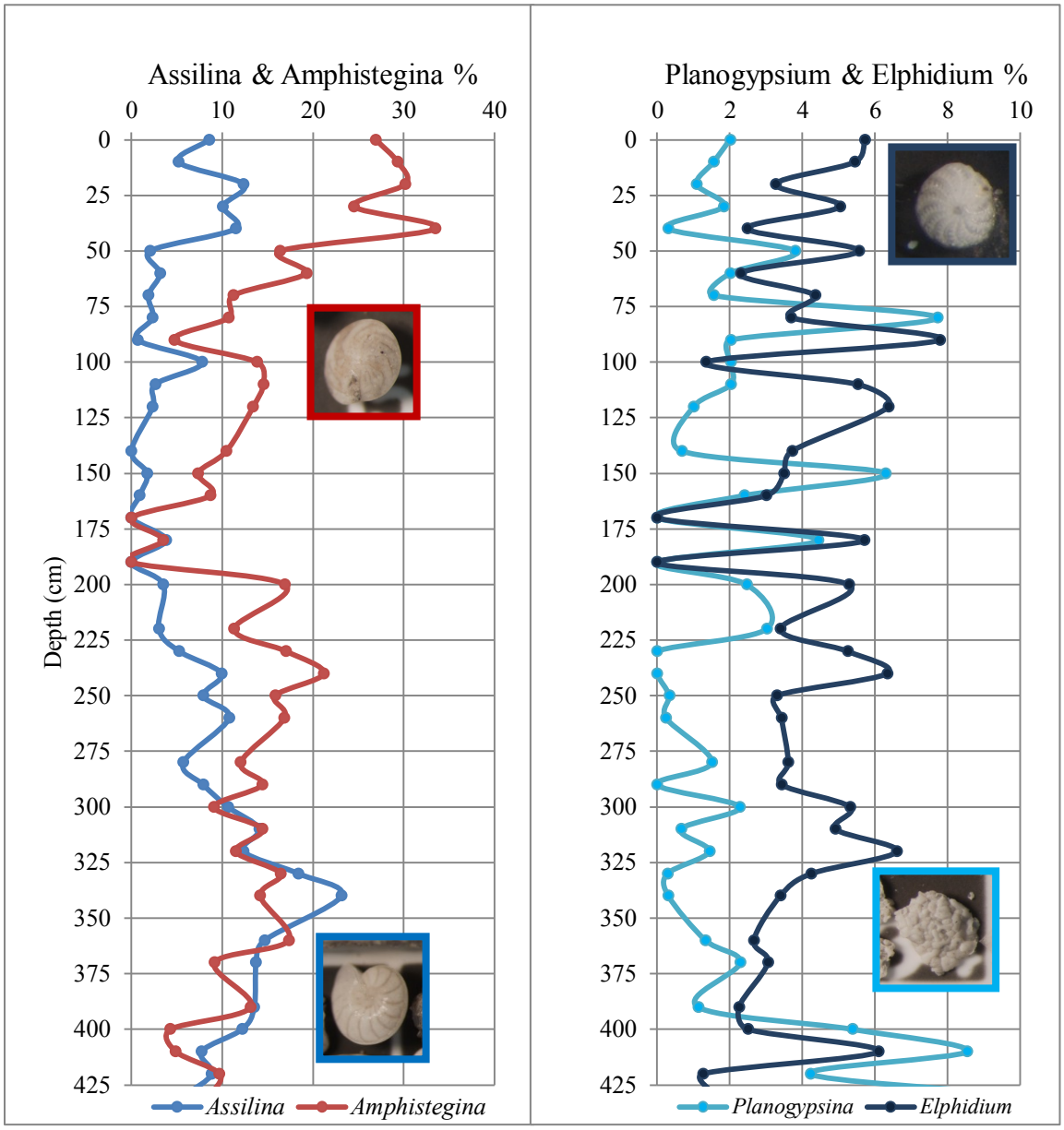

Figure 5.4 Suborder Rotaliina comparison. *Assilina* and *Amphistegina* and their relative percents (left). *Planogypsina* and *Elphidium* percent abundance (right). All shades of blue indicate opportunistic genera.

cm. *Assilina* is an opportunistic genera and the second most abundant Rotaliina with a maximum of 18% relative abundance at 330 cm (Figure 5.4). *Cibicides* appear more frequently at depths greater than 250 cm in the core, while *Elphidium* reaches its maximum of 8% at 90 cm. Though not identified to the species level, *Elphidium* commonly present in the Gulf of Aqaba are *E. advenum* (Cushman, 1922), *E. complanatum* (d'Orb. 1839). *E. craticulatum* (Fichtel and Moll 1798), *E. crispum* (Linne 1758), *E. macellum* (Fichtel and Moll 1798), and *E. reticulosum* (Cushman 1933) as described by Reiss and Hottinger (1984). *Elphidium* are opportunistic and typically occupy lagoons. At the genus level, *Elphidium* drastically increases from 420 to 410 cm and again from 100 to 90 cm. Less dramatic increases are noted from 400 to 320 cm and again from the foraminifera-barren layer at 170 to 120 cm. *Planogypsina* is also opportunistic and displays similar trends to both *Assilina* and *Elphidium.* Figure 5.3 illustrates this comparable relationship among the opportunistic genera *Assilina, Planogypsina* and *Elphidium* plotted with the abundant *Amphistegina.*

Of the Miliolina present in this study, *Hauerina, Triloculina,* and *Quinqueloculina* are dominant. *Hauerina* maintain a strong presence throughout the core ranging from a minimum of ~10% at 50, 350, and 400 cm and a maximum of ~30% at 150 cm. The most notable increase in *Hauerina* abundance is from the foraminifera-barren zone at 170 cm up to ~30% at 150 cm. Aside from this sharp increase, they display a gradual increase from 430 cm (bottom of core) up to the foraminifera-poor zone at 190 cm, once the ~30% maximum abundance is reached at 150 cm, they begin to gradually decrease up to 50 cm. They again gradually increase in the upper 50 cm. *Triloculina* are less abundant ranging from ~5-15%. On the other hand, *Quinqueloculina* have a similar abundance range to *Triloculina,* yet exhibit an inverse relationship. Although present in relatively low abundance (not exceeding

10%), small fluctuations in the opportunistic *Peneroplis planatus* and the Soritidae family are present. *Peneroplis planatus* relative abundance increases at 400, 200, 160, 90, and 20 cm. The Soritidae family including the genera *Sorites* and *Amphisorus* remain relatively constant from ~300-400 cm, but fluctuate greatly in the upper 150 cm of the core. Both Soritedae and *Penerolis* are associated with grassy marine habitats often attaching to the grass. Figure 5.5 illustrates the relationship between the Soritidae family, *Peneroplis planatus,* and the more abundant *Hauerina.*

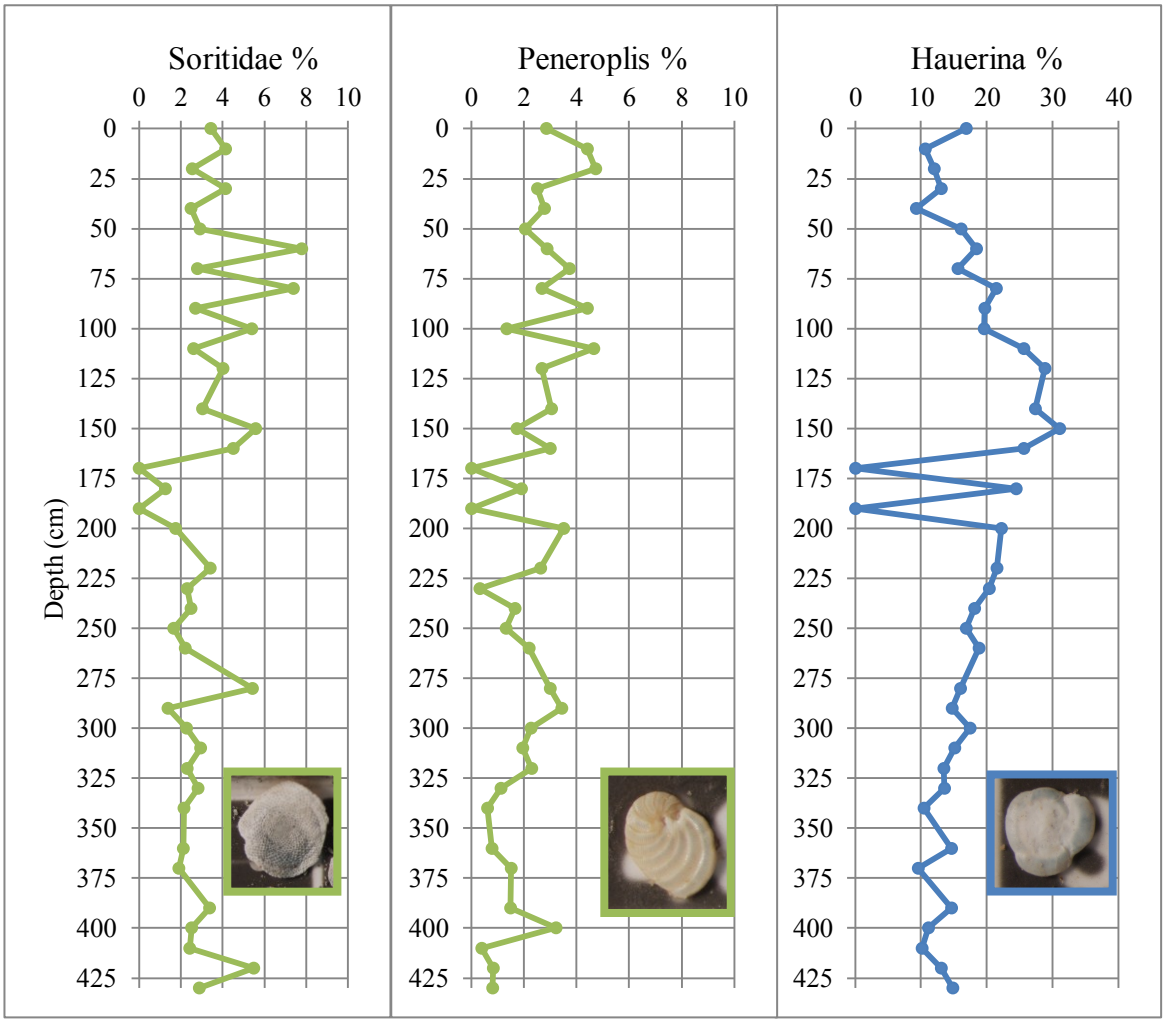

Figure 5.5 Graphical representation of the relationship between Soritidae family, *Peneroplis*, and Hauerina. Green indicates foraminifera associated with marine *Halophila* flora (blue is not associated with grass).

The suborder Textulariina fluctuated little throughout the core. Their maximum abundance remained under 10%. *Textularia* is the only genus of the suborder Textulariina present and is more abundant near 400 cm core depth. Their most notable increases are from 390 to 370 centimeters and from 120 to 100 centimeters.

Matrix Composition

After removing the foraminifera, the remaining samples are composed of varying proportions of bioclastic- and siliciclastic-dominated sediment. The visual percent estimate (Figure 5.6A) characterizes 0-120 cm and the 250-430 cm as bioclastic-dominated. Between 100 and 250 cm, the remaining sediment is predominately siliciclastic material and other minerals (Figure 5.6B). However, at 40-50 cm, siliciclastic sediment is more abundant.

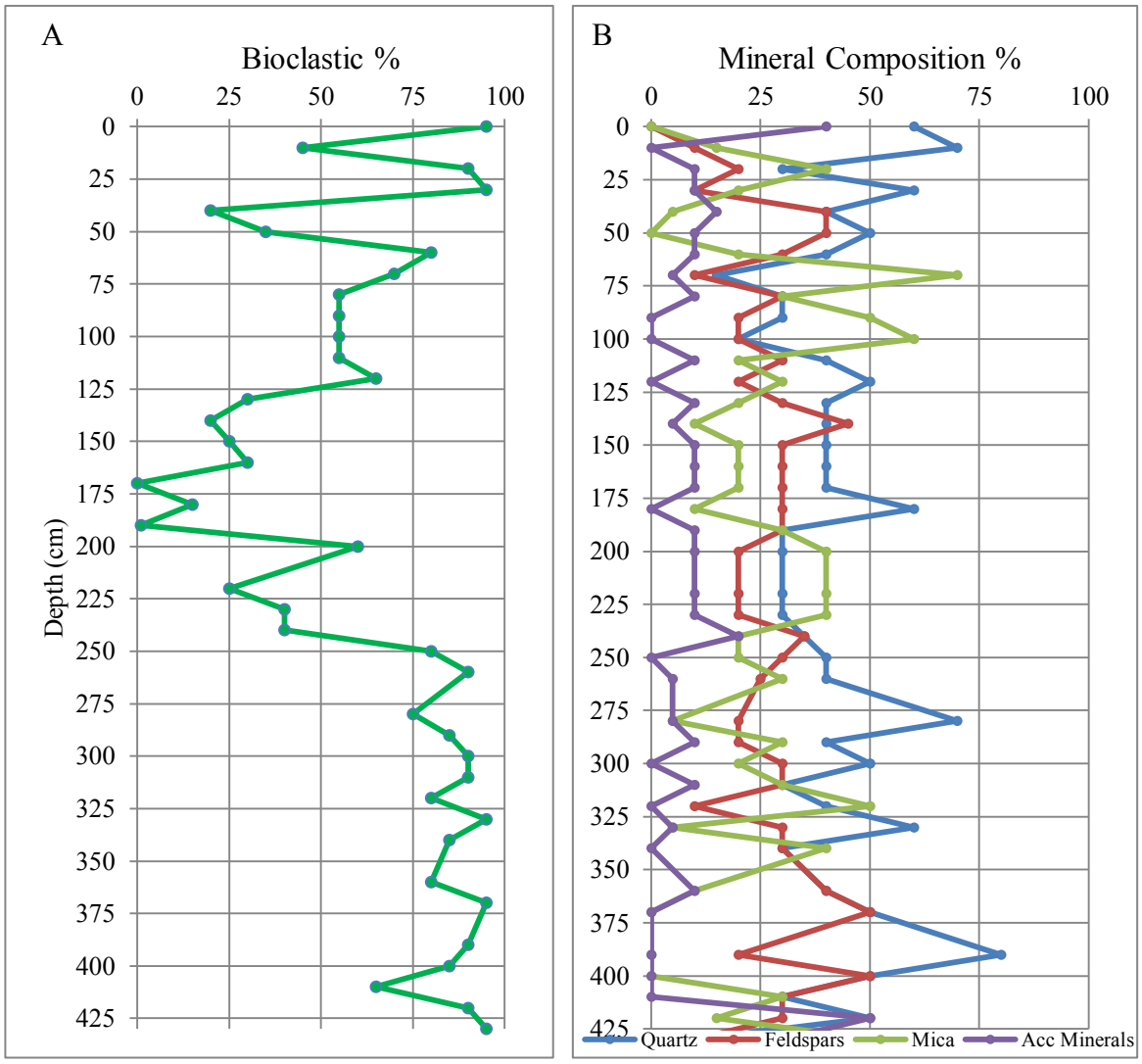

Figure 5.6 Graphical representation of (A) estimated percent bioclastic material and (B) estimated matrix mineral composition.

Grain Size

Fine-grain size distribution analysis displayed in Figure 5.7 and 5.8 presents anomalies at depths of 170 and 190 centimeters. Unimodal, leptokurtic, fine sands (127 microns) dominate these intervals and both have standard deviations of 516. Strong bimodal distribution is observed from 350 to 270 centimeters, a narrow band occurs at approximately 250 centimeters, and again in the upper 50 centimeters. Weaker bimodal distribution bands are present around 240, 210, 110, and between 50-75 centimeters. The lower 250 centimeters are coarsely skewed with maximum values in the very coarse sand ranges. Fine sands dominate in middle core portion between 250 and 50 centimeters.

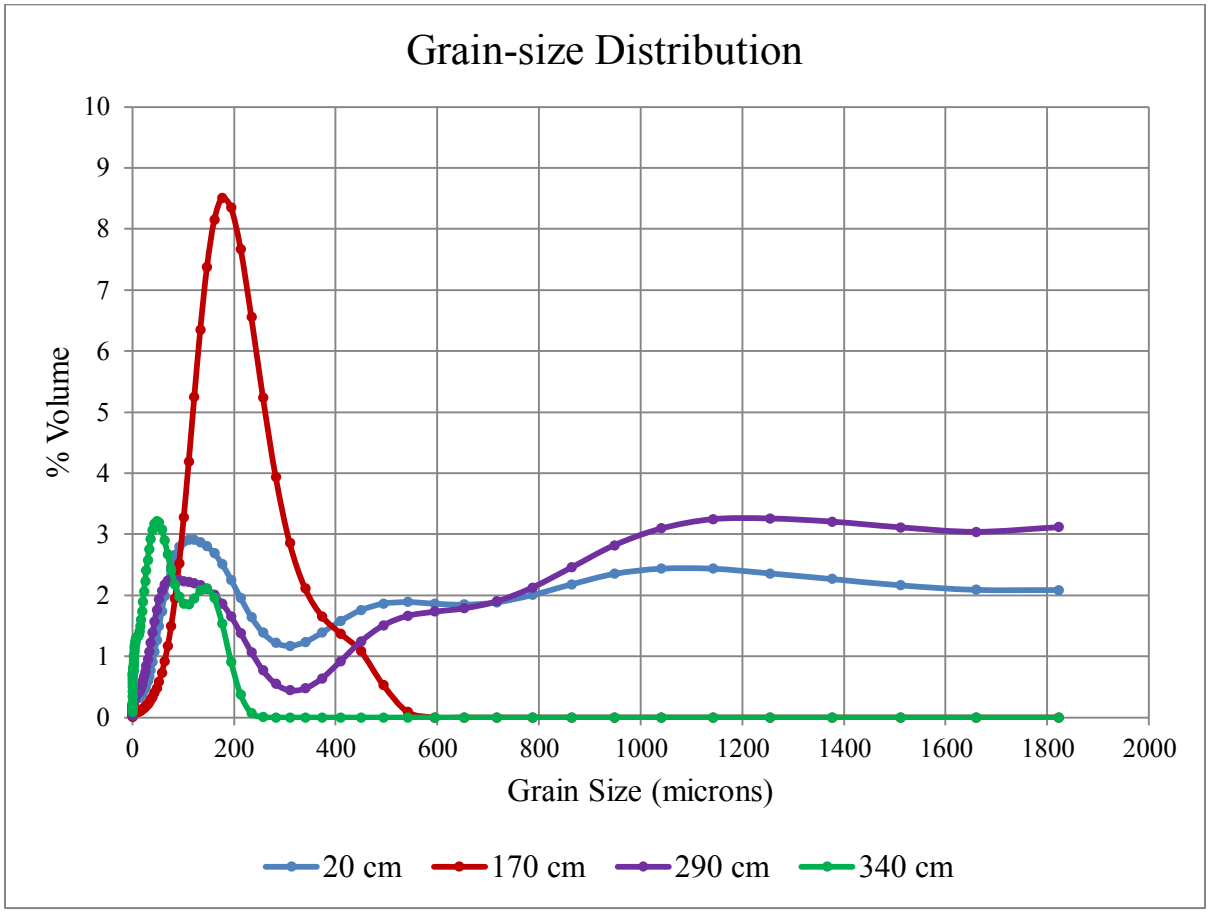

Figure 5.7 Grain size profiles illustrating bimodal distribution at 20, 290, and 340 cm and leptokurtic kurtosis at 170cm

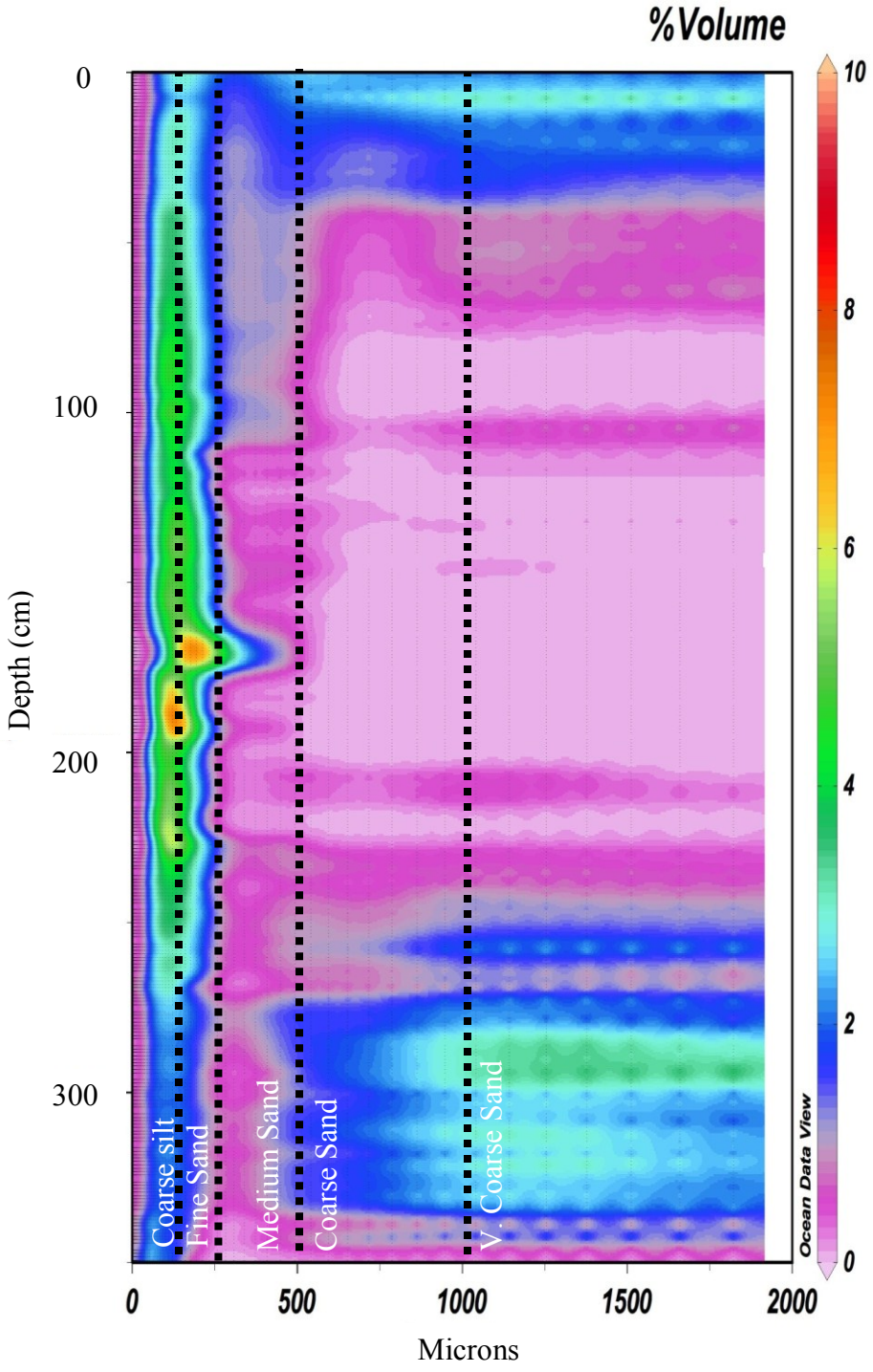

Figure 5.8 Grain-size distribution contour map. Upper and lower core portions demonstrate bimodal distribution of fine and coarse sand. Well-sorted, fine sand anomalies at 170 and 190 cm.

Statistical Analysis

Multivariate cluster analysis using foraminifera genus and abundance was used to generate five assemblage zones. Figure 5.9 identifies these boundaries. Image A displays these zones on the cluster diagram. Image B uses the statistically established zones and arranges them by depth. The upper and lower zones show a high level of correlation. The majority of clusters correlate to their overlying and underlying strata. This expected pattern confirms minimal mixing occurred during core collection.

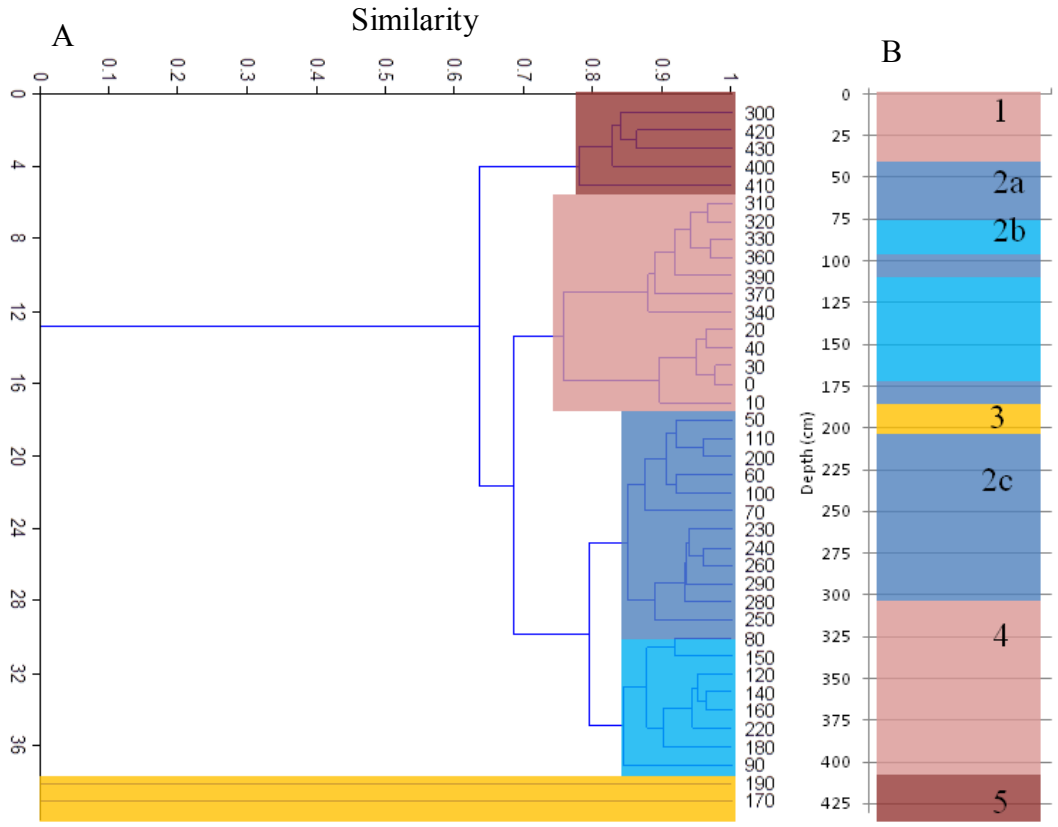

Figure 5.9 Multivariate cluster analyses from foraminifera genus and depth in cm. (A) Five statistically derived zones. (B) Five zones arranged with depth conveying their chronological relationship.

Radiocarbon Dates

Radiocarbon dates from 50, 160, 200, 260, and 400 cm depths yielded calibrated mean ages of 1127, 1792, 2194, 2479, and 3654 yr BP, respectively. Figure 5.10 provides the age ranges plotted against core depth and the decompaction model. Calibrated ages are rounded to the nearest decade. The top one meter of the core accommodates the majority of the core compaction. Radiocarbon dates suggest even a smaller interval, possibly only the top 50 cm, accounts for compaction. Table 5.1 presents Lawrence Livermore National Laboratory Center for Accelerator Mass Spectrometry ^{14}C data table.

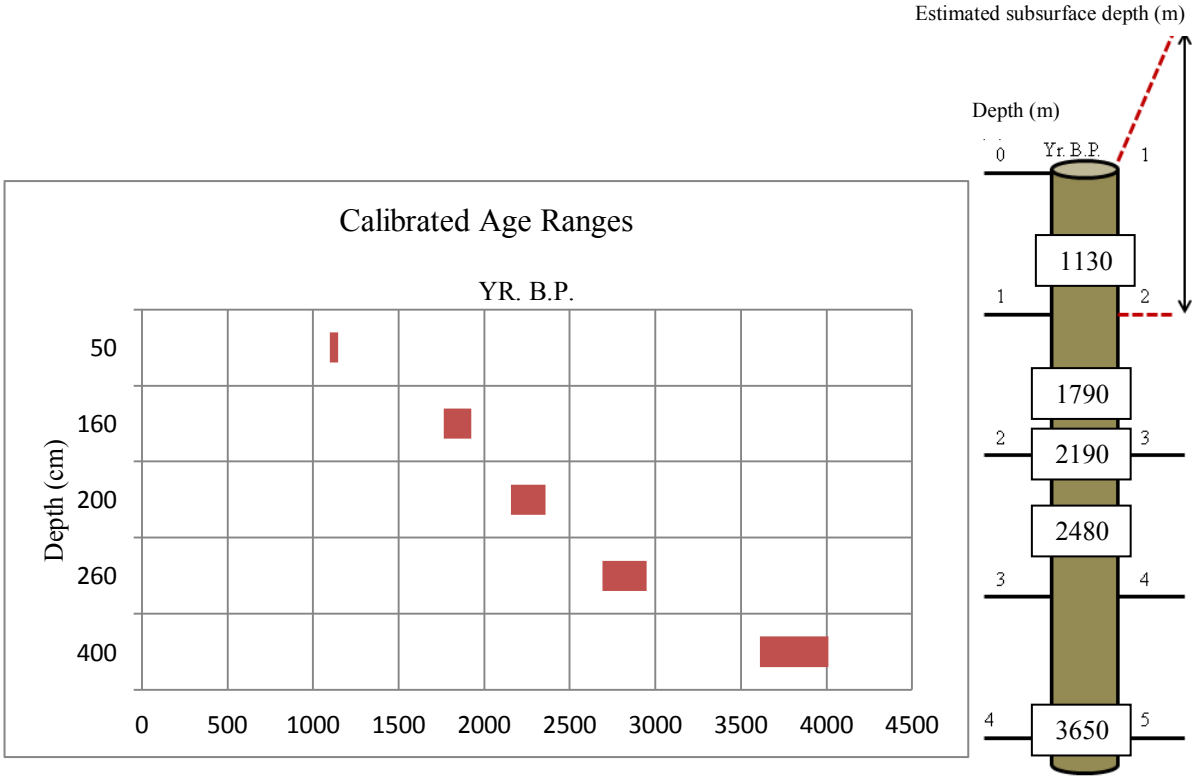

Figure 5.10 Calibrated age ranges plotted against core depth (left). Decompaction model with calibrated ages rounded to the nearest decade (right).

Table 5.1

Radiocarbon dates for samples 50, 160, 200, 260, and 400 cm.

CAMS #	Sample Name	Other ID	$d^{13}C$	Fraction Modern	±	$D^{14}C$	±	^{14}C age	±
154828	50-51	N98846	0	0.8235	0.0027	-176.5	2.7	1560	30
154829	160-161	N98847	0	0.7602	0.0027	-239.8	2.7	2200	30
154830	200-201	N98848	0	0.7277	0.0023	-272.3	2.3	2555	30
154831	260-261	N98849	0	0.7093	0.0025	-290.7	2.5	2760	30
154832	400-401	N98850	0	0.6291	0.0022	-370.9	2.2	3725	30
154833	200-201 DUP	N98851	0	0.7349	0.0023	-265.1	2.3	2475	30

Source: Center for Accelerator Mass Spectrometry at the Lawrence Livermore National Laboratory. Sample CAMS#154833 is a duplicate sample split of the CAMS#154830.

CHAPTER 6

DISCUSSION

Data Synthesis and Interpretation

This study interprets five ecostratigraphic zones from foraminifera assemblages, sediment composition, and grain size analysis. It defines these zones initially using abiotic and biotic proxies separately, and then combines them. Abiotic proxies include grain size, mineral composition, and lithology (Figure 6.1). Biotic proxies incorporate statistical and

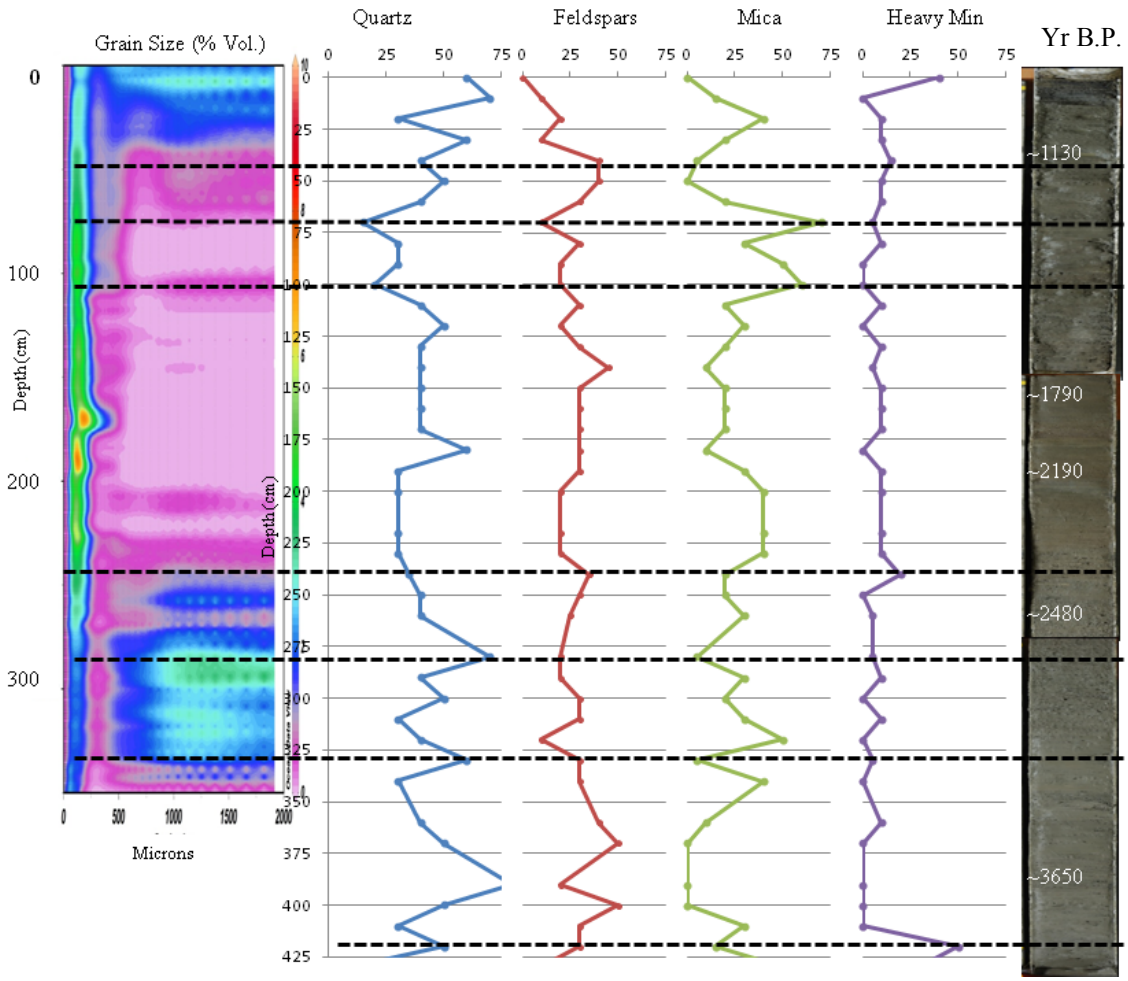

Figure 6.1 Abiotic zones defining ecostratigraphic boundaries. Grain size (left), mineral composition abundance (middle), and radiocarbon dates overlain on lithology (right).

graphical foraminifera assemblages and abundance (Figure 6.2). In some cases, the biological components lag in comparison to the abiotic zones. This represents a delay in the biological response to a change in environment and sediment supply and is apparent in the lower portion of the core. Mineralogical shifts at 420 and 340 cm may correlate to foraminifera changes at 400 and 330 cm, respectively.

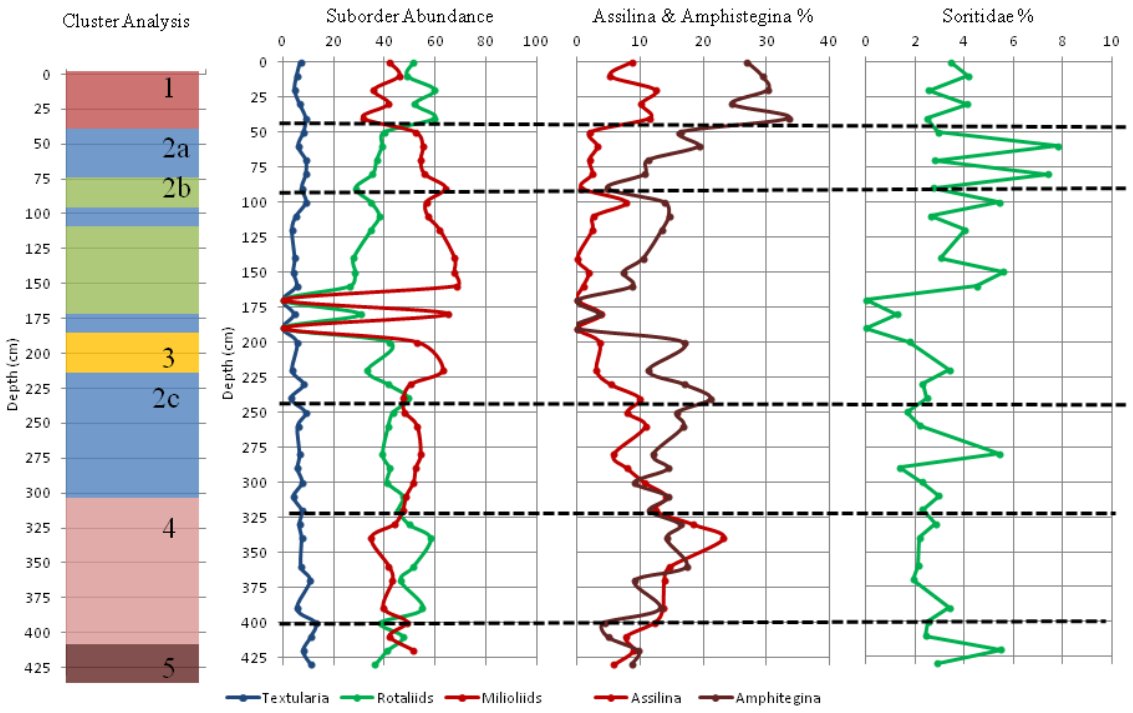

Figure 6.2 Foraminifera fluctuations defining climatic regimes. Multivariate cluster analysis (left). Suborder proportions, *Assilina* & *Amphistegina* percentages, and Soritidae abundance (graphs).

Grain size, suborder proportion, and foraminifera abundance data alternate in concert with each other. These changes represent either high or low energy regimes. Coarse-grained sediment, Rotaliina-dominated assemblages, and foraminifera-rich samples represent the high-energy environments. Oceanographic conditions associated with high energy regimes contain elevated oxygen and other nutrients levels necessary for foraminifera profusion and correspond to enhanced circulation. Atmospheric conditions driving these oceanic changes

are attributed to strong seasonality and large land surface-oceanographic temperature gradients. These temperature gradients increase wind and wave strength. We associate these conditions with arid environments where hot dry land mass temperatures and mild oceanic conditions result in strong circulation patterns.

Conversely, low-energy environments are characterized by fine-grained sediment, Miliolina-dominated assemblages, and foraminifera-poor samples. These data suggest weak circulation. Increased terrestrial runoff resulting in buoyant fresh-water lenses may decrease oceanic ventilation. We attribute these circumstances to enhanced precipitation and frequent seasonal flooding associated with a wetter climate. The flow diagram in Figure 6.3 illustrates this concept.

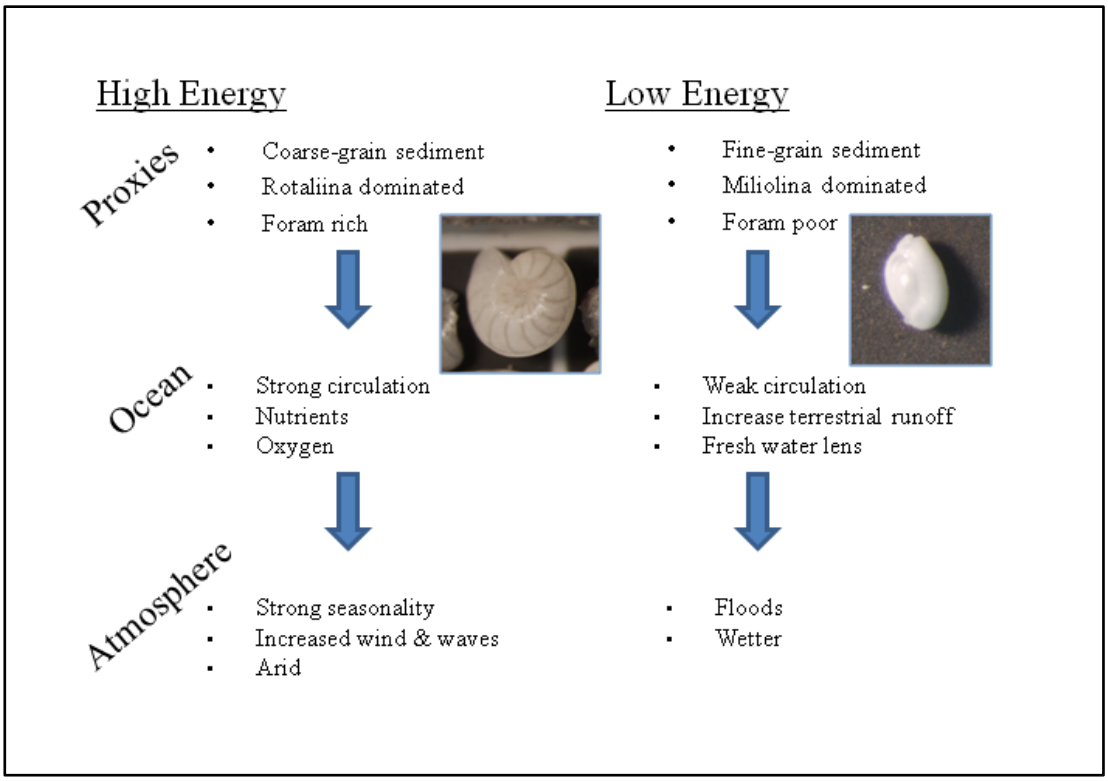

Figure 6.3 Flow diagram illustrating high energy conditions associated with arid environments (left) and low energy conditions associated with wetter climate (right).

The abiotic and biotic proxies are compiled in Figure 6.4. The figure incorporates grain size, suborder proportions of Textulariina, Rotaliina, and Miliolina, foraminifera abundance, and lithology combined with radiocarbon dates to generate a climatic chronology for the Gulf of Aqaba. We interpret five ecostratigraphic zones; two zones representing arid periods, a transitional zone, and wetter period punctuated by two foraminifera-barren horizons.

The core records nearly 1000 years of aridity at depths greater than 300 cm (zone 5). Sedimentation rates derived from radiocarbon dates indicate this period began over 3800 yr BP and continued to ~2900 yr BP. It exhibits coarse-grained sediment, Rotaliina-dominated assemblages, and increasing foraminifera abundance.

The interval from ~2900 and ~2500 yr BP represents a transitional zone from an arid to a less arid climate (zone 4). It displays varying grain size, alternating suborder proportions, and a peak in foraminifera abundance.

A wetter climate likely persisted between ~2500 to ~ 1100 yr BP (zones 2a and 2b). Fine-grained sediment, Miliolina-dominated assemblages, and low foraminifera abundances suggest this period experienced enhanced precipitation and decreased oceanic ventilation.

Two abrupt terrestrial deposits punctuate the core at 170 and 190 cm (zone 3). Radiocarbon dates confine these deposits between ~2200 and 1800 yr BP. These horizons are well-sorted terrestrial deposits that lack marine biota.

An arid climate is reestablished from ~1100 yr BP to present. Again, this is characterized by coarse-grained sediment, Rotaliina-dominated assemblages, and high foraminifera abundances. The arid period of the upper 50 cm in the core exhibits a low sedimentation rate of 0.44 mm/yr (compared to ~1.4 mm/yr for the majority of the core).

Sediment loss, core compaction, or extensive erosion may explain this phenomenon. These factors may also be responsible for lacking signatures of the Medieval Climatic Anomaly, the Little Ice Age, or other modern climate fluctuations in the past ~1130 years.

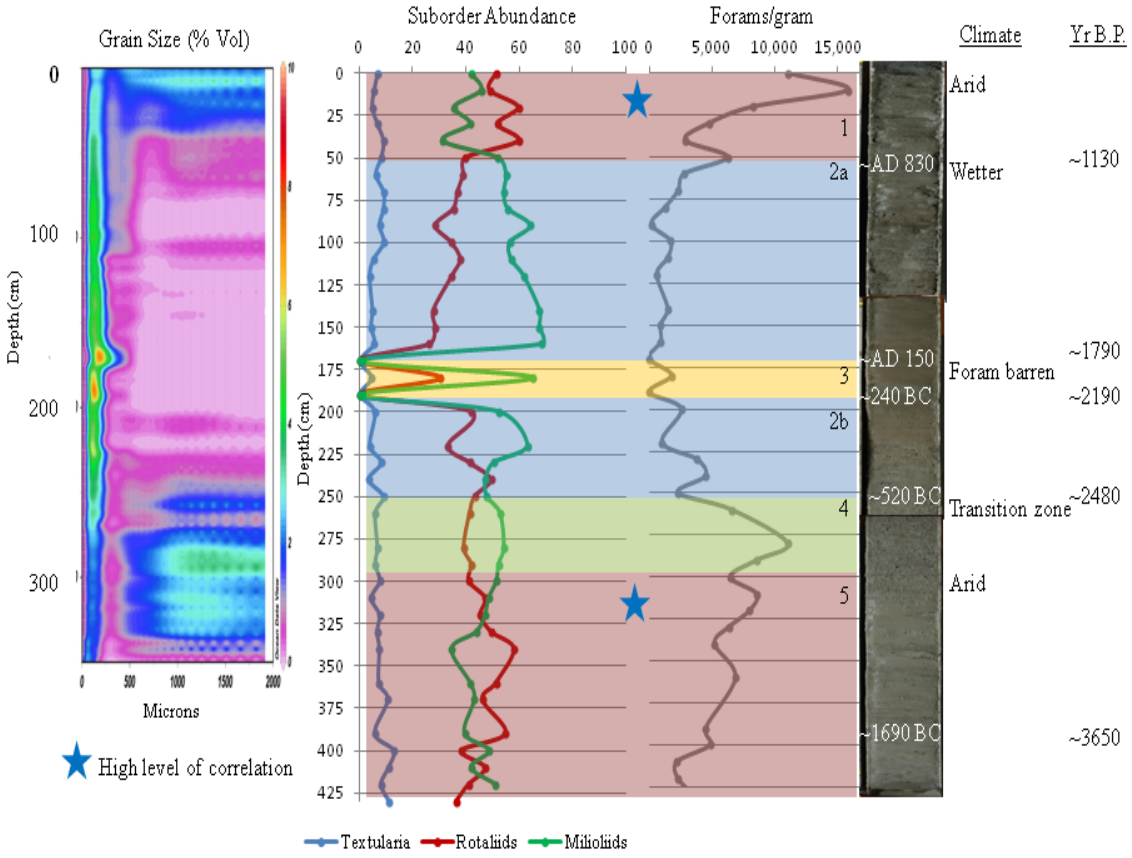

Figure 6.4 Combined representation of abiotic and biotic proxies. Image incorporates grain size (left), suborder proportions and foraminifera abundance (graphs), and core photograph with radiocarbon dates and interpreted climate periods. Red zones represent arid periods, the green zone indicates a transitional period, the blue zone represents a wet period, and the yellow zone signifies the foraminifera-barren horizons. Blue star correlates to high statistical similarity in foraminifera assemblages.

Climate

Modern Climate

Receiving less than 50 mm of annual precipitation, southern Israel and Jordan is defined as a hyperarid desert environment. The coastal cities of Eilat, Israel and Aqaba, Jordan report even less at ca. 30 mm of annual precipitation (World Meteorological Organization, 2011). The majority of this region's precipitation is greatest in the winter months (December-March). Consequently, little to no rainfall occurs during the summer months of June-September. This arid climate is accompanied by hot (95-104° F) summer temperatures and mild (50-70° F) winter temperatures (Israeli Meteorological Service, 2011). Two precipitation systems control the rainfall of southern Israel and Jordan. A cyclonic southward migrating moisture from the eastern Mediterranean and northward migrating Red Sea moisture from an extension of the tropical monsoon system are responsible for precipitation in this region. Monitoring modern (1950-2000) average cyclone tracks and their frequency, Enzel *et al.* (2003) provides evidence for a one degree latitudinal shift south in the Mediterranean moisture belt during the wettest winters studied. This implies that southward migrating Mediterranean cyclone tracks govern the modern moisture delivery at least in the area of the Dead Sea studied by Enzel *et al.* (2003).

Paleoclimate

Low precipitation and high evaporation characterizes the study area as an arid region. Such areas are capable of documenting small-scale environmental changes through preservation of the geologic and fossil record. Marine cores provide a unique look at changes in biology, sediment input, water chemistry including sea surface temperatures, sea surface salinity, and water column stratification. Several studies have identified Holocene

climatological shifts based on these parameters. Wright *et al.* (1993) synthesized an extensive network of data to reconstruct Middle Eastern early-Holocene climate on a continental spatial and temporal scale. Incorporating data from the Near East and southwest Asia, their research examined lake-level and vegetation records since the last glacial maximum, with an emphasis on 9000 to 6000 yr BP. The results of their work reveal the importance of studying the marginal Eastern Mediterranean climate zone. Multi-proxy evidence indicates a much wetter climate on the Saudi Arabian Peninsula (south of 30 degrees north latitude) from about 9000 to 6000 yr BP. North of roughly 35 degrees north latitude, the evidences points to slightly drier conditions than today. The Eastern Mediterranean region, however, appears to be a crucial transition zone for these observed changes.

Mayewski *et al.* (2004) reconstruct mid- to late-Holocene fluctuations by analyzing published global climate variability that incorporates multiproxy investigations from all continents (with the exception of Australia). They identify six rapid climate change events, four dating to mid- and late-Holocene. A collection of studies document a rapid shift to aridity circa 4200 yr BP which likely plays a roll in the collapse at the time of the Akkadian empire (e.g., Weiss et al., 1993; Almogi-Labin *et al.,* 1998; Cullen *et al.,* 2000; deMenocal, 2001; and Frumpkin, 2009). This event is identified through geochemical analysis of aeolian Mesopotamian sediments deposited in the Gulf of Oman (Cullen *et al.,* 2000), enriched ^{13}C and ^{15}N tree ring isotopes near the Dead Sea (Frumpkin, 2009), and rapid hydrological anomalies in Africa (Gasse, 2000). This study likely documents this aridification event prior to an abrupt increase in moisture ~2500 yr BP.

Using total organic carbon, foraminifera and pteropod species assemblages, and radiocarbon dates from deep water sediment of the northern Red Sea, Edelman-Furstenberg *et al.* (2009) documented five ecostratigraphic zones associated with periodic climatic shifts during the past ~6,000 yr BP. They suggest that low oxygen levels at the oxygen minimum zone (OMZ) were coupled with higher nutrients levels from 5700 to ~4400 yr BP indicating a wetter climate. The period from 4400 to ~3300 yr BP was relatively more arid, followed by a less arid phase from 3300 to ~2000 yr BP. They suggest from 2000 to ~700 yr BP the climate returned to more aridity. The final shift existed from 700 yr B.P. to present and is marked by less mixing of the water column suggesting a less arid dominated climate. The duration of these humid-arid cycles documented in the Red Sea last about 1200-1400 years since the early Holocene (Edelman-Furstenberg *et al.*, 2009).

The shift to a more arid period at ~4400 to 3300 yr BP noted by Edelman-Ferstenberg *et al.*, (2009) corresponds to a dry event identified by Arz *et al.* (2006) at circa 4200 yr BP. Gravity cores from the Shaban Deep in the northern Red Sea reveal a marked transition to aridity. Stable oxygen isotopes from surface dwelling (planktic) foraminifera and laminated anoxic brines document this event. At ~4200 yr BP, foraminifera isotope data reveal positive salinity anomalies implying an increase in SST and more arid conditions. The absence of laminated brines suggests a major evaporation event and subsequent enhanced deep water ventilation (Arz *et al.,* 2006).

Allison and Niemi (2010) present paleoclimate data from analysis of onshore cores and archaeological evidence from the coastal zone of Aqaba, Jordan. These cores reveal a basal marine unit overlain by regressional sequences of embayment lagoonal sediments. Supported by data from archaeological excavations of a late Chalcolithic site containing

water diversions and remains of extensive agricultural and husbandry (Khalil and Schmidt, 2009), Allison and Niemi (2010) recognize possible wetter-than-present conditions approximately 6000 to 5500 yr BP. By ~2800 yr BP, they conclude that the Gulf of Aqaba shoreline prograded seaward approximately 400 m, leaving the land dominated by aeolian and fluvial processes.

Possible Mechanisms

The driving force behind observed climatic changes is a subject of debate. Arz *et al.* (2003) proposes early to mid-Holocene climatic fluctuations are associated with a cyclical southward extension and retreat of the Mediterranean climate zone. Based on marine cores from the northern Red Sea, Arz *et al.* (2003) suggest that the Afro-Asian monsoonal rains (to the south) did not extend northward into the Gulf of Aqaba during this time. Rather, a southward extension of Mediterranean moisture sources is responsible for the humid periods documented in the northern Red Sea and likely also, the Gulf of Aqaba. Figure 6.5 represents the southward trough in summer Intertropical Convergence Zone (ITCZ) and the suggested path of a Mediterranean moisture source.

Conversely, Moustafa *et al.* (2000) suggest a northward migration of the African monsoon is responsible for the humid periods during the mid-Holocene. Using stable isotope records of corals near the Gulf of Aqaba, they conclude that summer monsoonal rains extended northward to the Northern Red Sea resulting in the more humid conditions. This is recorded by slowed growth rates (~4 mm/year) in mid-Holocene corals compared to their modern analog (~7.5 mm/year). They attribute this slowed growth rate to increased terrestrial sediment input caused by increased water runoff between 5750 to 4450 ^{14}C yr BP (not calibrated for reservoir effect).

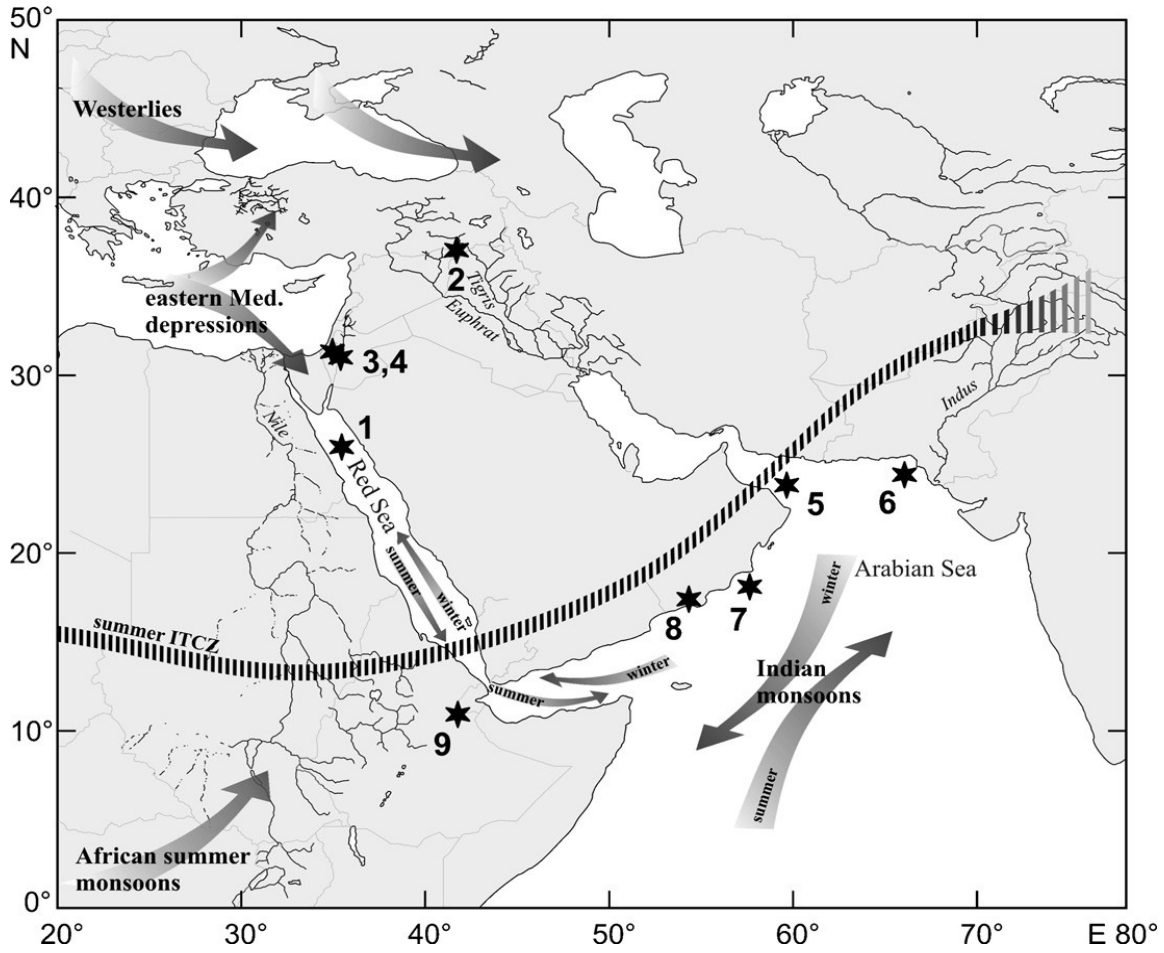

Figure 6.5 Proposed climatic patterns that influence the Gulf of Aqaba. Numbers represent previous studies. 1, Gravity cores (Arz *et al.,* 2006); 2, excavation site at Tell Leilan, northeast Syria (Weiss *et al.,* 1993); 3, Soreq Cave, Israel (e.g., Bar-Matthews *et al.,* 2000); 4, Dead Sea (Enzel *et al*., 2003); 5, Gulf of Oman (Cullen and deMenocal*,* 2000); 6, Indus delta (Staubwasser *et al.,* 2003); 7, northwestern Arabian Sea (Gupta *et al.,* 2003); 8, Qunf Cave, southern Oman (Fleitmann *et al.,* 2003); 9, northeast African Lakes Abhe and Ziway-Shala (Gasse, 2000). (After Arz *et al.,* 2006).

Fleitmann *et al.* (2007) propose that the seasonal ITCZ is responsible for the above climate variations by seasonal southward migration. Figure 6.6 is a generalized diagram of seasonal ITCZ. They suggest that a shortening of the summer monsoonal season is the response of this southward migration. Based on stalagmites from Oman and Yemen, they argue that the Indian Summer Monsoon (ISM) weakened due to the decreased orbital-induced solar insolation. Although, fluctuations exist throughout the Holocene, they claim

that abrupt monsoon events are superimposed on a long-term trend of decreasing monsoon precipitation.

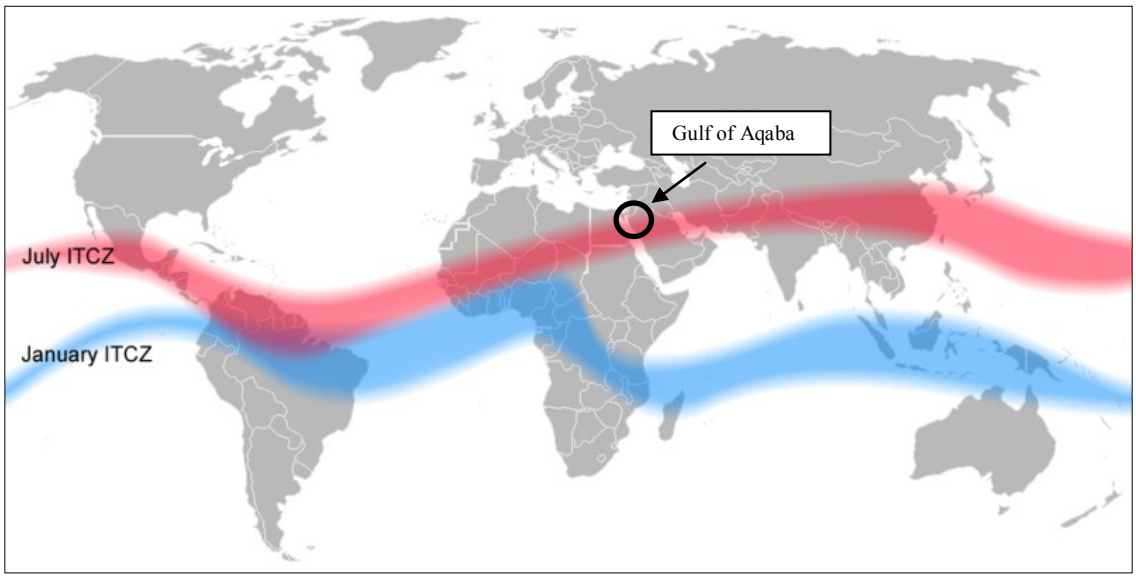

Figure 6.6 Image showing the approximate location of the summer and winter ITCZ in relation to the Gulf of Aqaba (Sedimentologist, 2011).

Mechanisms that dictate early-Holocene climate variability may, to a lesser extent, also drive late-Holocene changes. Because climatic boundary shifts are in part driven by the sun's zenith, it is reasonable to conclude climatic fluctuations in the geologic record are seasonal as well as on a decade-, century-, or millennium-scale. Global Holocene climate variability operates on documented and widely accepted intervals of ~2800-2000 and ~1500 cycles (Allen and Anderson, 1993; Bond *et al.,* 1997; Bray, 1971, 1972; Dansgaard *et al*., 1971; Denton and Karle´n, 1973; Johnsen *et al*., 1972; Mayewski *et al*., 1997; Naidu and Malmgren, 1996; Noren, 2002; O'Brien *et al*., 1995; Pisias *et al*., 1973; Sonett and Finney, 1990; Stager *et al*., 1997; Stuiver and Braziunas, 1989,1993). Southern regions of the Near East (below 30° N) have documented high lake levels between 9,000 to 6,000 yr BP from Saudi Arabia across the Red Sea into Africa and as far west as Ethiopia and the Saharan

Desert (Wright *et al.*, 1993). This east-west trend of enhanced precipitation may have extended throughout the Mediterranean. More specifically, palynologic records of deciduous oak trees from Crete may indicate amplified summer precipitation during the early Holocene (Wright *et al.*, 1993). Palynologic and lake level studies of 9000 yr B.P. by Wright *et al.* (1993) suggest that precessional (~26,000 year) cycles caused summer southwest Asian temperatures to increase 2-3° C and winter temperatures to drop about 1.5° C from modern values. Continental surface pressure gradients of large landmasses amplify the effects of cyclical solar insolation. Enhanced solar radiation 9000 yr B.P. likely drew in Indian Ocean moisture landward, thus increasing annual precipitation. Mayewski *et al.,* (2004) suggest these solar variability cycles documented throughout the Quaternary superimposed on long-term insolation changes dictate late-Holocene fluctuations.

Anthropogenic Influences

Humans and their ability to alter their environment play a critical role in paleoenvironment reconstruction and sediment supply into the Gulf of Aqaba. The earliest evidence for human occupancy dates to the Late Chalcolithic period (4^{th}-5^{th} millennia B.C.). This is apparent from tells excavated on alluvial fans of the Wadi Yutim north of present day Aqaba (Khalil and Schmidt, 2009). The sedentary lifestyle of Aqaba's early inhabitants necessitated water drainage management, consequently altering the region's hydrogeological processes (Niemi and Smith, 1999). The Iron-Hellenistic period (8^{th}-4^{th} centuries B.C.) is documented at Tell el-Kheleifeh along the present day Israeli-Jordanian border (Pratico, 1993). Settlement patterns of the Late Roman-Byzantine period (1^{st} century B.C.-7^{th} century A.D.) appear closer to the present day shoreline and extend under the modern city of Aqaba (Allison and Niemi, 2010). Continuous occupation persisted since the 7^{th} century A.D. from

Early Islamic period (7th-12th century; Whitcomb, 1994) to the Mamluk (13th-16th century), followed by the Ottoman empire (16th-20th century) (De Meulemeester and Al-Shqour, 2008).

Managing drainages and redirecting seasonal flash flood waters have played a significant roll among ancient settlements. These processes, coupled with climatic shifts govern sediment transport and deposition. Allison and Niemi (2010) offer archaeological and sedimentological evidence of a prograding shoreline that persisted until the 8th century B.C. and development of the coastal plain site of Tell el-Kheleifeh. The ensuing landscape became fluvial and aeolian controlled. They suggest the settlement patterns of the region's early inhabitants from alluvial fans, to the central valley, and then southeastward may have been in response to redirect or avoid flash floods from the Wadi Yutim. The effects settlement mobilization has on sediment supply are far-reaching and difficult to assess. Water diversion engineering techniques from the Chalcolithic to present may have played a central role in sedimentation processes in the Gulf of Aqaba.

Foraminifera Barren Zone

Possible Origin

The lack of foraminifera and marine microfossils at 170 and 190 cm in the studied core distinguish them from the remaining samples. Figure 6.7 illustrates the well-sorted, subangular quartz and feldspar dominated sediments. The lack of foraminifera and other marine biota suggests significant terrestrial input. A torrential flood event transporting and depositing terrestrial sediment on the shelf or either storm or tsunami waves drawing aeolian and other terrestrial sediments seaward are plausible mechanisms to account for this anomaly.

High frequency storm events in the Gulf of Aqaba have low preservation potential. Storm deposits that survive waning flow, which often erases structures created by storm-flow velocity, rarely survive bioturbation (Boggs, 2001 p. 387). This leaves a less than distinguishable signature in offshore stratigraphy.

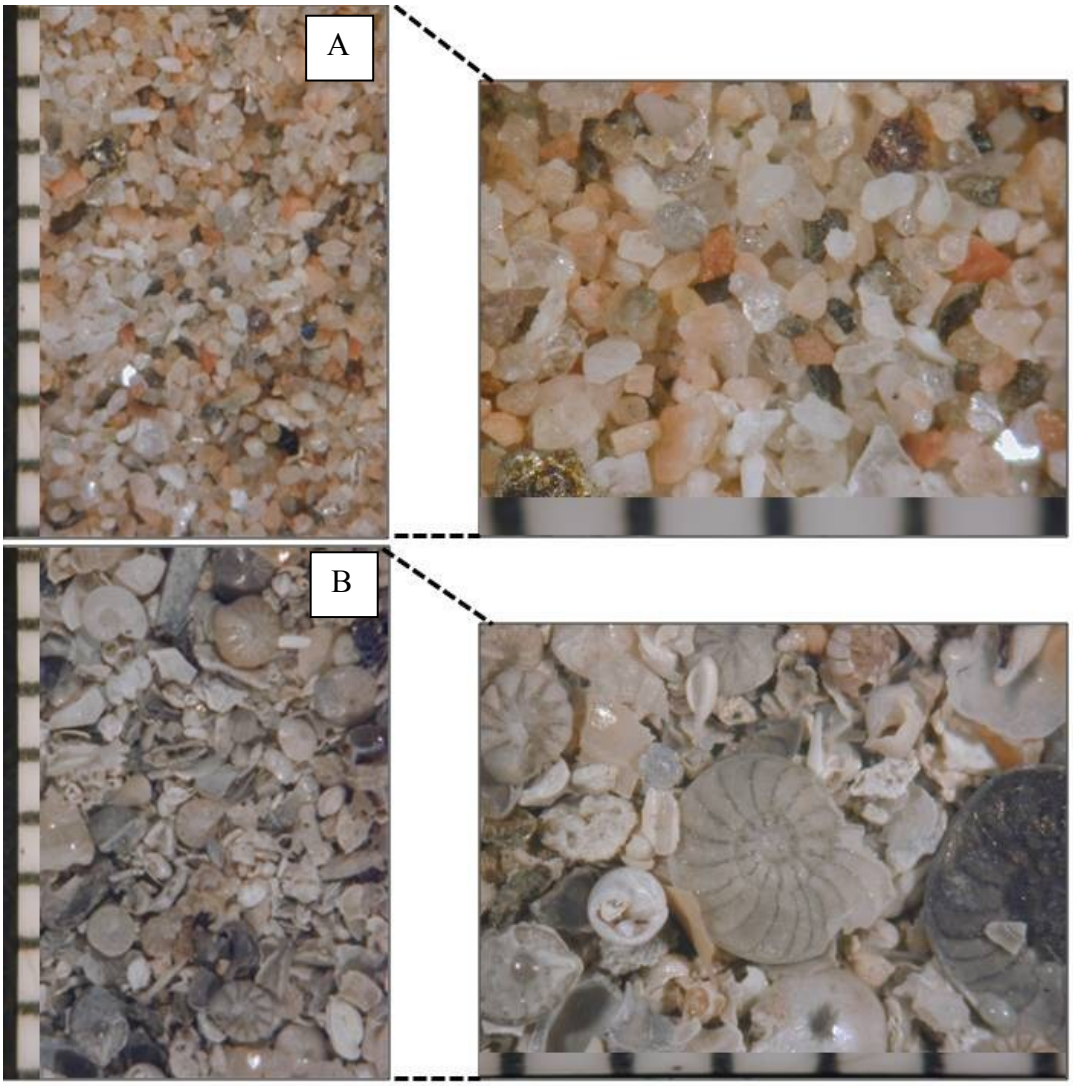

Figure 6.7 Photomicrographic images comparing foraminiferan-barren zone at 170 cm (A) with foraminiferan-rich sediment of 390 cm (B). Scale is in mm.

Flash Floods

Torrential flash floods frequently deposit terrestrial sediment onto the shelf. Figure 6.8 illustrates the effects of modern flooding in the Gulf of Aqaba. A clear distinction is visible between the turbid, terrestrial suspension load floodwater from the surrounding clear gulf water. This demonstrates the powerful impact torrential floods can have on sediment input in the gulf. Given the wave-dominated shoreline of the northern gulf and strong currents, most of the suspended load is likely carried farther offshore. Seasonal flooding alone is unlikely to account for the anomalous foraminifera-barren zones. Seasonal floods of this magnitude do not punctuate the sedimentological record as frequently as expected. Therefore, floods powerful enough to produce these terrestrial deposits require a temporally unique mechanism, such as a dam failure. Parker (1997: 22) reports accounts from 19th and early 20th century western travelers of a crude masonry dam in antiquity built across the mouth of the Wadi Yutim canyon. Presently, the dam is not in place and documentation of is existence is limited. Given the lack of information regarding the structure and the age of its collapse, it is difficult to explore dam failure as a possibility. Moreover, mapping the lateral extent of this shelf deposit and understanding the drainage patterns into the gulf is crucial when investigating fluvial origins as a possible mechanism.

Figure 6.8 Modern flood event and its impact on sediment supply in the Gulf of Aqaba. (A) January 2010 (Hartman, workshop lecture, 2010). (B) May 2006 (Goodman, workshop lecture, 2010 after Arava Drainage Authority).

Tsunamis

A tsunami wave and deposit may provide another explanation for the foraminifera-barren zone. Because this region is earthquake prone, it is reasonable to assume that earthquake triggered tsunamis have affected this area in the past. Written accounts of tsunamis are well documented along the Levant coast on the Eastern Mediterranean. However, because the coast along the Gulf of Aqaba was less populated than those on the Mediterranean over the past 4,000 years, written records of tsunami events are sparse. Nonetheless, earthquake catalogs document at least one account of a potential large sea wave in the Gulf of Aqaba associated with an earthquake in AD 1068. The late 12th century author, Ibn al-Jauzi, states that Aila (the present day city Aqaba, Jordan) was completely destroyed, leaving only 12 surviving inhabitants and mentions "the withdrawal and return of the sea" (Ambraseys, 2009, p. 274). Archaeological evidence of rebuilt structures during the time supports the destruction of Aila in A.D. 1068 (Whitcomb, 1994). A decrease in bioclastic material and normal grain size distribution at ~40 cm depth in the core may represent a poorly preserved signature of this event.

As written records decrease with older tsunamigenic earthquakes, the geologic record and other proxies provide accounts of catastrophic events. Studies of onshore tsunami deposits prevail, but identifying these deposits offshore is an emerging field. The foremost question regarding offshore tsunami deposits is how to distinguish them from storm or flood deposits. Reinhardt *et al*. (2006) identifies large tsunami deposits from offshore cores in the King Herod's ancient harbor in Caesarea. A thickly stratified shell layer characterizes the deposits coupled with a wider grain size distribution than a storm deposit.

Goodman *et al.* (2009) examines grain size distribution as a primary tsunami deposit proxy offshore at Caesarea. They distinguish tsunami deposits based on wide particle-size distributions. They interpret three distinguishable horizons from contour map particle-size distribution from Caesarea. Those horizons are 1) normal marine conditions as narrow grain size distribution on fine fraction grains, 2) relatively wider grain size distribution representing storm horizons, and 3) very wide grain size distribution in tsunami deposits containing coarse-grained material. This interpretation however, does not correspond to particle distribution found in the possible tsunami horizon in the Gulf of Aqaba. Perhaps conditions controlling sediment deposition or marine dissimilarities between the Mediterranean and the Gulf of Aqaba prevent comparative analysis of this nature.

Fluvial and aeolian processes transporting granitic sediment presently controls deposition into the Gulf of Aqaba (Allison and Niemi, 2010). Due to the close granitic source proximity, fluvial sediments transported through the Wadi Yutim drainage display high angularity, low sphericity, and a poorly sorted grain size distribution. The well-sorted angular texture of the foraminifera-barren horizons suggest a first generation sediment deposit. A likely source of the fine-grained sand is either beach sand or sand dunes found inland of the beach rather than a direct fluvial input. Beach and aeolian sands are both well-sorted. Additionally, these layers are unique in that a foraminifera horizon is present between the two barren zones. The foraminifera-present sample at 180 cm suggests multiple events. It is possible that this study documents at two wave events (at 170 and 190 cm).

It is important to recognize that all earthquakes are not tsunamigenic nor do all tsunamis occur in response to earthquakes. Volcanoes, extra-terrestrial impacts, sub-aqueous slumping, and mass wasting are recognized tsunamigenic mechanisms. Differentiating the

mechanism based solely on the deposit is rarely unequivocal. However, tsunamis can occur as an indirect response to seismic activity. In the Gulf of Aqaba, Tibor *et al.* (2010) described large detached blocks and collapsed walls in submarine canyons from multibeam sonar mapping of the seafloor. They suggest these deformation features may be triggered by seismic activity. Even though this region is earthquake prone, the lack of tsunami deposits in the marine record suggests earthquakes in the Gulf of Aqaba are typically not tsunamigenic. If a unique seismically-triggered tsunamigenic mass wasting event were responsible for the foraminiferan barren horizons, this might explain the paucity of such tsunamis deposits in the offshore record.

Because investigations of offshore tsunami deposits are sparse, onshore studies provide a general analog. Peters and Jaffe (2010) compiled a series of onshore investigations in order to develop criteria for identifying tsunami deposits in the geologic record. This study incorporates the parameters deposit thickness, grain size distribution, and kurtosis drawn from their compilation. Onshore tsunami deposits are typically <20 cm thick, but often to do exceed 10 cm. Grain size distributions are less diagnostic and range from clay to boulders. However, sand-size fractions tend to dominate the sediment, yet this parameter remains largely a function of source material. Grain size statistics potentially provide a reliable means for differentiation, yet until a uniform protocol in tsunami deposit sampling is established, this criterion varies largely among studies. The statistical parameter kurtosis again varies, yet similar patterns persist. Deposits from Yale, Sri Lanka and the majority of sites from Phuket, Thailand display leptokurtic to very leptokurtic kurtosis (Peters and Jaffe, 2010).

The foraminiferan-barren horizons in the Gulf of Aqaba display features comparable to onshore tsunami deposits. Thickness criteria is within the boundaries established by (Peters and Jaffe, 2010) of less than 20 cm thick. The exact thickness is unknown due to the 10 cm sampling resolution. However, grain size anomalies suggest 5 and 10 cm thickness for 170 and 190 cm depths, respectively. Source material is likely aeolian sands drawn seaward with the retreat of the tsunami and its subsequent wave events. The unimodal particle-size distribution exhibits leptokurtic kurtosis implying sand finer then modern beach deposits suggesting backshore sand dunes as the most likely single source of sediment supply. An aeolian supply also indicates run-up height several meters above sea level reaching the sand dune fields.

Correlation to Seismic Stratigraphy

Identifying and dating seismic reflectors generated from GAE seismic data was a primary goal and influenced selection of the core location. The target represents the boundary between previously recognized seismic units U8 and U9 (Hartman, 2011). From the seismic profile, a two-way travel time of 4 ms and a velocity range between 1.53 and 2 m/ms revealed a target depth between ~3 and ~4 m (Equation 2). Due to coring compaction accounted for primarily in the top meter (first 50 cm of the core is equivalent to 100 cm of sediment), the presumed U8-U9 boundary should lie approximately at 200 to 300 cm. As discussed above, this may correlate with the foraminifera-barren zones of 170 and 190 m.

Equation 2. Depth (m) = (TWTT (ms) * velocitym/ms)/2

Where TWTT is the two way travel time = between 3.06 and 4 m and 4 second TWTT corresponds to a depth of 3.06 to 4 m.

Hartman (2011) describes the expected lithology of U8 and U9 based on seismic reflection characteristics. U8 displayed low-amplitude, sub-horizontal reflections characteristic of chaotic heterogenetic strata. This unit thins seaward terminating at ~30 m. These data suggest U8 is a heterogenic unit deposited in a high-energy regime. The overlying U9 is continuously present throughout the shelf capping all other units and does not exceed 5 m. Figure 6.9 A and B are seismic profiles of the described units with the approximate location of MG10H-02.

The U8/U9 boundary is associated with a shallow (< 30 m) relict fringing reef, labeled R6.2 (Figure 6.9). The reef extends approximately one kilometer subparallel to the present shoreline and is ~50 m wide. The northwest portion of the reef is exposed at the seafloor surface off the city of Eilat, while the greater part is buried by U9 to the east.

Reef development and termination are a response to changing environmental conditions and sediment supply in the Gulf of Aqaba. The abrupt terrestrial input events at 170 and 190 cm documented in this study may have initially weakened the fringing reef. Additional changes in sediment input through drainage modification and coastal human occupancy may also be responsible for choking this reef system.

The age of the U8/U9 boundary, if it correlates to the foraminiferan barren zone, is bracketed by the radiocarbon dates of the sediment below and above these horizons at core depths of 200 cm and 160 cm, respectively, or approximately between ~2200 and ~1800 yr BP. This age data correlates well with a sediment-buried reef along the Eilat coast that dates to 2400 yr BP (Skaked *et al*., 2004). Shaked *et al*. (2004) attribute the burial of the reef to a large earthquake that resulted in 0.6 m localized subsidence relating to a down-faulting event. The buried reef remained in growth position and displayed pristine preservation suggesting

rapid burial by a thick sequence of siliciclastic sediments. These overlying sediments do not resemble local fluvial sources in lithic composition, thus discrediting flash-flood origins. Rather, sedimentary structures and marine bioclasts suggest sediment transportation and deposition by sea waves. The abrupt burial suggests a large earthquake accompanied by a tsunami wave is likely responsible for the demise of the reef.

It is possible, however, that the U8/U9 boundary is as deep at 4 m. Depending on the amount and manner of core compaction, the boundary could lie near 3 m represented by the abrupt change in particle size. Or, it may lie much deeper and the full transition is not recorded in the core. Processing grain size between 350 to 430 cm of this core and analyzing proxies in additional cores is necessary before unequivocal interpretation of the boundary is possible. Nonetheless, the foraminifera-barren horizons remain a reasonable interpretation for the U8/U9 boundary.

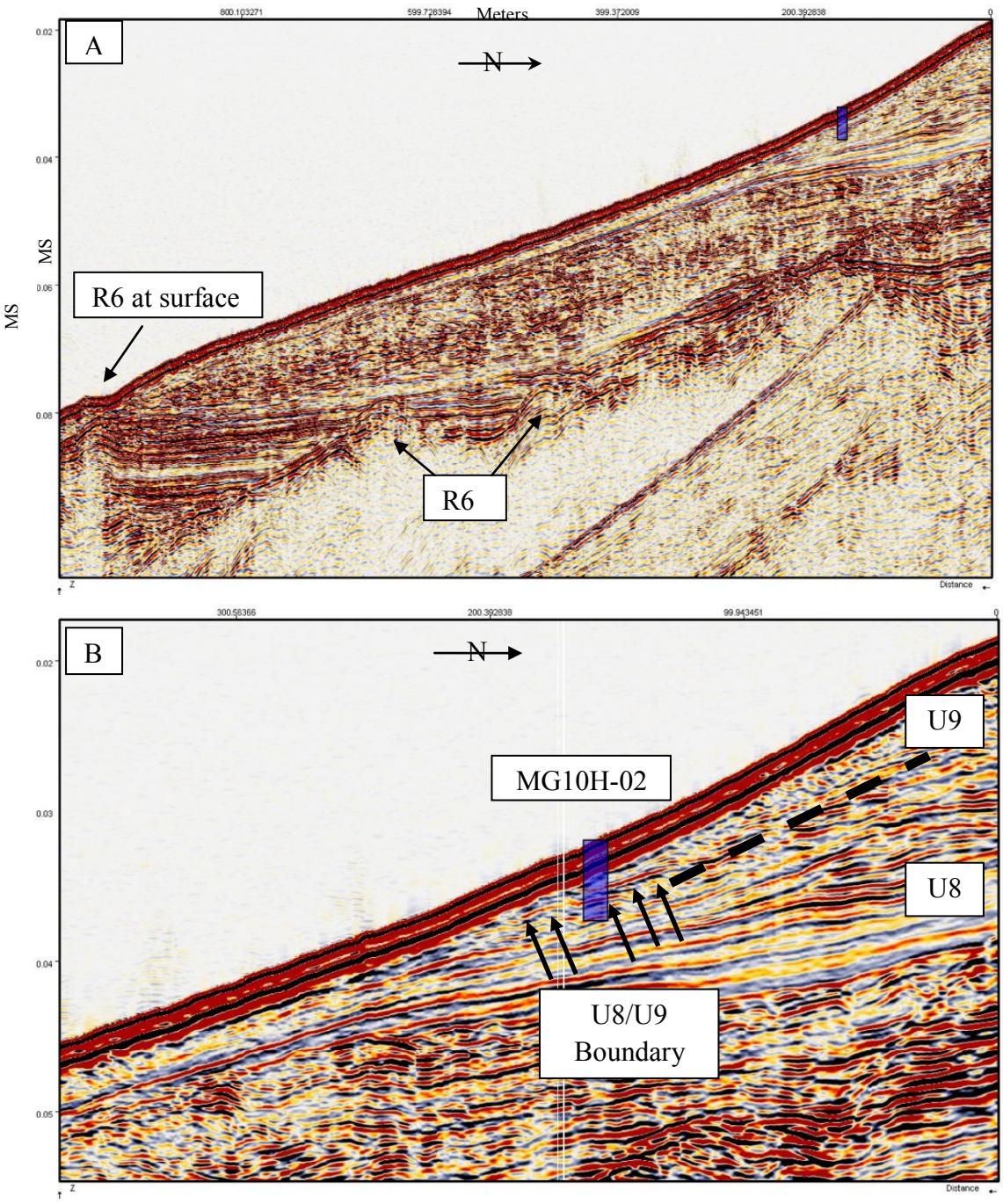

Figure 6.9 Seismic profiles with core location plotted in blue. (A) Buried relict reef. (B) Higher resolution than A, note core may penetrate U8/U9 boundary (After Hartman, 2011).

CHAPTER 7

CONCLUSION

Foraminifera, grain size, lithological analyses, and sediment characterization, from a 4.3 m marine core collected from 25 m water depth of the Northern Gulf of Aqaba documents late-Holocene climatic fluctuations, two foraminifera-barren horizons, and possible correlation to a subsurface seismic boundary associated with reef mortality and burial.

Multiproxy analyses record coarse-grained sediment, Rotaliina-dominated assemblages, containing high foraminifera abundance, and are interpreted as periods of aridity from ~3900 to ~2900 and ~1130 yr BP to present. Aridity is inferred from large land surface-ocean temperature gradients inducing strong wind and wave action leading to a high energy shelf environment. Fluctuating grain-size distribution, alternating Rotaliina- and Miliolina-dominated assemblages, and a foraminifera abundance peak indicate a transitional period from an arid to less arid climate between ~2900 to ~2500 yr BP. An abrupt decrease in particle size, Miliolina proportions, and foraminifera abundance mark a climatic shift ~2500 yr BP. This is followed by approximately 1400 years of increased runoff from precipitation in the northern gulf watershed between ~2500 to ~1100 yr BP. Fine-grain sediment, Miliolina-dominated assemblages, and low foraminifera abundance characterize this as a low energy shelf environment. We associate low energy offshore environments with wetter climatic periods in response to weak circulation patterns restricted by buoyant fresh water input from enhanced terrestrial runoff.

Punctuating the wetter period are two foraminifera-barren zones. Dating between ~2200 and ~1800 yr BP, these horizons lack marine microfossils and correspond to grain size

anomalies at that depth. The deposits are quartz-dominated, leptokurtic, normally distributed fine-grained sands. The lack of marine biota and the well-sorted particle size suggest terrestrial backbeach sand origins, possible aeolian sand. These deposits may signify a dam failure in the Wadi Yutim of the Jordanian mountains that possibly produced a unique flood event. Alternatively, these deposits represent a tsunamigenic earthquake or tsunamigenic mass wasting event. The distinct terrestrial input indicates an abrupt event showing no evidence of bioturbation. A tsunami wave drawing well sorted, first generation granitic aeolian sands onto the shelf is a plausible explanations for this anomaly.

The depth of the foraminifera-barren strata corresponds approximately to a seismic reflector separating inferred stratigraphic units U8 and U9. The rapid terrestrial input event may have initially weakened the reef system. This event coupled with climatic and anthropogenic factors may be responsible for the coral reef termination and partial burial by the overlying U9 deposits.

APPENDIX A

Foraminifera Spreadsheet

MG10H02	**Rotaliina**							
Depth	Amphistegina	%	Assilina	%	Ammonia	%	Cibicides refulgens	%
0-1	94	27	30	9	13	4	6	2
10-11	113	29	20	5	8	2	1	0
20-21	83	30	34	12	16	6	11	4
30-31	107	25	44	10	22	5	5	1
40-41	108	34	37	11	28	9	3	1
50-51	56	16	7	2	19	6	4	1
60-61	67	19	11	3	32	9	0	0
70-71	36	11	6	2	23	7	9	3
80-81	32	11	7	2	19	6	2	1
90-91	14	5	2	1	18	6	8	3
100-101	41	14	23	8	18	6	7	2
110-111	50	15	9	3	17	5	9	3
120-121	40	13	7	2	10	3	8	3
140-141	31	10	0	0	7	2	10	3
150-151	21	7	5	2	8	3	2	1
160-161	29	9	3	1	10	3	6	2
170-171	0	0	0	0	0	0	0	0
180-181	11	3	12	4	14	4	8	3
190-191	0	0	0	0	0	0	0	0
200-201	48	17	10	4	7	2	7	2
220-221	30	11	8	3	12	5	4	2
230-231	52	17	16	5	9	3	15	5
240-241	77	21	36	10	7	2	17	5
250-251	48	16	24	8	4	1	7	2
260-261	69	17	44	11	10	2	11	3
280-281	40	12	19	6	7	2	12	4
290-291	42	14	23	8	5	2	12	4
300-301	36	9	42	11	9	2	15	4
310-311	44	14	43	14	5	2	17	6
320-321	40	11	43	12	9	3	16	5
330-331	58	16	65	18	7	2	6	2
340-341	46	14	75	23	16	5	9	3
360-361	65	17	55	15	10	3	15	4
370-371	24	9	36	14	9	3	14	5
390-391	35	13	36	14	8	3	14	5
400-401	12	4	34	12	2	1	0	0
410-411	12	5	19	8	7	3	5	2
420-421	23	10	21	9	8	3	5	2
430-431	21	9	14	6	3	1	1	0

MG10H02								
Depth	Cibicides lobatula	%	Dyocibicides	%	Elphidium	%	Bolivinellina	%
0-1	4	1	0	0	20	6	2	1
10-11	7	2	4	1	21	5	1	0
20-21	2	1	2	1	9	3	0	0
30-31	9	2	2	0	22	5	1	0
40-41	5	2	0	0	8	2	0	0
50-51	7	2	1	0	19	6	3	1
60-61	9	3	0	0	8	2	0	0
70-71	10	3	5	2	14	4	2	1
80-81	5	2	4	1	11	4	0	0
90-91	2	1	8	3	23	8	2	1
100-101	0	0	1	0	4	1	2	1
110-111	9	3	3	1	19	6	0	0
120-121	9	3	3	1	19	6	0	0
140-141	6	2	4	1	11	4	2	1
150-151	6	2	9	3	10	3	1	0
160-161	6	2	5	2	10	3	1	0
170-171	0	0	0	0	0	0	0	0
180-181	3	1	7	2	18	6	3	1
190-191	0	0	0	0	0	0	0	0
200-201	6	2	4	1	15	5	7	2
220-221	5	2	4	2	9	3	3	1
230-231	4	1	1	0	16	5	6	2
240-241	8	2	3	1	23	6	5	1
250-251	21	7	7	2	10	3	7	2
260-261	9	2	4	1	14	3	1	0
280-281	14	4	10	3	12	4	5	2
290-291	6	2	9	3	10	3	12	4
300-301	3	1	12	3	21	5	9	2
310-311	9	3	3	1	15	5	3	1
320-321	5	1	8	2	23	7	5	1
330-331	10	3	6	2	15	4	3	1
340-341	9	3	8	2	11	3	5	2
360-361	14	4	4	1	10	3	8	2
370-371	6	2	2	1	8	3	9	3
390-391	12	5	5	2	6	2	14	5
400-401	5	2	13	5	7	3	17	6
410-411	0	0	23	9	15	6	11	4
420-421	3	1	4	2	3	1	20	8
430-431	3	1	8	3	4	2	5	2

MG10H02						
Depth	Epistomaroides	%	Planogypsina	%	Reussella	%
0-1	2	1	7	2	1	0
10-11	1	0	6	2	6	2
20-21	2	1	3	1	2	1
30-31		0	8	2	6	1
40-41	2	1	1	0	0	0
50-51	5	1	13	4	2	1
60-61	1	0	7	2	0	0
70-71	5	2	5	2	3	1
80-81	2	1	23	8	0	0
90-91	1	0	6	2	0	0
100-101	0	0	6	2	0	0
110-111	5	1	7	2	2	1
120-121	2	1	3	1	2	1
140-141	6	2	2	1	3	1
150-151	1	0	18	6	0	0
160-161	9	3	8	2	0	0
170-171	0	0	0	0	0	0
180-181	4	1	14	4	2	1
190-191	0	0	0	0	0	0
200-201	6	2	7	2	2	1
220-221	5	2	8	3	0	0
230-231	5	2	0	0	2	1
240-241	3	1	0	0	0	0
250-251	1	0	1	0	1	0
260-261	4	1	1	0	2	0
280-281	4	1	5	2	2	1
290-291	3	1	0	0	0	0
300-301	2	1	9	2	4	1
310-311	2	1	2	1	1	0
320-321	3	1	5	1	1	0
330-331	4	1	1	0	0	0
340-341	7	2	1	0	1	0
360-361	3	1	5	1	3	1
370-371	4	2	6	2	3	1
390-391	4	2	3	1	9	3
400-401	2	1	15	5	0	0
410-411	1	0	21	9	2	1
420-421	0	0	10	4	0	0
430-431	4	2	25	10	0	0

MG10H02	**Miliolina**						
Depth	Borelis	%	Peneroplis planatus	%	Sorites	%	Amphisorus
0-1	17	5	10	3	2	1	10
10-11	20	5	17	4	13	3	3
20-21	11	4	13	5	3	1	4
30-31	13	3	11	3	8	2	10
40-41	11	3	9	3	6	2	2
50-51	16	5	7	2	2	1	8
60-61	19	5	10	3	26	7	1
70-71	12	4	12	4	8	2	1
80-81	11	4	8	3	20	7	2
90-91	6	2	13	4	6	2	2
100-101	24	8	4	1	13	4	3
110-111	10	3	16	5	9	3	0
120-121	6	2	8	3	12	4	0
140-141	12	4	9	3	9	3	0
150-151	11	4	5	2	11	4	5
160-161	18	5	10	3	14	4	1
170-171	0	0	0	0	0	0	0
180-181	10	3	6	2	2	1	2
190-191	0	0	0	0	0	0	0
200-201	16	6	10	4	4	1	1
220-221	11	4	7	3	7	3	2
230-231	17	6	1	0	4	1	3
240-241	31	9	6	2	5	1	4
250-251	23	8	4	1	0	0	5
260-261	29	7	9	2	3	1	6
280-281	22	7	10	3	13	4	5
290-291	17	6	10	3	2	1	2
300-301	20	5	9	2	1	0	8
310-311	16	5	6	2	6	2	3
320-321	19	5	8	2	6	2	2
330-331	15	4	4	1	5	1	5
340-341	14	4	2	1	6	2	1
360-361	19	5	3	1	3	1	5
370-371	10	4	4	2	5	2	0
390-391	7	3	4	2	8	3	1
400-401	11	4	9	3	7	3	0
410-411	11	4	1	0	6	2	0
420-421	13	5	2	1	13	5	0
430-431	12	5	2	1	7	3	0

MG10H02								
Depth	Hauerina	%	Articulina	%	Spiroloculina	%	Nodophthalmidium	%
0-1	59	17	3	1	2	1	0	0
10-11	41	11	7	2	4	1	2	1
20-21	33	12	1	0	3	1	1	0
30-31	57	13	5	1	3	1	1	0
40-41	30	9	2	1	1	0	1	0
50-51	55	16	10	3	1	0	3	1
60-61	64	18	4	1	7	2	4	1
70-71	50	16	4	1	4	1	5	2
80-81	64	21	0	0	6	2	11	4
90-91	58	20	12	4	5	2	12	4
100-101	58	20	3	1	5	2	2	1
110-111	88	26	14	4	1	0	2	1
120-121	86	29	11	4	3	1	5	2
140-141	81	27	8	3	1	0	4	1
150-151	89	31	9	3	7	2	10	3
160-161	85	26	8	2	10	3	5	2
170-171	0	0	0	0	0	0	0	0
180-181	77	24	13	4	3	1	10	3
190-191	0	0	0	0	0	0	0	0
200-201	63	22	6	2	4	1	5	2
220-221	57	22	12	5	4	2	5	2
230-231	62	20	7	2	4	1	6	2
240-241	66	18	3	1	4	1	3	1
250-251	51	17	7	2	6	2	1	0
260-261	77	19	9	2	10	2	4	1
280-281	53	16	11	3	6	2	4	1
290-291	43	15	11	4	5	2	1	0
300-301	69	17	12	3	6	2	4	1
310-311	46	15	11	4	4	1	3	1
320-321	47	14	8	2	9	3	4	1
330-331	48	14	12	3	10	3		0
340-341	34	10	6	2	9	3	1	0
360-361	55	15	15	4	9	2	2	1
370-371	25	10	8	3	12	5	3	1
390-391	39	15	4	2	11	4	1	0
400-401	31	11	10	4	22	8	1	0
410-411	25	10	19	8	8	3	1	0
420-421	31	13	12	5	14	6	0	0
430-431	36	15	16	7	12	5	0	0

MG10H02								
Depth	Cycloforina pulchella	%	Cycloforina sulcata	%	Prygo	%	Triloculina	%
0-1	1	0	0	0	0	0	11	3
10-11	0	0	0	0	0	0	54	14
20-21	0	0	0	0	1	0	5	2
30-31	1	0	1	0	0	0	25	6
40-41	1	0	0	0	0	0	23	7
50-51	0	0	0	0	0	0	55	16
60-61	0	0	0	0	0	0	36	10
70-71	1	0	0	0	0	0	27	8
80-81	0	0	0	0	0	0	29	10
90-91	2	1	1	0	0	0	36	12
100-101	0	0	0	0	0	0	39	13
110-111	0	0	0	0	0	0	49	14
120-121	2	1	0	0	0	0	11	4
140-141	1	0	0	0	5	2	22	7
150-151	0	0	0	0	0	0	35	12
160-161	1	0	0	0	9	3	25	8
170-171	0	0	0	0	0	0	0	0
180-181	1	0	0	0	0	0	28	9
190-191	0	0	0	0	0	0	0	0
200-201	0	0	0	0	0	0	30	11
220-221	0	0	0	0	1	0	25	9
230-231	0	0	0	0	2	1	16	5
240-241	0	0	0	0	1	0	17	5
250-251	0	0	0	0	0	0	34	11
260-261	0	0	0	0	2	0	33	8
280-281	2	1	0	0	0	0	18	5
290-291	0	0	0	0	3	1	17	6
300-301	0	0	0	0	0	0	52	13
310-311	0	0	0	0	1	0	15	5
320-321	1	0	1	0	0	0	14	4
330-331	2	1	0	0	3	1	11	3
340-341	0	0	2	1	0	0	16	5
360-361	0	0	0	0	0	0	11	3
370-371	3	1	0	0	3	1	9	3
390-391	0	0	0	0	2	1	7	3
400-401	0	0	0	0	0	0	41	15
410-411	0	0	0	0	0	0	21	9
420-421	0	0	0	0	0	0	24	10
430-431	0	0	0	0	0	0	35	14

MG10H02			*Quinqueloculina*					
Depth	Lachlanella	%	Pseudotriloculina	%	mosharrafai	%	seminulum	%
0-1	6	2	7	2	4	1	1	0
10-11	6	2	6	2	3	1	0	0
20-21		0	4	1		0	6	2
30-31	7	2	15	3	3	1	5	1
40-41	3	1	0	0	0	0	0	0
50-51	9	3	10	3	2	1	0	0
60-61	11	3	8	2	1	0	0	0
70-71	14	4	8	2	4	1	1	0
80-81	4	1	9	3	2	1	0	0
90-91	4	1	5	2	8	3	17	6
100-101	8	3	8	3	0	0	0	0
110-111	1	0	6	2	0	0	0	0
120-121	4	1	8	3	8	3	3	1
140-141	11	4	10	3	0	0	4	1
150-151	7	2	4	1	0	0	0	0
160-161	7	2	1	0	9	3	6	2
170-171	0	0	0	0	0	0	0	0
180-181	10	3	15	5	4	1	2	1
190-191	0	0	0	0	0	0	0	0
200-201	7	2	2	1	1	0	0	0
220-221	1	0	8	3	3	1	4	2
230-231	1	0	7	2	1	0	9	3
240-241	9	2	5	1	3	1	9	2
250-251	9	3	5	2	0	0	0	0
260-261	4	1	7	2	2	0	4	1
280-281	8	2	10	3	1	0	5	2
290-291	0	0	8	3	4	1	15	5
300-301	8	2	13	3	1	0	0	0
310-311	5	2	9	3	0	0	4	1
320-321	11	3	7	2	4	1	2	1
330-331		0	5	1	7	2	6	2
340-341	7	2	3	1	1	0	4	1
360-361	4	1	5	1	1	0	0	0
370-371	7	3	3	1	0	0	1	0
390-391	0	0	2	1	3	1	4	2
400-401	1	0	3	1	0	0	0	0
410-411	7	3	4	2	0	0	0	0
420-421	6	3	3	1	3	1	0	0
430-431	2	1	4	2	2	1	0	0

MG10H02					**Textulariina**	
Depth	lamarkiana	%	ludwigi	%	Textularia	%
0-1	12	3	1	0	16	5
10-11	0	0	0	0	16	4
20-21	13	5	0	0	13	5
30-31	16	4	0	0	18	4
40-41	12	4	0	0	23	7
50-51	0	0	0	0	22	6
60-61	0	0	0	0	18	5
70-71	23	7	0	0	22	7
80-81	0	0	0	0	21	7
90-91	2	1	0	0	15	5
100-101	0	0	0	0	24	8
110-111	0	0	0	0	14	4
120-121	17	6	0	0	10	3
140-141	23	8	0	0	9	3
150-151	0	0	0	0	12	4
160-161	18	5	0	0	12	4
170-171	0	0	0	0	0	0
180-181	22	7	0	0	11	3
190-191	0	0	0	0	0	0
200-201	0	0	0	0	16	6
220-221	18	7	2	1	8	3
230-231	14	5	0	0	19	6
240-241	6	2	0	0	11	3
250-251	0	0	0	0	14	5
260-261	17	4	0	0	19	5
280-281	12	4	0	0	16	5
290-291	14	5	0	0	13	4
300-301	0	0	0	0	24	6
310-311	19	6	0	0	12	4
320-321	21	6	0	0	18	5
330-331	22	6	0	0	18	5
340-341	6	2	0	0	17	5
360-361	24	6	0	0	23	6
370-371	20	8	0	0	15	6
390-391	12	5	0	0	8	3
400-401	0	0	0	0	19	7
410-411	0	0	0	0	14	6
420-421	0	0	0	0	15	6
430-431	0	0	0	0	22	9

MG10H02	**Globigerinina**				
Depth	Globigerinoides	%	Globigerinoides	**%**	**Total Forams**
0-1	8	2	0	**0**	**349**
10-11	5	1	0	**0**	**385**
20-21	0	0	0	**0**	**275**
30-31	11	3	0	**0**	**436**
40-41	6	2	0	**0**	**322**
50-51	6	2	0	**0**	**342**
60-61	3	1	0	**0**	**347**
70-71	7	2	0	**0**	**321**
80-81	6	2	0	**0**	**298**
90-91	6	2	1	**0**	**295**
100-101	3	1	0	**0**	**296**
110-111	4	1	0	**0**	**344**
120-121	0	0	1	**0**	**298**
140-141	5	2	0	**0**	**296**
150-151	0	0	0	**0**	**286**
160-161	5	2	1	**0**	**332**
170-171	0	0	0	0	**0**
180-181	3	1	0	**0**	**315**
190-191	0	0	0	**0**	**0**
200-201	0	0	0	**0**	**284**
220-221	2	1	0	**0**	**265**
230-231	6	2	0	**0**	**305**
240-241	1	0	0	**0**	**363**
250-251	13	4	0	**0**	**303**
260-261	5	1	0	**0**	**409**
280-281		0	6	**2**	**332**
290-291	4	1	0	**0**	**291**
300-301	6	2	0	**0**	**395**
310-311	1	0	0	**0**	**305**
320-321	8	2	0	**0**	**348**
330-331	5	1	0	**0**	**353**
340-341	7	2	0	**0**	**324**
360-361	4	1	0	**0**	**375**
370-371	13	5	0	**0**	**262**
390-391	7	3	0	**0**	**266**
400-401	17	6	0	**0**	**279**
410-411	13	5	0	**0**	**246**
420-421	4	2	0	**0**	**237**
430-431	5	2	0	**0**	**243**

Whole Sample Wt	Picked Sample Wt	Forams per Gram	Depth cm
1.7730	0.056	11,050	**0**
2.3341	0.0568	15,821	**10**
2.0320	0.0675	8,279	**20**
1.7135	0.1575	4,743	**30**
0.9306	0.1049	2,857	**40**
1.0584	0.0581	6,230	**50**
1.0528	0.1312	2,784	**60**
0.6497	0.0902	2,312	**70**
0.7398	0.1745	1,263	**80**
0.2943	0.5169	168	**90**
1.2333	0.2144	1,703	**100**
0.8803	0.2056	1,473	**110**
0.3135	0.1534	609	**120**
1.1985	0.2426	1,462	**140**
0.9179	0.2916	900	**150**
1.0079	0.3643	919	**160**
3.8475	no foram	0	**170**
1.0137	0.1782	1,792	**180**
0.7606	no foram	0	**190**
0.4724	0.0522	2,570	**200**
0.6412	0.1664	1,021	**220**
1.2187	0.0976	3,808	**230**
1.8094	0.1464	4,486	**240**
1.6650	0.22	2,293	**250**
1.9433	0.121	6,569	**260**
2.0421	0.0615	11,024	**280**
1.5146	0.0514	8,575	**290**
1.3682	0.0841	6,426	**300**
2.1428	0.0765	8,543	**310**
1.6889	0.0734	8,007	**320**
1.8052	0.1008	6,322	**330**
1.5064	0.0937	5,209	**340**
1.9830	0.1082	6,873	**360**
Missing	0.0526		**370**
1.0771	0.0637	4,498	**390**
0.7344	0.0419	4,890	**400**
0.3847	0.0425	2,227	**410**
0.6769	0.0704	2,279	**420**
0.9616	0.0653	3,578	**430**

Depth	**Quinqueloculina (%)**	**Triloculina (%)**
0-1	9	3
10-11	4	14
20-21	8	2
30-31	11	6
40-41	5	7
50-51	6	16
60-61	6	10
70-71	16	8
80-81	5	10
90-91	12	12
100-101	5	13
110-111	2	14
120-121	13	4
140-141	16	7
150-151	4	12
160-161	12	8
170-171	0	0
180-181	17	9
190-191	0	0
200-201	4	11
220-221	14	9
230-231	10	5
240-241	9	5
250-251	5	11
260-261	8	8
280-281	11	5
290-291	14	6
300-301	6	13
310-311	12	5
320-321	13	4
330-331	11	3
340-341	6	5
360-361	9	3
370-371	12	3
390-391	8	3
400-401	1	15
410-411	4	9
420-421	5	10
430-431	3	14

MG10H02			
Depth	**Rotaliina %**	**Miliolina %**	**Textulariina %**
0-1	51	42	7
10-11	49	46	5
20-21	60	36	5
30-31	52	42	7
40-41	60	31	9
50-51	40	52	8
60-61	39	55	6
70-71	37	54	9
80-81	35	56	9
90-91	28	64	7
100-101	34	56	9
110-111	38	57	5
120-121	35	62	4
140-141	28	68	5
150-151	28	67	4
160-161	26	68	5
170-171	0	0	0
180-181	30	65	4
190-191	0	0	0
200-201	42	52	6
220-221	33	63	4
230-231	41	50	8
240-241	49	47	3
250-251	43	48	9
260-261	41	53	6
280-281	39	54	7
290-291	42	52	6
300-301	41	51	8
310-311	47	49	4
320-321	45	47	7
330-331	50	44	7
340-341	58	35	7
360-361	51	42	7
370-371	46	43	11
390-391	55	39	6
400-401	38	49	13
410-411	47	42	11
420-421	41	51	8
430-431	36	53	11

APPENDIX B

Foraminifera Graphs

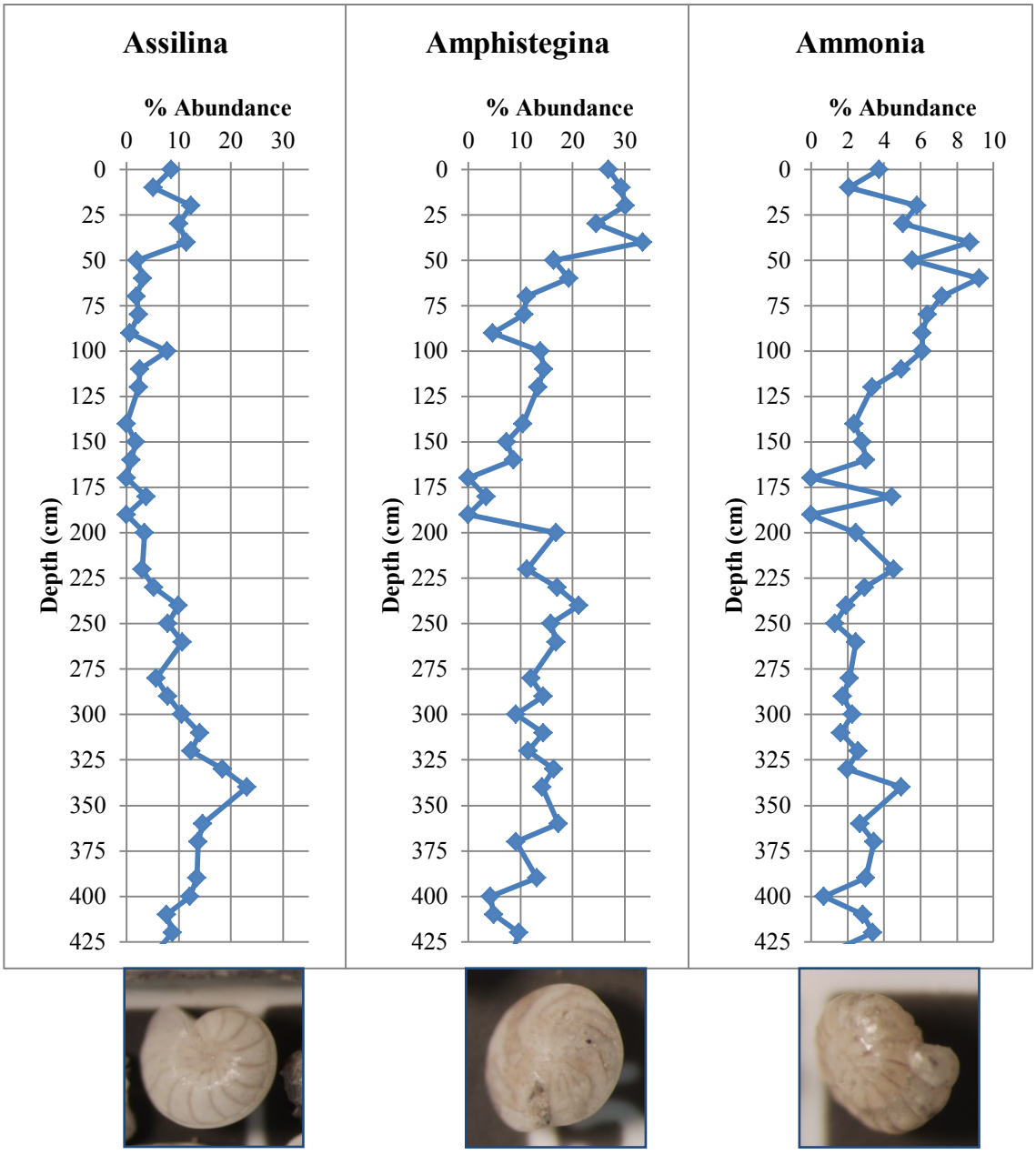
Assilina
% Abundance
0 10 20 30
Depth (cm)
0 25 50 75 100 125 150 175 200 225 250 275 300 325 350 375 400 425
Amphistegina
% Abundance
0 10 20 30
Depth (cm)
0 25 50 75 100 125 150 175 200 225 250 275 300 325 350 375 400 425
Ammonia
% Abundance
0 2 4 6 8 10
Depth (cm)
0 25 50 75 100 125 150 175 200 225 250 275 300 325 350 375 400 425

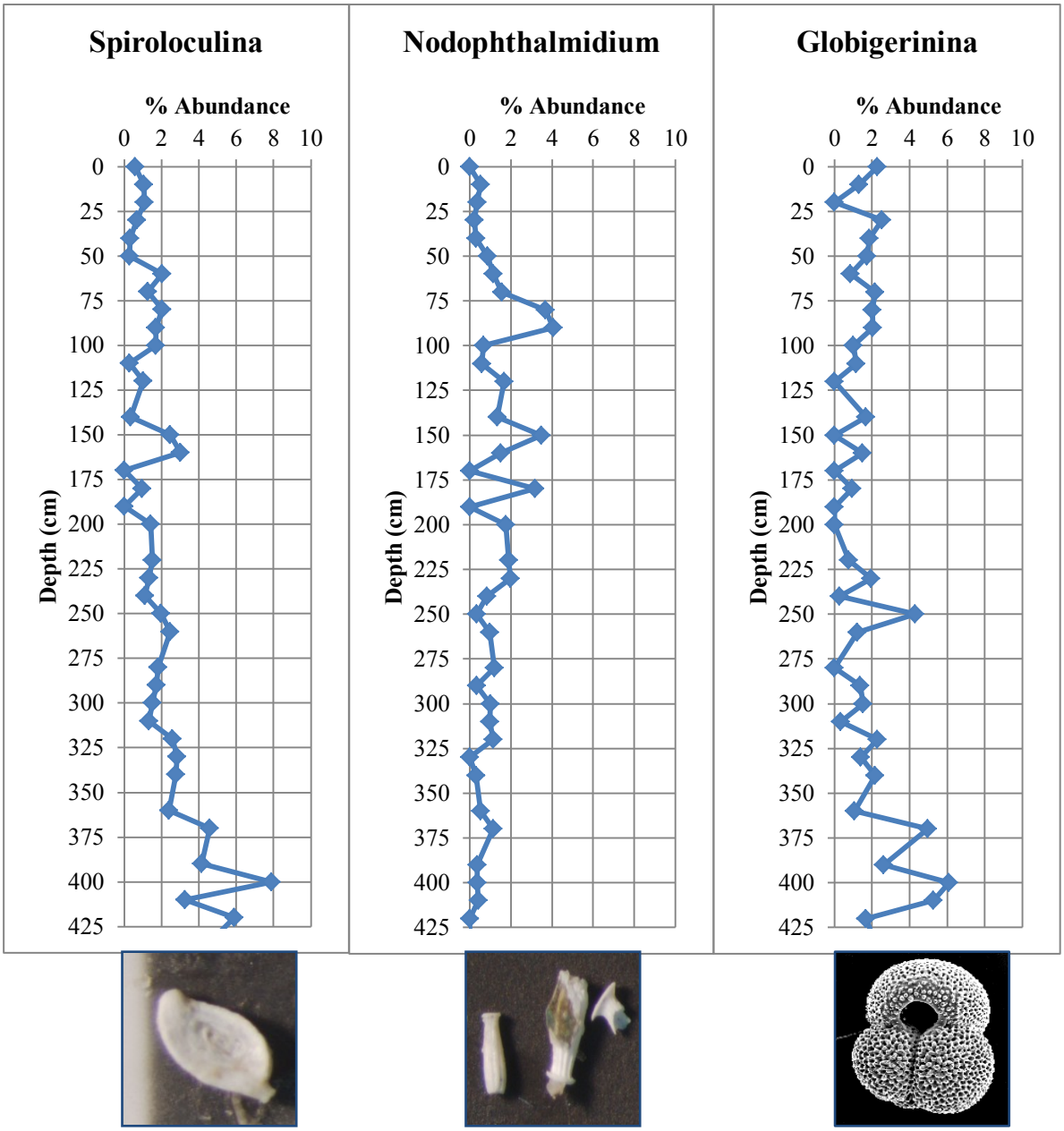
Spiroloculina
% Abundance
0 2 4 6 8 10
Depth (cm)
0 25 50 75 100 125 150 175 200 225 250 275 300 325 350 375 400 425
Nodophthalmidium
% Abundance
0 2 4 6 8 10
Depth (cm)
0 25 50 75 100 125 150 175 200 225 250 275 300 325 350 375 400 425
Globigerinina
% Abundance
0 2 4 6 8 10
Depth (cm)
0 25 50 75 100 125 150 175 200 225 250 275 300 325 350 375 400 425

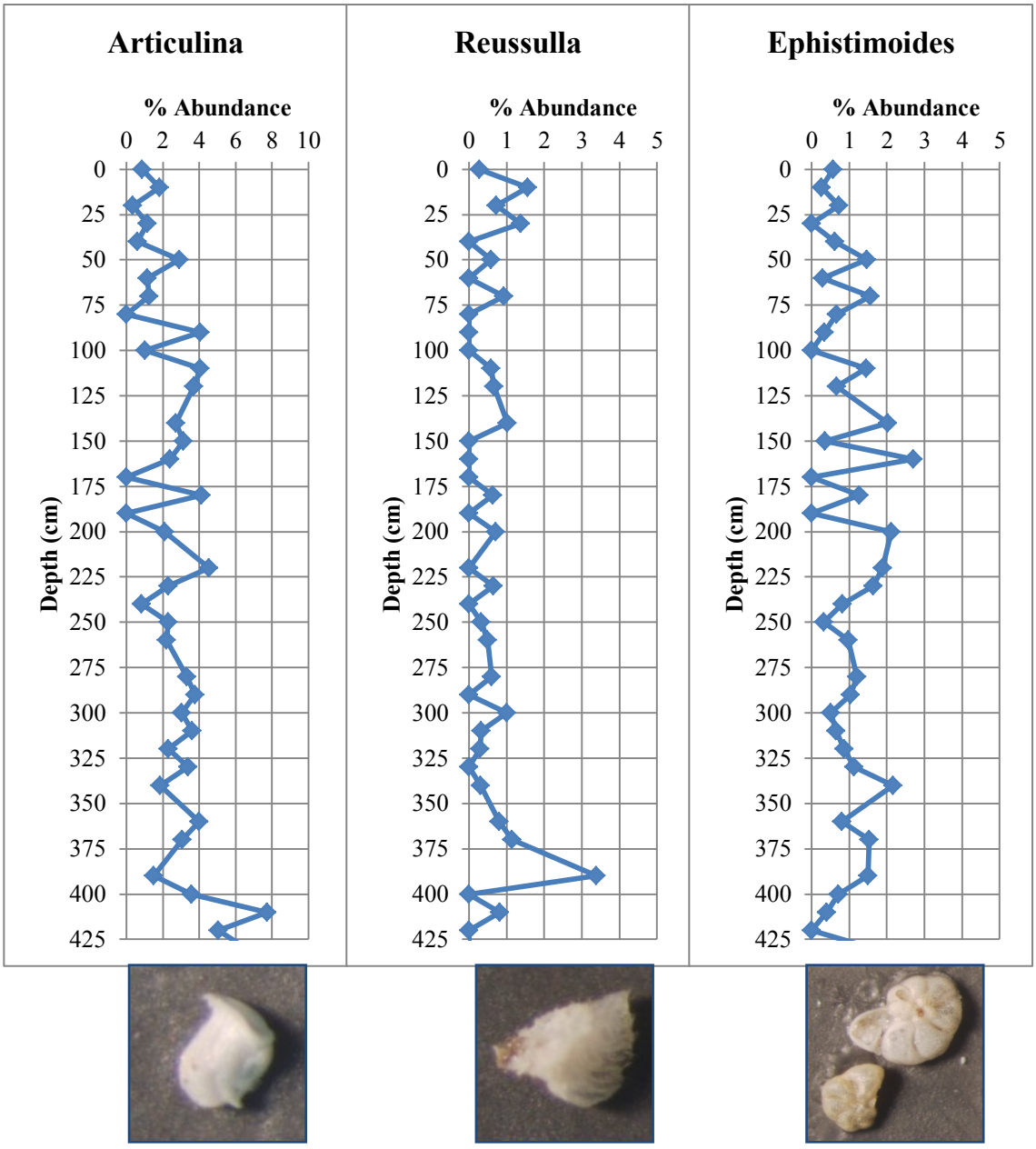
Articulina
% Abundance
0 2 4 6 8 10
Depth (cm)
0 25 50 75 100 125 150 175 200 225 250 275 300 325 350 375 400 425
Reussulla
% Abundance
0 1 2 3 4 5
Depth (cm)
0 25 50 75 100 125 150 175 200 225 250 275 300 325 350 375 400 425
Ephistimoides
% Abundance
0 1 2 3 4 5
Depth (cm)
0 25 50 75 100 125 150 175 200 225 250 275 300 325 350 375 400 425

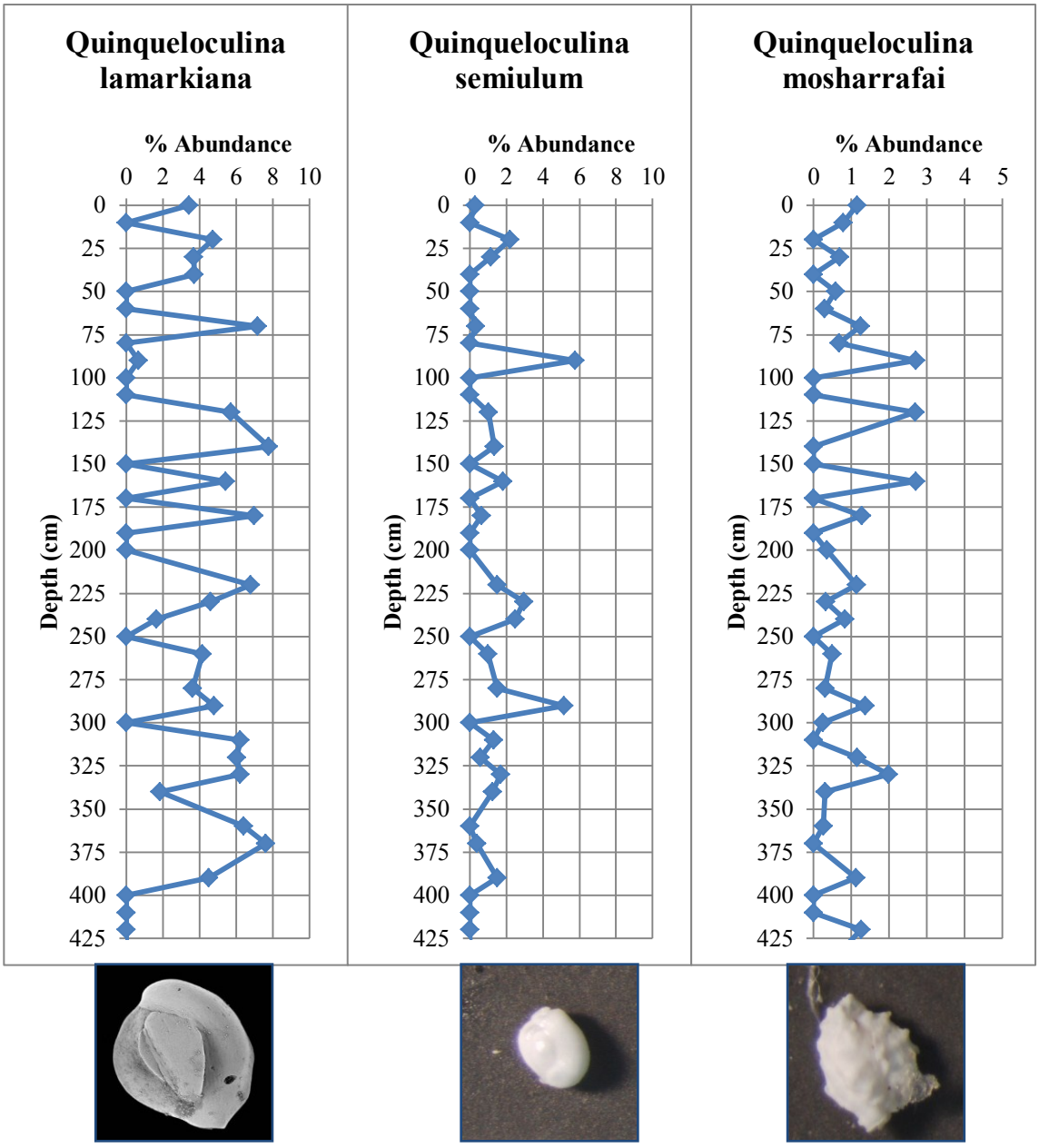
Quinqueloculina lamarkiana
% Abundance
0 2 4 6 8 10
Depth (cm)
0 25 50 75 100 125 150 175 200 225 250 275 300 325 350 375 400 425
Quinqueloculina semiulum
% Abundance
0 2 4 6 8 10
Depth (cm)
0 25 50 75 100 125 150 175 200 225 250 275 300 325 350 375 400 425
Quinqueloculina mosharrafai
% Abundance
0 1 2 3 4 5
Depth (cm)
0 25 50 75 100 125 150 175 200 225 250 275 300 325 350 375 400 425

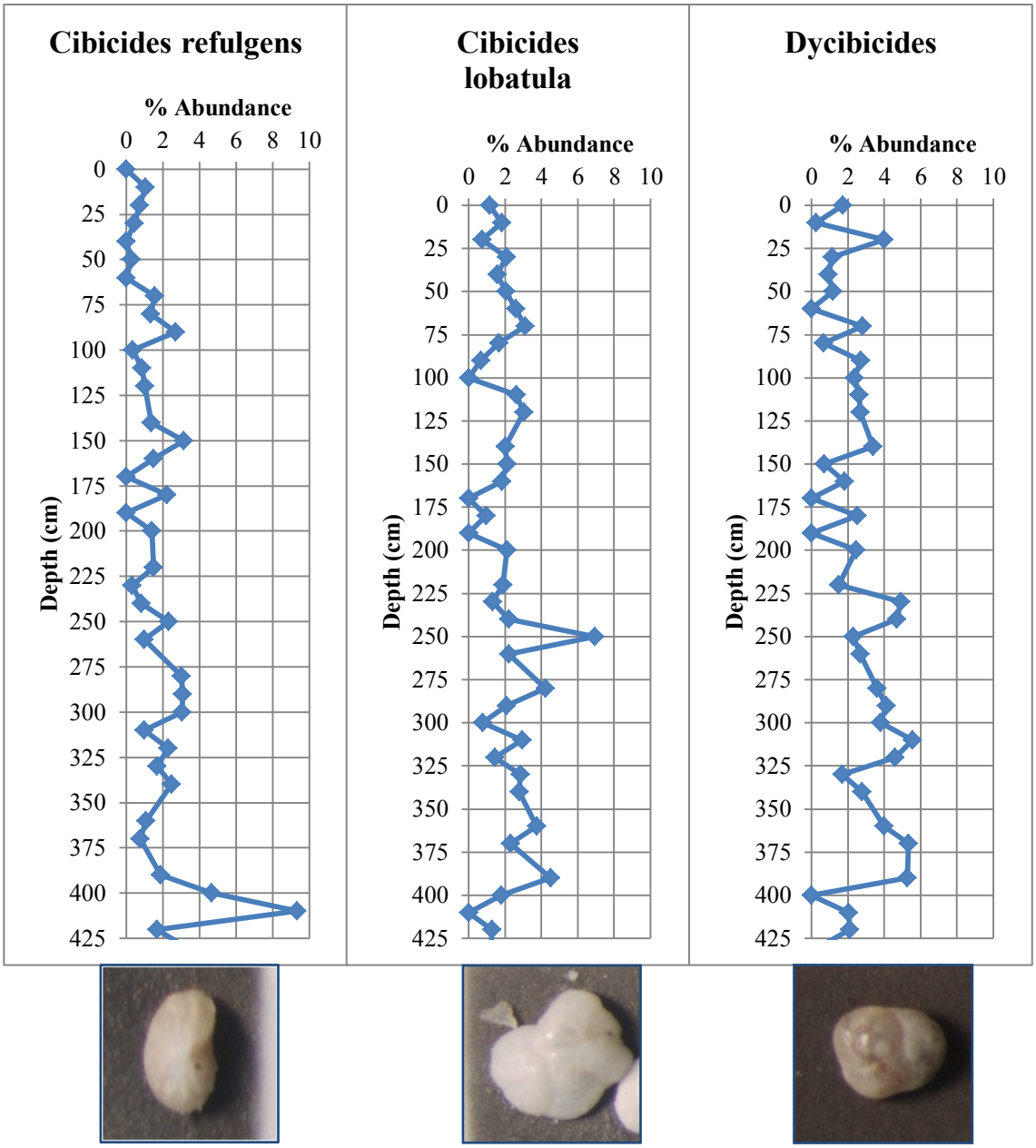
Cibicides refulgens
% Abundance
0 2 4 6 8 10
Depth (cm)
0 25 50 75 100 125 150 175 200 225 250 275 300 325 350 375 400 425
Cibicides lobatula
% Abundance
0 2 4 6 8 10
Depth (cm)
0 25 50 75 100 125 150 175 200 225 250 275 300 325 350 375 400 425
Dycibicides
% Abundance
0 2 4 6 8 10
Depth (cm)
0 25 50 75 100 125 150 175 200 225 250 275 300 325 350 375 400 425

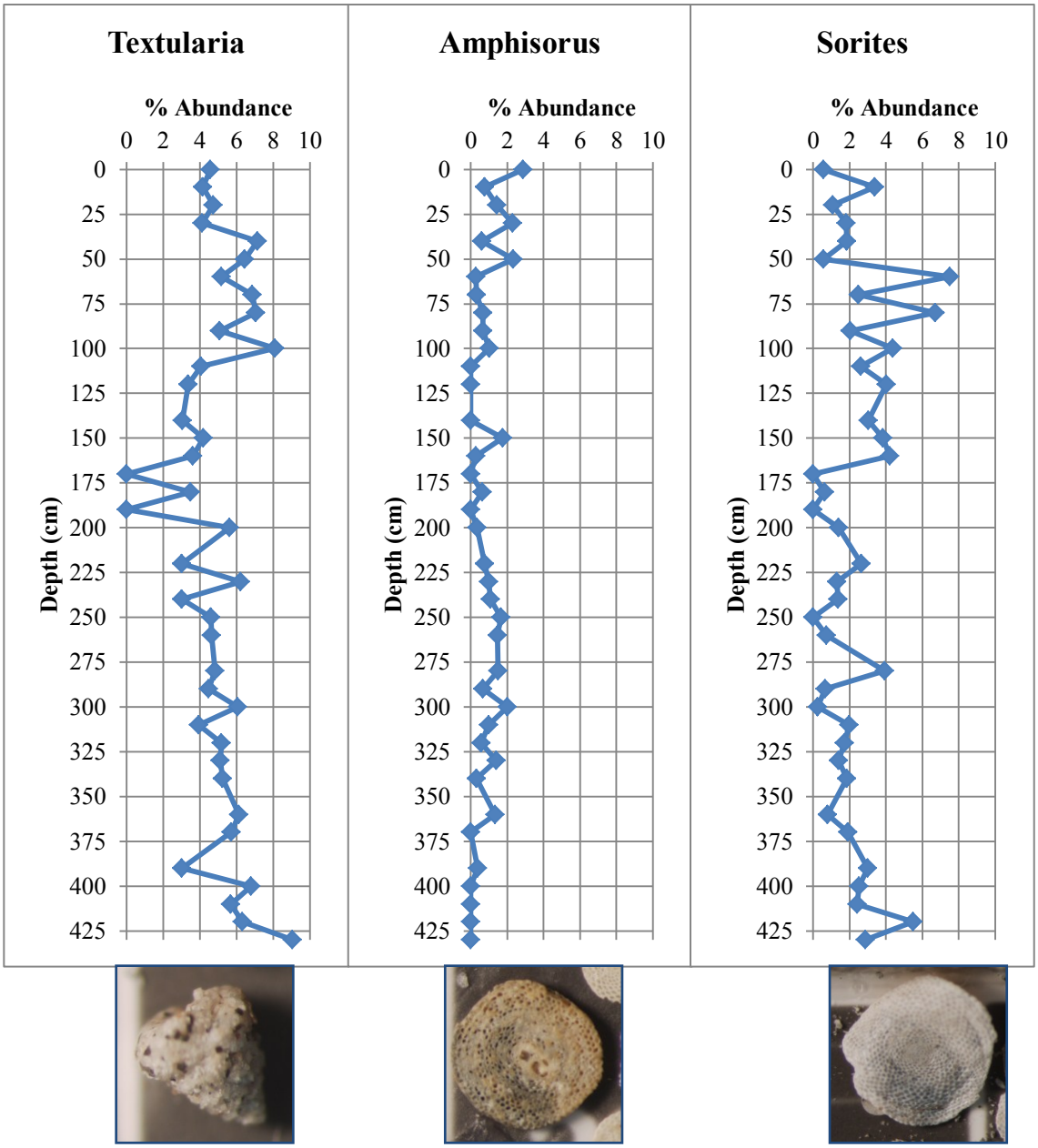
Textularia
% Abundance
0 2 4 6 8 10
Depth (cm)
0 25 50 75 100 125 150 175 200 225 250 275 300 325 350 375 400 425
Amphisorus
% Abundance
0 2 4 6 8 10
Depth (cm)
0 25 50 75 100 125 150 175 200 225 250 275 300 325 350 375 400 425
Sorites
% Abundance
0 2 4 6 8 10
Depth (cm)
0 25 50 75 100 125 150 175 200 225 250 275 300 325 350 375 400 425

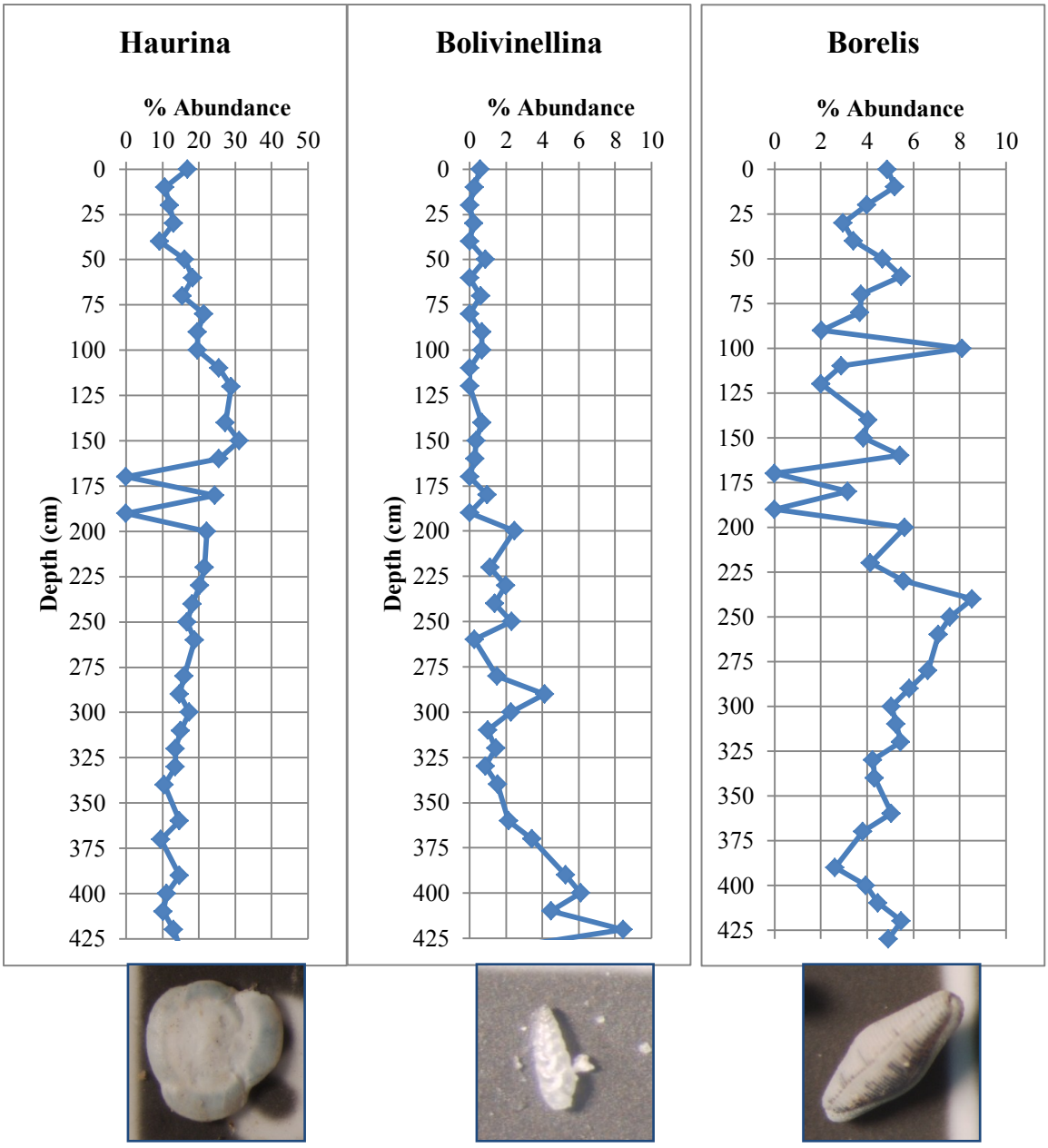
Haurina
% Abundance
0 10 20 30 40 50
Depth (cm)
0 25 50 75 100 125 150 175 200 225 250 275 300 325 350 375 400 425
Bolivinellina
% Abundance
0 2 4 6 8 10
Depth (cm)
0 25 50 75 100 125 150 175 200 225 250 275 300 325 350 375 400 425
Borelis
% Abundance
0 2 4 6 8 10
0 25 50 75 100 125 150 175 200 225 250 275 300 325 350 375 400 425

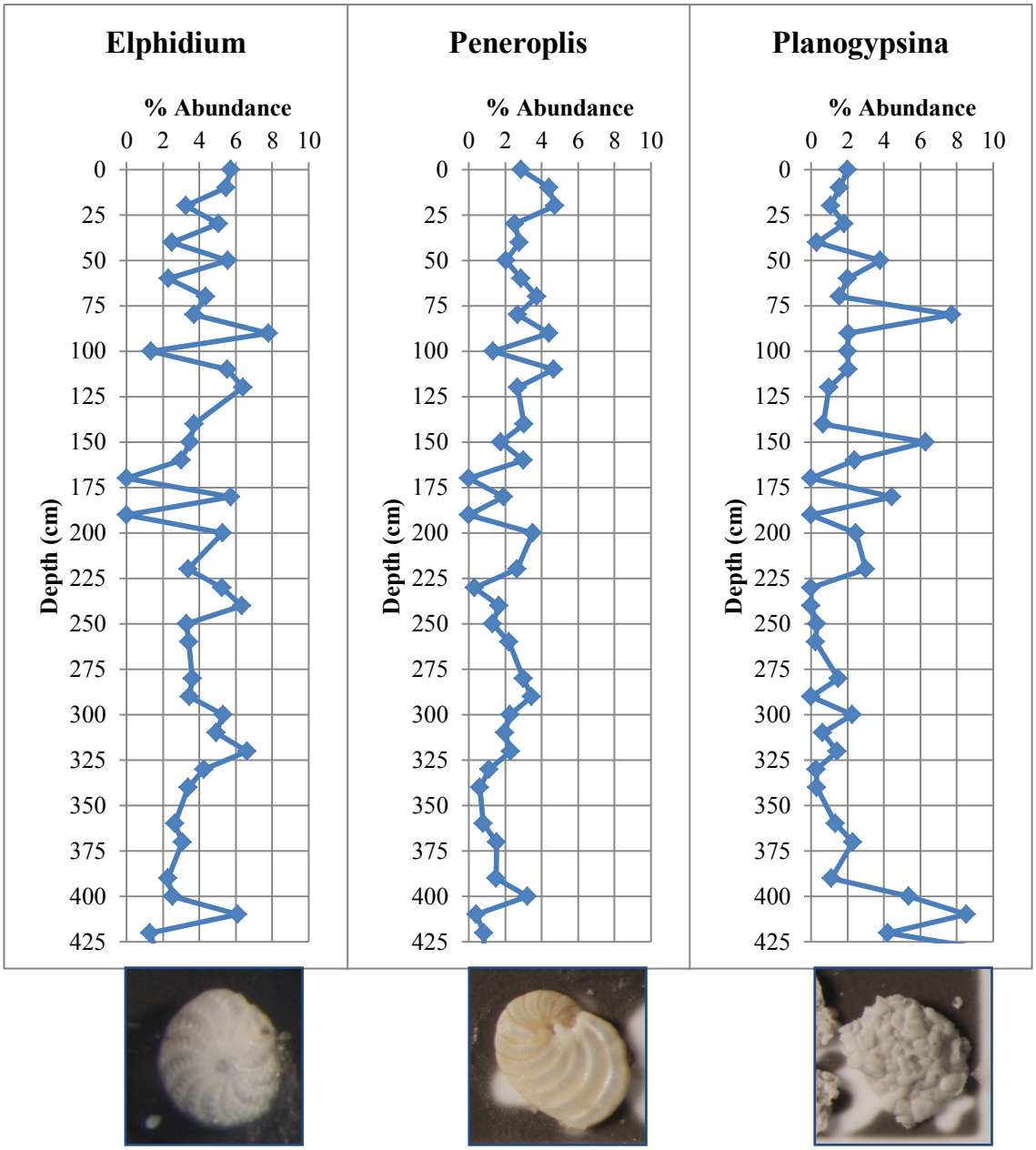
Elphidium
% Abundance
0 2 4 6 8 10
Depth (cm)
0 25 50 75 100 125 150 175 200 225 250 275 300 325 350 375 400 425
Peneroplis
% Abundance
0 2 4 6 8 10
Depth (cm)
0 25 50 75 100 125 150 175 200 225 250 275 300 325 350 375 400 425
Planogypsina
% Abundance
0 2 4 6 8 10
Depth (cm)
0 25 50 75 100 125 150 175 200 225 250 275 300 325 350 375 400 425

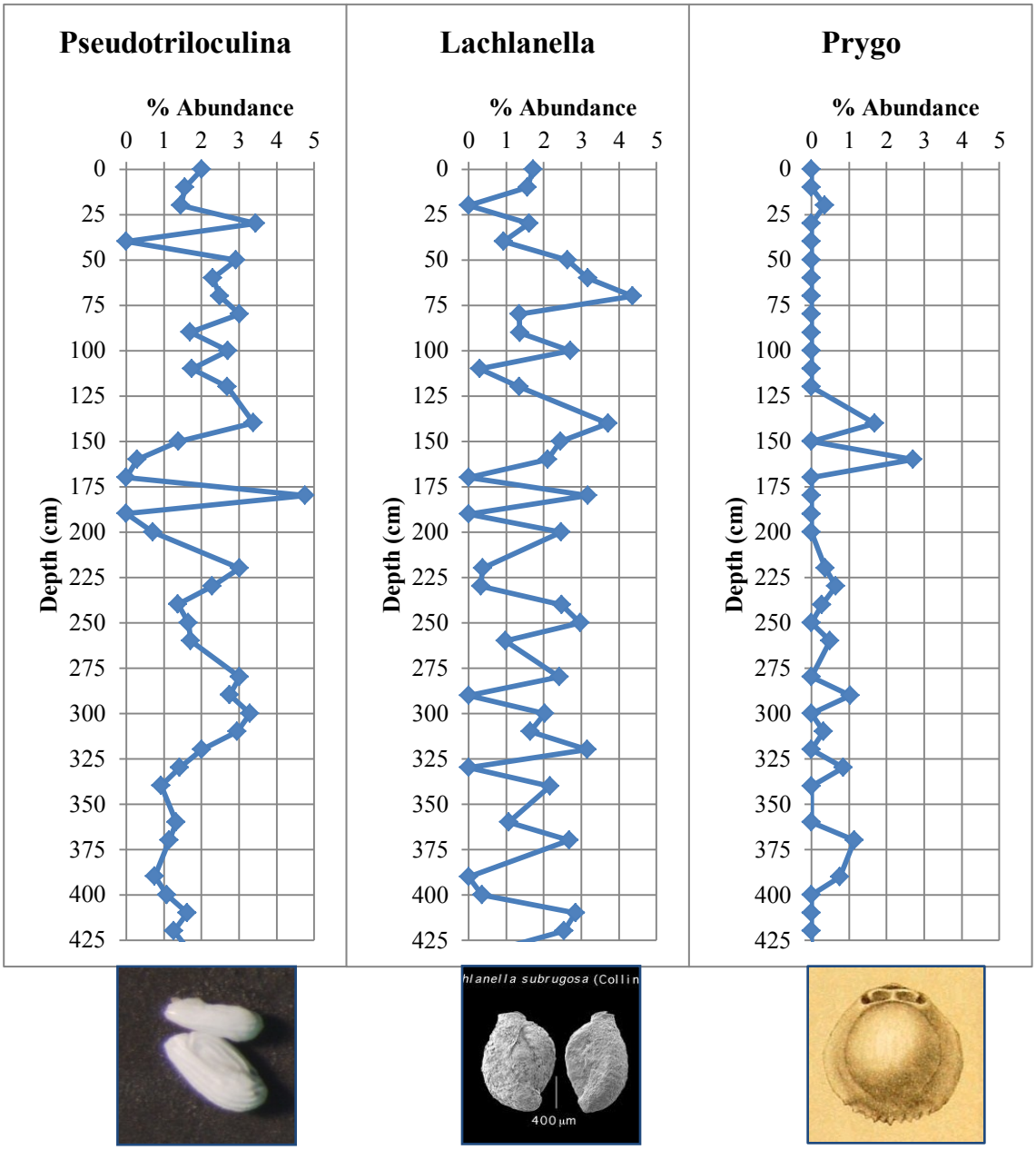
Pseudotriloculina
Lachlanella
Prygo
% Abundance
0 1 2 3 4 5
Depth (cm)
0 25 50 75 100 125 150 175 200 225 250 275 300 325 350 375 400 425
hlanella subrugosa (Collin
400 µm

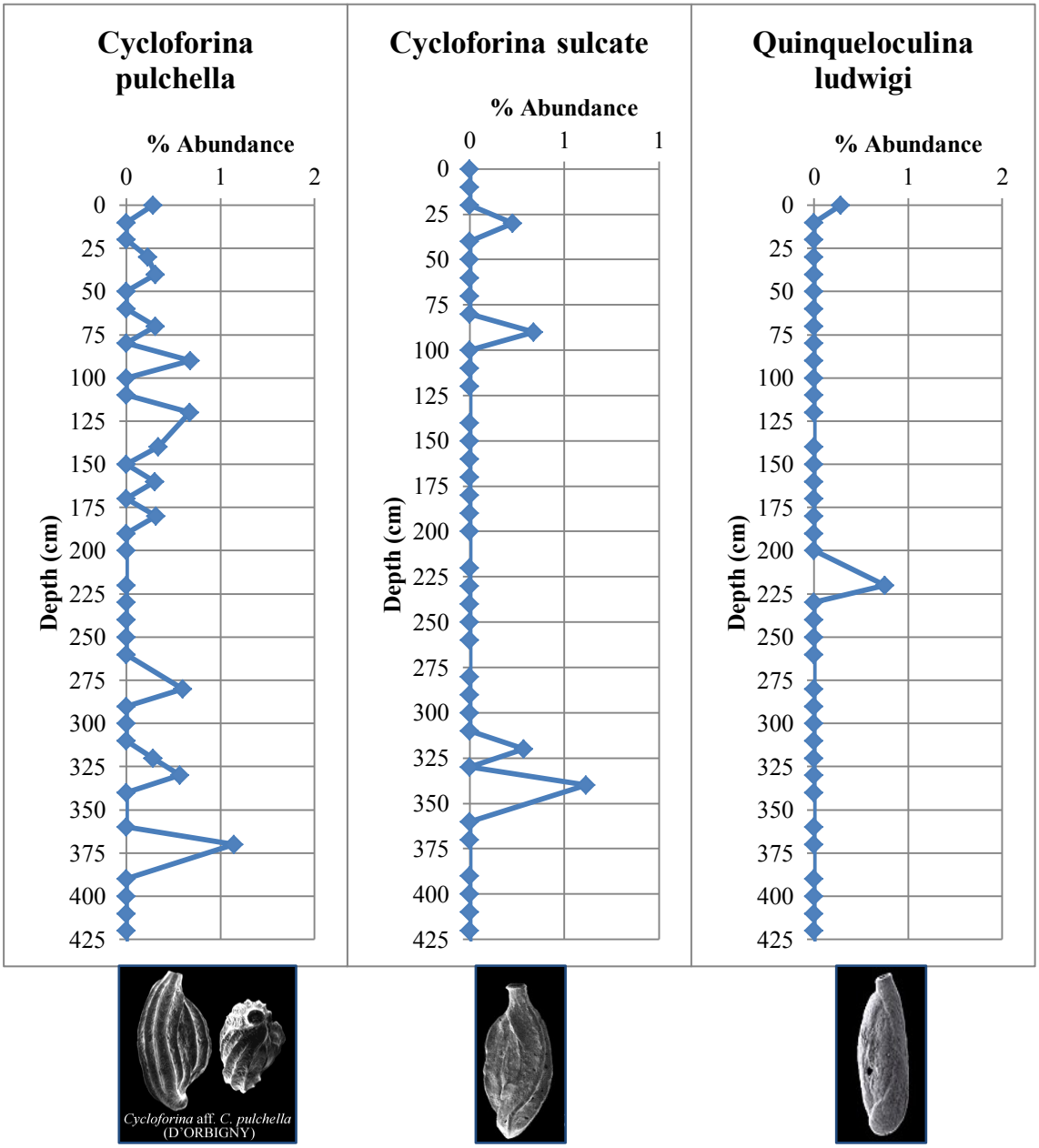
Cycloforina pulchella
% Abundance
0
1
2
Depth (cm)
0
25
50
75
100
125
150
175
200
225
250
275
300
325
350
375
400
425
Cycloforina sulcate
% Abundance
0
1
1
Depth (cm)
Quinqueloculina ludwigi
% Abundance
0
1
2
Depth (cm)
Cycloforina aff. C. pulchella
(D'ORBIGNY)

APPENDIX C

Grain Size

Sample	Depth cm	Diff.	Mean	Median	Mean/Median	Mode	S. D.
1	0	0.0116552	387	188	2.06113	140	442.283
1002	1	0.0106066	416	220	1.88949	154	451.579
2003	2	0.0119097	495	244	2.03163	169	524.323
3004	3	0.0159284	487	296	1.6467	568	484.138
4005	4	0.0110817	501	250	2.00539	154	528.032
6007	6	0.0106927	531	324	1.6421	905	517.906
7008	7	0.00741128	721	630	1.14439	994	557.95
8009	8	0.00653905	833	768	1.08388	1909	574.655
9010	9	0.0192711	421	161	2.61902	140	517.17
10011	10	0.0211634	506	225	2.24793	1197	547.01
11012	11	0.027707	469	213	2.20477	169	522.121
12013	12	0.0274084	406	191	2.11999	169	473.177
14015	14	0.0332728	332	141	2.34724	128	423.329
16017	16	0.0323059	366	152	2.40622	140	467.77
17018	17	0.0217551	440	175	2.5136	128	517.316
18019	18	0.0254528	369	159	2.32218	140	459.244
19020	19	0.0185527	427	166	2.56518	128	516.236
20021	20	0.0232157	440	176	2.50216	116	515.461
21022	21	0.0211671	414	154	2.68354	140	529.776
22023	22	0.0246714	432	148	2.92613	116	549.446
23024	23	0.0223604	407	163	2.49929	128	497.405
24025	24	0.0329548	296	108	2.7258	106	449.183
26027	26	0.0254443	385	151	2.55175	140	499.177
27028	27	0.0272688	353	135	2.60833	116	469.209
28029	28	0.0335054	400	145	2.751	128	508.22
29030	29	0.0336248	356	128	2.7829	116	495.254
30031	30	0.0259499	306	123	2.49742	116	429.078
31032	31	0.049976	295	115	2.57825	128	414.542
32033	32	0.030009	390	147	2.65575	116	497.657
33034	33	0.0382794	309	125	2.47236	116	409.814
34035	34	0.0356607	320	130	2.45857	128	434.533
36037	36	0.0392239	317	114	2.77359	116	463.811
37038	37	0.0361039	309	116	2.66986	96	426.92
38039	38	0.0445284	293	106	2.76718	116	445.039
39040	39	0.0380606	291	113	2.56215	116	423.21
40041	40	0.0331793	268	106	2.5197	106	411.244
41042	41	0.0423801	188	97	1.94409	128	289.074
42043	42	0.0375177	177	94	1.88297	116	271.287
43044	43	0.0389022	116	86	1.34509	116	115.818

44045	44	0.0370873	218	100	2.18014	116	353.81
46047	46	0.0390311	246	100	2.45966	116	403.426
47048	47	0.0442806	197	94	2.08352	116	311.123
48049	48	0.0431417	168	92	1.84023	116	255.661
49050	49	0.044803	183	92	1.99374	116	296.628
5051	50	0.0302123	287	116	2.47321	128	434.975
51052	51	0.038728	228	97	2.34333	106	381.589
52053	52	0.0397205	234	101	2.32171	116	379.536
53054	53	0.0403769	199	97	2.05201	116	311.928
54055	54	0.0375818	188	96	1.95847	106	301.505
56057	56	0.0478161	181	91	1.98985	106	300.438
57058	57	0.0461915	187	94	1.99418	116	291.527
58059	58	0.0401943	219	100	2.17607	116	346.943
59060	59	0.0459023	172	91	1.88337	116	279.633
60061	60	0.0422142	224	102	2.19066	116	365.895
61062	61	0.0364015	181	96	1.88795	106	293.596
62063	62	0.036384	115	87	1.32059	106	113.398
63064	63	0.0304767	256	111	2.31171	128	409.994
64065	64	0.0376006	229	100	2.28662	106	377.912
66067	66	0.0305952	224	108	2.08014	128	352.115
67068	67	0.0290002	248	107	2.31811	106	396.513
68069	68	0.0358698	122	93	1.31217	116	116.074
69070	69	0.0331067	189	101	1.87691	116	308.768
70071	70	0.0316594	155	92	1.68372	106	248.447
71072	71	0.0411011	115	89	1.2998	106	110.553
72073	72	0.0376814	120	92	1.30393	106	114.758
73074	73	0.0397828	146	92	1.58057	106	212.915
74075	74	0.0403768	177	94	1.87475	106	280.479
76077	76	0.0413864	165	100	1.65185	116	218.552
77078	77	0.0425034	118	89	1.3261	106	114.388
78079	78	0.0366833	125	98	1.27807	116	114.041
79080	79	0.0350989	125	97	1.29254	116	115.16
80081	80	0.024133	119	99	1.20753	116	98.9087
81082	81	0.034332	126	96	1.30915	106	115.475
82083	82	0.0289125	123	98	1.25896	106	107.471
83084	83	0.032412	121	95	1.27447	106	107.727
84085	84	0.02501	113	93	1.21513	106	94.1491
86087	86	0.030069	118	96	1.2364	106	102.127
87088	87	0.0342571	124	97	1.27971	106	112.053
88089	88	0.0320912	128	101	1.26433	116	112.068
89090	89	0.0269063	122	100	1.21794	116	102.279

90091	90	0.0240939	117	94	1.24093	106	100.32
91092	91	0.0207873	118	98	1.21066	106	94.664
92093	92	0.0401148	75	1	87.9022	88	7782.83
93094	93	0.0579531	101	73	1.38291	128	102.856
94095	94	0.0462301	114	86	1.32296	106	111.881
96097	96	0.0391615	122	97	1.24967	140	107.912
97098	97	0.0290299	127	104	1.22413	128	107.363
98099	98	0.0255918	139	114	1.2224	140	115.626
99100	99	0.0218363	124	106	1.16223	116	93.676
100101	100	0.0138799	141	113	1.24708	106	102.88
101102	101	0.0181465	141	109	1.29444	96	110.802
102103	102	0.0261981	124	95	1.30807	106	112.932
103104	103	0.0246241	170	104	1.64218	128	273.954
104105	104	0.0216159	352	129	2.7224	128	498.893
106107	106	0.0255149	220	108	2.0391	128	355.601
107108	107	0.0269141	136	109	1.2397	128	116.746
108109	108	0.0297029	198	115	1.72458	140	299.571
109110	109	0.0332366	208	104	1.99715	128	333.709
110111	110	0.0269226	161	104	1.54312	128	237.699
150151	150	0.0225879	116	101	1.14544	128	87.1958
151152	151	0.0247799	123	106	1.16189	140	92.9272
152153	152	0.0239811	120	101	1.18326	128	93.6387
153154	153	0.025375	117	101	1.16118	128	90.7694
154155	154	0.0251807	101	94	1.07828	106	59.5484
156157	156	0.0253531	98	92	1.06927	116	61.3538
157158	157	0.0255113	111	98	1.1327	128	81.5907
158159	158	0.0257227	104	100	1.04896	140	66.5237
159160	159	0.0271838	109	99	1.10062	140	80.1291
160161	160	0.0477163	120	94	1.28322	140	115.76
161162	161	0.0471653	109	94	1.16308	154	93.886
162163	162	0.0235678	133	126	1.05498	154	84.7998
163164	163	0.0296125	122	110	1.11468	154	92.6514
164165	164	0.0256696	115	100	1.14845	140	88.8362
166167	166	0.0180112	142	129	1.10363	169	98.6216
167168	167	0.0104411	189	178	1.06276	185	97.1901
168169	168	0.00881878	194	181	1.07211	185	98.2125
169170	169	0.00900753	194	182	1.06594	185	94.9355
170171	170	0.0106361	187	177	1.05781	185	95.1003
171172	171	0.00943051	214	200	1.07159	204	106.906
172173	172	0.0113014	202	193	1.0454	204	96.696
173174	173	0.00946308	197	184	1.07386	185	99.0999

174175	174	0.00977499	206	191	1.07669	204	103.64
176177	176	0.0281763	96	81	1.18657	80	74.8258
177178	177	0.0234524	109	89	1.21898	88	82.7115
178179	178	0.0546032	81	74	1.08493	96	60.4978
179180	179	0.0293317	113	97	1.16953	116	141.981
180181	180	0.0243374	106	103	1.02254	116	56.4965
181182	181	0.0270066	103	100	1.02655	116	57.0376
182183	182	0.0228245	102	100	1.02241	116	57.2481
183184	183	0.0247537	100	99	1.01271	116	52.7424
184185	184	0.0268845	121	103	1.17096	128	101.321
186187	186	0.0251396	106	105	1.01173	116	54.3177
187188	187	0.0235669	105	103	1.01436	116	52.3035
188189	188	0.0179565	107	107	1.00546	116	45.7444
189190	189	0.0163949	111	109	1.02363	116	48.1151
190191	190	0.0130712	139	129	1.07435	140	73.2305
191192	191	0.0139661	128	124	1.03883	128	59.7081
192193	192	0.0143405	151	136	1.10815	140	87.9712
193194	193	0.0176965	137	125	1.09556	128	81.4219
194195	194	0.0138932	133	125	1.06323	128	69.917
196197	196	0.0149345	133	124	1.07204	128	72.554
197198	197	0.0305402	100	87	1.1573	88	70.2597
198199	198	0.02781	85	75	1.13769	73	55.965
199200	199	0.0331895	81	71	1.14467	73	57.0999
200201	200	0.0326722	87	81	1.06923	106	56.8418
201202	201	0.0310998	84	78	1.07036	106	54.2753
202203	202	0.0339522	106	83	1.27513	96	99.8677
203204	203	0.0399913	82	73	1.13126	88	60.7714
204205	204	0.0480615	74	69	1.07907	128	53.3451
206207	206	0.0297083	150	97	1.54032	116	212.927
207208	207	0.0284894	183	97	1.89475	106	288.094
208209	208	0.0264604	170	96	1.7736	106	263.948
209210	209	0.029718	97	91	1.06625	116	63.6367
210211	210	0.0237172	202	100	2.01855	116	362.423
211212	211	0.0235638	159	104	1.52512	116	211.343
212213	212	0.0197705	136	100	1.36789	116	211.687
213214	213	0.0252966	223	104	2.15061	116	370.181
214215	214	0.0259571	146	100	1.46394	116	196.877
216217	216	0.0240564	108	94	1.15557	106	109.516
217218	217	0.0296048	88	85	1.0431	96	50.31
218219	218	0.0358847	80	74	1.07923	88	52.3774
219220	219	0.0345655	90	78	1.16036	88	71.8595

220221	220	0.0298196	88	86	1.01601	128	52.1889
221222	221	0.0324235	78	78	0.991128	116	44.9638
222223	222	0.0286023	99	92	1.07258	106	62.3363
223224	223	0.0243651	92	89	1.03545	96	45.6109
224225	224	0.0202738	105	98	1.08094	96	57.1811
226227	226	0.0132405	153	132	1.16224	128	98.1901
227228	227	0.0182411	127	115	1.11129	128	83.0722
228229	228	0.0132833	154	133	1.15735	128	98.0275
229230	229	0.016361	285	126	2.26323	128	412.711
230231	230	0.018373	272	122	2.23352	116	400.767
231232	231	0.0275361	144	104	1.39144	116	185.442
232233	232	0.0428856	130	89	1.46739	96	145.438
233234	233	0.0460696	129	83	1.5527	96	157.001
234235	234	0.0267855	288	109	2.63684	106	436.884
236237	236	0.0210044	289	120	2.39866	116	426.073
237238	237	0.0457228	105	80	1.31052	96	108.81
238239	238	0.0476143	79	70	1.13229	73	58.4288
239240	239	0.0759767	75	67	1.12872	154	62.7676
240241	240	0.0310423	425	151	2.80777	140	534.015
241242	241	0.0371308	92	85	1.08046	106	63.3045
242243	242	0.0410249	148	86	1.7313	96	219.087
243244	243	0.0432157	285	95	2.98966	88	453.726
244245	244	0.0263596	261	102	2.5428	96	407.094
246247	246	0.0204326	414	139	2.98819	116	536.666
247248	247	0.0567465	88	75	1.1637	96	70.7329
248249	248	0.0176002	269	117	2.29889	128	395.229
249250	249	0.0197547	288	116	2.49373	116	431.321
250251	250	0.0251905	225	99	2.266	96	370.506
251252	251	0.025405	321	110	2.91846	88	473.068
252253	252	0.0265825	283	103	2.74128	88	433.011
253254	253	0.0227397	255	105	2.42279	96	388.596
254255	254	0.023968	329	108	3.0376	96	484.989
256257	256	0.0268077	410	125	3.29375	116	551.68
257258	257	0.0292131	357	120	2.96513	116	498.07
258259	258	0.021301	516	177	2.91274	1909	589.082
259260	259	0.0274288	564	194	2.91143	1314	605.316
260261	260	0.0488668	84	73	1.14773	169	63.984
261262	261	0.0255272	272	108	2.52565	96	408.718
262263	262	0.0231785	317	118	2.6801	96	453.786
263264	263	0.0305213	278	106	2.61407	116	423.496
264265	264	0.0669405	76	61	1.25921	169	66.8939

266267	266	0.0410719	193	89	2.18026	128	286.11
267268	267	0.0387136	409	108	3.76945	80	549.207
268269	268	0.0893624		40	1.33719	128	50.2078
269270	269	0.110839	46	30	1.55163	128	46.6555
270271	270	0.0616575	55	47	1.15347	106	43.6654
271272	271	0.028073	464	142	3.26192	1584	575.556
272273	272	0.0340577	419	124	3.38891	1314	543.85
273274	273	0.0278982	521	188	2.77273	1443	580.725
274275	274	0.0325317	337	116	2.90697	106	477.029
276277	276	0.0248639	418	152	2.75936	96	509.531
277278	277	0.0223535	480	197	2.44001	1197	536.703
278279	278	0.0535507	210	86	2.44175	80	298.359
279280	279	0.0420222	347	114	3.05012	80	482.954
280281	280	0.03063	471	167	2.81341	1314	553.383
281282	281	0.0482222	284	100	2.82973	80	407.658
282283	282	0.028351	540	177	3.05957	1584	607.76
283284	283	0.0246715	509	217	2.3496	1091	549.447
284285	284	0.0267366	563	187	3.0041	1443	603.702
286287	286	0.0235978	571	247	2.31352	1443	592.845
287288	287	0.0278776	493	165	2.99028	1584	579.349
288289	288	0.0281795	550	180	3.05247	1314	595.377
290291	289	0.0270139	511	170	3.00855	1314	583.183
291292	290	0.0204418	530	194	2.73189	1909	579.212
292293	291	0.0219213	491	170	2.8822	1909	569.725
293294	292	0.0211745	605	169	3.59076	1909	640.36
294295	293	0.0331188	548	152	3.59575	1909	617.376
296297	296	0.0273597	549	149	3.68106	1909	621.203
297298	297	0.021279	589	319	1.84618	1909	593.063
298299	298	0.0306432	506	178	2.83894	1197	566.991
299300	299	0.0398391	554	212	2.6087	1314	601.485
300301	300	0.0816049	60	45	1.33307	66	55.9155
301302	301	0.046725	436	117	3.72532	1091	556.24
302303	302	0.0528593	410	99	4.12751	1314	548.754
303304	303	0.0382469	528	176	3.00721	1314	591.138
304305	304	0.0486342	396	114	3.49014	1197	529.185
306307	306	0.0327168	408	130	3.15244	88	534.728
307308	307	0.0371982	457	159	2.88175	1197	548.315
308309	308	0.0489557	342	108	3.15641	994	457.45
309310	309	0.0562788	346	97	3.5829	66	488.588
310311	310	0.0311457	492	181	2.71666	1091	544.689
311312	311	0.0376919	528	173	3.05574	1197	589.513

312313	312	0.0408293	505	177	2.8518	1314	579.517
313314	313	0.0276335	546	261	2.08941	1091	565.305
314315	314	0.0366451	390	125	3.122	1197	514.059
316317	316	0.0278506	527	163	3.22372	1443	593.53
317318	317	0.0288841	429	128	3.36138	1584	550.023
318319	318	0.0894306	48	36	1.3312	61	45.4246
319320	319	0.0349754	587	233	2.51496	1443	615.115
320321	320	0.0317944	513	160	3.20914	1443	594.489
321322	321	0.030519	500	194	2.57777	1197	553.307
322323	322	0.0345622	548	210	2.60891	1314	591.911
323324	323	0.0312545	472	160	2.94526	1197	552.228
324325	324	0.0384105	328	94	3.50256	73	486.156
326327	326	0.0415533	446	128	3.47987	1443	561.471
327328	327	0.0337509	396	118	3.35282	66	515.807
328329	328	0.0512504	333	91	3.66891	66	487.76
329330	329	0.049911	413	103	3.99235	1443	553.485
330331	330	0.0428296	551	299	1.84105	1091	569.216
331332	331	0.0429573	424	111	3.80199	1197	554.916
332333	332	0.0437789	391	113	3.45833	994	505.743
333334	333	0.033728	473	165	2.86622	1739	567.106
334335	334	0.0511821	460	121	3.80214	1443	576.096
336337	336	0.0501189	454	93	4.86076	1584	590.122
337338	337	0.0729095	58	40	1.45133	55	57.7978
338339	338	0.0955648	44	29	1.52524	50	46.0654
339340	339	0.0925868	48	32	1.47082	50	49.1465
340341	340	0.0924861	47	31	1.52406	50	50.245
341342	341	0.0553626	395	70	5.6171	1314	549.047
342343	342	0.0430873	565	122	4.64414	1584	644.27
343344	343	0.0555952	374	71	5.29148	50	543.128
344345	344	0.0748336	132	43	3.06858	50	217.93
346347	346	0.0828129	54	37	1.48713	50	55.8185
347348	347	0.113704	37	23	1.61339	46	40.2617
348349	348	0.124808	36	21	1.7416	50	40.45
349350	349	0.11925	33	19	1.694	46	36.4144

Sample	Depth cm	Variance	C. V.	Skewness	Kurtosis
1	0	195614	114.421	1.66411	2.13979
1002	1	203923	108.435	1.57072	1.7956
2003	2	274915	105.964	1.1961	0.31546
3004	3	234389	99.408	1.2226	0.649777
4005	4	278818	105.493	1.1933	0.292364
6007	6	268227	97.4651	1.07691	0.109544
7008	7	311309	77.4328	0.534007	-0.844814
8009	8	330228	69.0104	0.298556	-1.08697
9010	9	267465	122.948	1.45304	0.937977
10011	10	299220	108.019	1.07056	-0.0634924
11012	11	272610	111.43	1.21778	0.359969
12013	12	223897	116.595	1.49861	1.33774
14015	14	179207	127.613	1.8082	2.69279
16017	16	218809	127.788	1.70748	2.01718
17018	17	267616	117.475	1.35987	0.702604
18019	18	210905	124.499	1.69853	2.04082
19020	19	266500	120.937	1.43682	0.878099
20021	20	265700	117.076	1.32631	0.635706
21022	21	280663	128.12	1.52841	1.07635
22023	22	301891	127.241	1.39799	0.618735
23024	23	247412	122.242	1.51495	1.26961
24025	24	201765	151.915	2.1579	3.73208
26027	26	249178	129.644	1.63873	1.58452
27028	27	220157	132.903	1.75785	2.15846
28029	28	258287	127.014	1.45795	0.976063
29030	29	245276	138.941	1.76119	1.96671
30031	30	184108	140.209	2.05011	3.45621
31032	31	171845	140.342	1.93295	3.10123
32033	32	247662	127.641	1.54751	1.3401
33034	33	167947	132.508	1.8003	2.59748
34035	34	188819	135.917	1.9118	2.9275
36037	36	215121	146.309	1.98704	3.04205
37038	37	182261	138.132	1.89287	2.87558
38039	38	198059	152.02	2.10083	3.52803
39040	39	179107	145.541	2.10527	3.73044
40041	40	169122	153.529	2.36083	4.92416
41042	41	83563.8	153.685	3.21029	11.5263
42043	42	73596.5	153.625	3.3791	12.9789
43044	43	13413.8	99.933	1.92892	4.36227
44045	44	125181	162.469	2.95285	8.62481

46047	46	162752	163.816	2.61977	6.20293
47048	47	96797.4	158.25	3.02806	9.70362
48049	48	65362.5	151.811	3.43382	13.7032
49050	49	87988.2	161.667	3.36776	12.3202
5051	50	189203	151.711	2.24185	4.11179
51052	51	145610	167.174	2.83752	7.54452
52053	52	144047	162.354	2.76752	7.25773
53054	53	97299.4	156.471	3.0261	9.6956
54055	54	90905.3	160.002	3.27141	11.2391
56057	56	90263.2	166.331	3.42985	12.5516
57058	57	84988	155.902	3.07341	10.1713
58059	58	120369	158.669	2.84931	8.10725
59060	59	78194.4	162.588	3.65771	14.8944
60061	60	133879	163.384	2.9443	8.53344
61062	61	86198.6	162.647	3.73744	15.4946
62063	62	12859.1	98.4899	2.05671	4.95903
63064	63	168095	160.29	2.63204	6.1977
64065	64	142818	164.858	2.84731	7.68411
66067	66	123985	157.396	2.96946	8.81872
67068	67	157223	160.065	2.69696	6.67038
68069	68	13473.2	95.0193	1.78257	3.67713
69070	69	95337.6	163.484	3.63676	13.9593
70071	70	61725.9	159.928	4.37487	22.1451
71072	71	12222.1	95.871	1.83784	3.97535
72073	72	13169.5	95.581	1.89515	4.22452
73074	73	45332.8	146.328	4.38744	24.3537
74075	74	78668.5	158.503	3.53442	13.9645
76077	76	47765.1	132.679	3.18587	13.1913
77078	77	13084.6	97.0391	1.73922	3.38576
78079	78	13005.4	90.936	1.56302	2.75379
79080	79	13261.8	91.8415	1.61424	2.92751
80081	80	9782.92	83.1477	1.93969	5.25826
81082	81	13334.4	91.9413	1.67551	3.09318
82083	82	11550	87.0933	1.71507	3.60128
83084	83	11605.1	89.096	1.65208	3.25168
84085	84	8864.05	83.151	1.95981	5.38203
86087	86	10429.9	86.188	1.70622	3.74041
87088	87	12555.8	90.6935	1.75355	3.56547
88089	88	12559.3	87.3612	1.61581	2.98511
89090	89	10461	83.8135	1.74516	4.05544
90091	90	10064.2	85.7039	2.00671	5.28603

91092	91	8961.27	79.97	1.82631	4.5829
92093	92	93.0024	2.02367	5.59557	
93094	93	10579.4	101.793	1.62338	2.97817
94095	94	12517.3	98.1639	1.82738	3.85504
96097	96	11645	88.7429	1.35572	1.96489
97098	97	11526.7	84.5848	1.49982	2.75525
98099	98	13369.3	82.9536	1.48074	2.52866
99100	99	8775.2	75.717	1.68422	4.19697
100101	100	10584.3	72.8975	1.61779	2.83668
101102	101	12277.1	78.8044	1.59552	2.51475
102103	102	12753.6	91.3429	1.95845	4.5111
103104	103	75050.9	160.808	4.46029	21.7896
104105	104	248894	141.627	1.80876	2.01298
106107	106	126452	161.774	3.09629	9.3801
107108	107	13629.7	86.0372	1.66456	3.32615
108109	108	89742.7	151.35	3.61908	14.2838
109110	109	111362	160.639	3.16628	10.2425
110111	110	56500.7	147.565	4.20264	20.8084
150151	150	7603.11	75.3169	1.59117	4.52648
151152	151	8635.46	75.5527	1.29195	2.5828
152153	152	8768.21	78.2202	1.54199	3.69501
153154	153	8239.08	77.4271	1.56717	4.09424
154155	154	3546.01	58.9858	0.505115	-0.113489
156157	156	3764.29	62.6965	0.535803	-0.019141
157158	157	6657.04	73.7649	1.42373	3.78083
158159	158	4425.41	63.6882	0.383051	-0.455451
159160	159	6420.67	73.6213	1.45476	4.91016
160161	160	13400.5	96.2983	1.67136	3.31532
161162	161	8814.58	86.2757	1.4083	3.04485
162163	162	7191.01	63.7719	1.00531	2.23796
163164	163	8584.29	75.8126	1.23388	2.53459
164165	164	7891.87	77.3446	1.72169	5.27427
166167	166	9726.21	69.2233	1.07113	1.75554
167168	167	9445.91	51.329	0.796185	1.16545
168169	168	9645.69	50.5276	0.829222	1.09214
169170	169	9012.75	48.8378	0.799451	1.15428
170171	170	9044.07	50.8315	0.7387	1.06962
171172	171	11428.9	49.9226	0.636101	0.437792
172173	172	9350.11	47.8975	0.535163	0.671788
173174	173	9820.79	50.2861	0.778384	0.908766
174175	174	10741.3	50.3627	0.705823	0.600284

176177	176	5598.9	78.3238	2.23738	8.2256
177178	177	6841.19	76.137	1.67098	4.29546
178179	178	3659.98	74.8488	0.579241	-0.265751
179180	179	20158.5	125.72	7.06777	64.8733
180181	180	3191.85	53.4693	0.247691	-0.193694
181182	181	3253.29	55.5531	0.293086	-0.19204
182183	182	3277.34	56.0899	0.277716	-0.230948
183184	183	2781.76	52.6751	0.121525	-0.470994
184185	184	10265.8	84.0257	2.10048	6.29294
186187	186	2950.41	51.2177	0.111964	-0.246064
187188	187	2735.66	49.9082	0.0972322	-0.305196
188189	188	2092.55	42.7165	-0.118367	-0.186895
189190	189	2315.07	43.1649	0.0968532	-0.00574204
190191	190	5362.71	52.709	1.41589	4.41025
191192	191	3565.05	46.5299	0.441023	0.802473
192193	192	7738.92	58.3967	1.33531	2.80541
193194	193	6629.52	59.6395	1.39476	3.51432
194195	194	4888.38	52.4549	1.43988	5.0371
196197	196	5264.08	54.5645	1.14785	3.32733
197198	197	4936.43	70.0926	1.38439	3.61623
198199	198	3132.09	65.5718	0.670297	-0.0102681
199200	199	3260.39	70.3998	0.819359	0.365083
200201	200	3230.99	65.6487	0.433238	-0.45586
201202	201	2945.81	64.6284	0.402739	-0.52581
202203	202	9973.55	94.5194	2.16896	6.40956
203204	203	3693.16	73.8824	0.681477	-0.150905
204205	204	2845.7	72.0808	0.443171	-0.642835
206207	206	45338	142.197	3.93754	18.0999
207208	207	82998.4	157.43	2.98549	8.57633
208209	208	69668.6	155.371	3.36968	11.704
209210	209	4049.63	65.369	0.534002	-0.0794082
210211	210	131350	179.244	3.30909	10.1938
211212	211	44665.7	133.314	3.44969	12.854
212213	212	44811.5	155.512	5.67389	35.6753
213214	213	137034	166.115	2.90929	7.8841
214215	214	38760.7	135.118	3.77164	15.7615
216217	216	11993.8	101.27	6.04908	52.9484
217218	217	2531.09	56.956	0.215284	-0.659201
218219	218	2743.4	65.4661	0.480457	-0.338535
219220	219	5163.79	79.7834	2.01393	8.13133
220221	220	2723.69	59.6417	0.148909	-0.71285

221222	221	2021.75	57.9348	0.0264883	-0.78096
222223	222	3885.81	63.0292	0.430962	-0.336589
223224	223	2080.36	49.6807	0.16846	-0.295302
224225	224	3269.68	54.2062	0.664506	0.611167
226227	226	9641.3	64.1532	1.51272	2.97304
227228	227	6900.98	65.261	1.93287	6.4081
228229	228	9609.4	63.5249	1.47753	2.84887
229230	229	170330	144.907	2.36064	4.78518
230231	230	160614	147.222	2.47414	5.49596
231232	231	34388.8	128.427	3.90645	17.5639
232233	232	21152.3	111.673	2.3246	6.06665
233234	233	24649.2	121.704	2.57734	7.38184
234235	234	190868	151.873	2.1796	3.78722
236237	236	181538	147.415	2.27085	4.28715
237238	237	11839.6	103.62	2.36186	7.05507
238239	238	3413.92	73.9096	0.615372	-0.329762
239240	239	3939.77	83.2532	0.560352	-0.68296
240241	240	285172	125.599	1.36373	0.599185
241242	241	4007.46	68.7485	0.459627	-0.479198
242243	242	47999.1	147.595	3.16802	10.4504
243244	243	205868	158.943	2.11704	3.41442
244245	244	165726	156.206	2.40466	5.05081
246247	246	288010	129.502	1.44579	0.775024
247248	247	5003.15	80.7012	0.683116	-0.319543
248249	248	156206	146.999	2.42811	5.36161
249250	249	186038	149.539	2.28224	4.35154
250251	250	137275	164.576	2.90628	8.02642
251252	251	223793	147.459	1.9305	2.61041
252253	252	187499	153.161	2.19777	3.94147
253254	253	151007	152.215	2.43592	5.39247
254255	254	235215	147.273	1.83564	2.14684
256257	256	304351	134.492	1.39827	0.537713
257258	257	248074	139.451	1.69808	1.71992
258259	258	347018	114.09	1.03194	-0.344908
259260	259	366407	107.348	0.794105	-0.790732
260261	260	4093.95	76.5486	0.55634	-0.630835
261262	261	167050	150.171	2.28578	4.53041
262263	262	205922	143.368	1.99208	2.98852
263264	263	179349	152.22	2.21084	4.06024
264265	264	4474.8	87.4597	0.798194	-0.2827
266267	266	81859	147.908	2.30664	4.55653

267268	267	301628	134.378	1.33203	0.42099
268269	268	2520.82	93.4249	0.863301	-0.223618
269270	269	2176.73	100.779	0.958503	-0.135981
270271	270	1906.66	79.8106	0.603501	-0.587812
271272	271	331265	124.104	1.19341	0.0154572
272273	272	295773	129.77	1.32832	0.455389
273274	273	337242	111.398	0.960517	-0.421043
274275	274	227557	141.646	1.81887	2.27479
276277	276	259622	121.8	1.36407	0.755573
277278	277	288050	111.729	1.13783	0.119395
278279	278	89018	142.402	2.03236	3.38519
279280	279	233245	139.244	1.70903	1.88159
280281	280	306233	117.465	1.14024	-0.00274888
281282	281	166185	143.771	1.91509	2.91712
282283	282	369372	112.504	0.909317	-0.62814
283284	283	301892	107.961	0.983054	-0.270742
284285	284	364456	107.279	0.805963	-0.752638
286287	286	351465	103.787	0.792651	-0.734623
287288	287	335645	117.55	1.08897	-0.183663
288289	288	354473	108.338	0.806847	-0.757058
290291	289	340102	114.068	0.990568	-0.389209
291292	290	335487	109.191	0.955399	-0.414502
292293	291	324587	116.135	1.11757	-0.0808543
293294	292	410061	105.801	0.684773	-1.03691
294295	293	381154	112.676	0.832302	-0.770342
296297	296	385893	113.095	0.851446	-0.745903
297298	297	351724	100.658	0.773109	-0.73605
298299	298	321478	112.147	0.957366	-0.391131
299300	299	361784	108.591	0.806089	-0.742533
300301	300	3126.54	93.7492	0.948142	0.00719162
301302	301	309403	127.526	1.19919	0.134012
302303	302	301130	133.899	1.29593	0.360217
303304	303	349444	112.004	0.895018	-0.57271
304305	304	280037	133.566	1.39593	0.707385
306307	306	285934	130.923	1.42447	0.768641
307308	307	300649	119.999	1.1811	0.133705
308309	308	209261	133.73	1.54013	1.45308
309310	309	238718	141.234	1.59905	1.48245
310311	310	296686	110.701	0.973284	-0.281108
311312	311	347526	111.724	0.899004	-0.547994
312313	312	335840	114.673	0.987251	-0.386203

313314	313	319569	103.567	0.835775	-0.558048
314315	314	264256	131.653	1.44858	0.904012
316317	316	352278	112.699	0.901387	-0.58801
317318	317	302525	128.309	1.31021	0.408547
318319	318	2063.39	93.9404	0.891422	-0.135716
319320	319	378367	104.855	0.713985	-0.906575
320321	320	353417	115.923	0.9759	-0.458275
321322	321	306149	110.674	0.991273	-0.282255
322323	322	350358	108.089	0.841077	-0.680259
323324	323	304956	116.897	1.08866	-0.0949027
324325	324	236347	148.433	1.78869	2.11051
326327	326	315250	125.937	1.20237	0.123884
327328	327	266057	130.21	1.39695	0.779495
328329	328	237910	146.268	1.70837	1.82024
329330	329	306346	133.984	1.30555	0.363096
330331	330	324007	103.293	0.753172	-0.692602
331332	331	307932	131.005	1.27431	0.309272
332333	332	255776	129.332	1.31667	0.584785
333334	333	321609	119.985	1.16576	0.0467876
334335	334	331886	125.194	1.11645	-0.104984
336337	336	348244	129.855	1.13174	-0.149303
337338	337	3340.58	99.3895	1.19579	0.650512
338339	338	2122.02	105.707	1.36889	1.23208
339340	339	2415.38	103.361	1.31881	1.09803
340341	340	2524.56	106.254	1.38199	1.28529
341342	341	301452	138.993	1.31803	0.407203
342343	342	415084	113.987	0.742346	-0.969631
343344	343	294988	145.411	1.46182	0.814298
344345	344	47493.3	165.703	2.19167	3.65406
346347	346	3115.7	102.624	1.29097	0.939743
347348	347	1621	108.661	1.38446	1.27112
348349	348	1636.21	111.29	1.3577	1.11911
349350	349	1326.01	110.97	1.45684	1.57903

APPENDIX D

Matrix Composition

Bioclasts %						
Depth cm	Gastropods	Ostracods	Bivalves	Foram Frag	Plants	Worm Tubes
0-1	10	0	10	80	0	0
10-11	60	0	30	0	5	5
20-21	10	0	10	70	5	5
30-31	30	0	0	65	0	5
40-41	20	0	20	50	10	0
50-51	40	0	20	20	15	5
60-61	30	0	10	40	20	0
70-71	20	0	10	40	10	10
80-81	40	0	30	20	10	0
90-91	10	0	40	15	30	5
100-101	40	0	10	30	10	10
110-111	30	0	20	45	0	5
120-121	25	0	25	25	15	10
130-131	30	0	20	30	10	10
140-141	30	0	10	30	30	0
150-151	25	0	20	10	40	5
160-161	20	0	20	20	30	10
170-171	Negligible forams and other bioclasts					
180-181	30	0	30	30	10	0
190-191	Negligible forams and other bioclasts					
200-201	40	0	10	40	10	0
220-221	20	0	20	60	0	0
230-231	20	0	40	30	0	10
240-241	40	5	20	20	0	0
250-251	40	0	20	40	0	0
260-261	30	0	20	40	5	5
280-281	35	0	30	35	0	0
290-291	30	0	30	40	0	0
300-301	30	0	10	60	0	0
310-311	40	0	10	40	10	0
320-321	15	0	15	70	0	0
330-331	20	0	10	60	0	10
340-341	30	10	0	50	0	10
360-361	40	0	20	30	0	10
370-371	10	0	40	40	0	10
390-391	20	0	20	50	5	5
400-401	20	0	20	40	0	0
410-411	30	0	50		15	5
420-421	20	0	40	40	0	0

430-431	40	0	20	40	0	0
Mineral %						
Cm	**Qrtz**	**Feldspars**	**Mica**	**Hvy Min**	**Sorting**	**Angular**	**Dominant**
0-1	60	0	0	40	Moderate	Angular	Bioclasts 95%
10-11	70	10	15	0	Moderate	Angular	Silicates 55%
20-21	30	20	40	10	Moderate	Angular	Bioclasts 90%
30-31	60	10	20	10	Poor	Angular	Bioclasts 95%
40-41	40	40	5	15	Moderate	Subangular	Siliclasts 80%
50-51	50	40	0	10	Poor	Angular	Silicates 65%
60-61	40	30	20	10	Well	Angular	Bioclasts 80%
70-71	15	10	70	5	Moderate	Subangular	Bioclasts 70%
80-81	30	30	30	10	Poor	Angular	Bioclast 55%
90-91	30	20	50	0	Moderate	Subangular	Bioclast 55%
100-101	20	20	60	0	Moderate	Subangular	Bioclast 55%
110-111	40	30	20	10	Moderate	Subangular	Bioclasts 55%
120-121	50	20	30	0	Moderate	Subangular	Bioclasts 65%
130-131	40	30	20	10	Well	Subangular	Silicates 70%
140-141	40	45	10	5	Well	Subangular	Silicates 80%
150-151	40	30	20	10	Well	Angular	Silicates 75%
160-161	40	30	20	10	Well	Subangular	Silicates 70%
170-171	40	30	20	10	Well	Subround	Silicates 100%
180-181	60	30	10	0	Well	Subangular	Silcates 85%
190-191	30	30	30	10	Well	Subround	Silcates 99%
200-201	30	20	40	10	Moderate	Subangular	Bioclasts 60%
220-221	30	20	40	10	Moderate	Angular	Silcates75%
230-231	30	20	40	10	Well	Subround	Silicates 60%
240-241	35	35	20	20	Well	Subangular	Silicates 60%
250-251	40	30	20	0	Well	Angular	Bioclasts 80%
260-261	40	25	30	5	Moderate	Angular	Bioclasts 90%
280-281	70	20	5	5	Moderate	Angular	Bioclasts 75%
290-291	40	20	30	10	Moderate	Angular	Bioclasts 85%
300-301	50	30	20	0	Well	Angular	Bioclasts 90%
310-311	30	30	30	10	Moderate	Angular	Bioclast 90%
320-321	40	10	50	0	Well	Angular	Bioclasts 80%
330-331	60	30	5	5	Moderate	Angular	Bioclasts 95%
340-341	30	30	40	0	Well	Angular	Bioclasts 85%
360-361	40	40	10	10	Moderate	Angular	Bioclasts 80%
370-371	50	50	0	0	Moderate	Angular	Bioclast 95%
390-391	80	20	0	0	Moderate	Subangular	Bioclast 90%
400-401	50	50	0	0	Moderate	Angular	Bioclasts 85%
410-411	30	30	30	0	Moderate	Angular	Bioclasts 65%

420-421	50	30	15	50	Moderate	Angular	Bioclasts 90%
430-431	10	10	50	30	Moderate	Angular	Bioclasts 95%

APPENDIX E

Core Lithology

MG10-H02

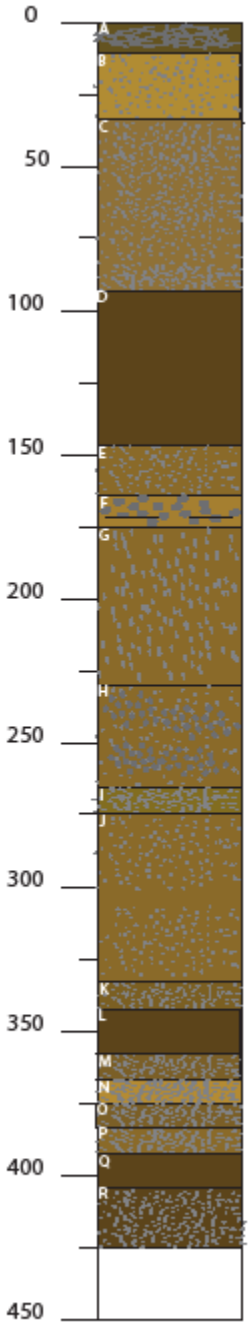

A) Organic, mottled, abundant bioturbation.
Med grain, dark blue/gray

B) Silty sand

C) Silty sand with interbedded clay.
Shell fragments

D) Clay. Organic matter at 112 cm

E) Fine grained slightly mottled
silty sand with moderate bioturbation

F) Medium grained slightly laminated sand

G) Fine/Medium grained silty sand.
Laminated with some clay lenses and darker patches

H) Silty sand. Pitted. Slightly more coarse than
above unit w/large shell fragments

I) Medium grainded silty sand. Petted w/lots of shell fragments

J) Sandy silt. Lots of shell framentsand visible whole shells.
Bioclastic and visible large forams

K) Sandy clay

L) Clay

M) Sandy clay

N) Silt

O) Sandy clay

P) Silty clay. Possible fining upwards

Q) Clay

R) Clayey silt

REFERENCES

Allen, B.D., Anderson, R.Y., 1993. Evidence from Western North America for Rapid Shifts in Climate During the Last Glacial Maximum. Science 260, 5116, 1920.

Allison, A.J., Niemi, T.M., 2010. Paleoenvironmental Reconstruction of Holocene Coastal Sediments Adjacent to Archaeological Ruins in Aqaba, Jordan. Geoarchaeology: An International Journal 25, 5.

Almogi-Labin A., 1982. Stratigraphic and paleoceanographic significance of Late Quaternary pteropods from deep sea cores in the Gulf of Aqaba (Elat) and northernmost Red Sea. Mar Micropaleontol 7, 53.

Almogi-Labin, A., Hemleben, C., Meischner, D., 1998. Paleoenvironmental events during the last 13,000 years in the central Red Sea as recorded by pteropoda. Paleoceanography 6, 1, 83.

Almogi-Labin, A., 2010. Pteropods as indicators of Red Sea paleoclimate during the last ~400,000 years. Geological Survey Israel website http://www.gsi.gov.il/_Uploads/4638almogi.pdf.

Al-Rousan, S.A., Rasheed, M., Badran, M., 2004. Nutrient diffusive fluxes from sediments in the northern Gulf of Aqaba, Red Sea. Scientia Marina, 68, 4.

Ambraseys, N., 2009. Earthquakes in the Mediterranean and Middle East *A Multidisciplinary Strudy of Seismicity up to 1900.* Cambridge University Press, New York.

Armstrong, H.A., Brasier, M.D., 2005. Microfossils: Second Edition. Blackwell Publishing, U.S.A., U.K., Australia.

Arz, H.W., Lamy, F., Pätzold, J., 2006. A pronounced dry event recorded around 4.2 ka in brine sediments from the northern Red Sea. Quaternary Research 66, 432–441.

Arz, H.W., Lamy, F., Pätzold, J., Muller, P.J., Prins, M., 2003. Mediterranean Moisture Source for an Early-Holocene Humid Period in the Northern Red Sea. Science, 3000.

Bar-Matthews, M., Ayalon, A., Kaufman, A., 2000. Timing and hydrological conditions of Sapropel events in the Eastern Mediterranean, as evident from speleothems, Sorel cave, Israel. Chemical Geology 169, 145–156.

Ben-Avraham, Z., Al-Zoubi, A., Tibor, G., Niemi, T., 2009.High Resolution Imaging of Active Faults in the Aqaba-Eilat Region, Final Report Middle East Regional Cooperation Project TA-MOU-05-M25-004, 33 p.

Ben-Avraham, Z., Al-Zoubi, A., Tibor, G., Niemi, T., 2011. Middle East Regional Cooperation (MERC) Semi-annual report. High Resolution Imaging of Active Faults in the Aqaba-Eilat Region —Leg 2: Marine Coring and Onshore Correlations.

Ben-Avraham, Z., Al-Zoubi, A., Tibor, G., Niemi, T., 2010. Middle East Regional Cooperation (MERC) Semi-annual report. High Resolution Imaging of Active Faults in the Aqaba-Eilat Region —Leg 2: Marine Coring and Onshore Correlations

Ben-Avraham, Z., 1985, Structural framework of the Gulf of Elat (Aqaba), Northern Red Sea: *Journal of Geophysical Research*, 90, B1, 703-726.

Ben-Avraham, Z., Almagor, G., and Garfunkel, Z., 1979, Sediments and structure of the Gulf of Elat (Aqaba)-Northern Red Sea: *Sedimentary Geology,* 23, 239-267.

Bender, F., 1974. The Geology of Jordan. Gebrüder Borntraeger, Berlin.

BiblicalZionist, 2011. http://www.biblicalzionist.com/images/GeMaApRedSea.jpg.

Boggs, S., 2001. Principles of Sedimentology and Stratigraphy: Third Edition. Prentice Hall, New Jersey.

Bond, G., Showers, W., Cheseby, M., Lotti, R., Almasi, P., deMenocal, P., Priore, P., Cullen, H., Hajdas, I., Bonani, G., 1997. A pervasive millenial-scale cycle in North Atlantic Holocene and glacial climates. Science 278, 1257.

Bray, J.R., 1971. Solar–climate relationships in the post-Pleistocene. Science 171, 1242.

Bray, J.R., 1972. Cyclic temperature oscillations from 0–20,300 yr BP. Nature 237, 277.

Burdon, D.J., 1959. Handbook of the Geology of Jordan. Benham and Company Limited, Colchester.

Cavalier-Smith, T., 1993. Kingdom protozoa and its 18 phyla. Microbiol Molecular Biology Reviews 57, 4, 953-994.

Cavalier-Smith, T., 1998. A revised six-kingdom system of life. Biological Reviews 73, 3, 203–266.

Cullen, H.M., deMenocal, P.B., 2000. North Atlantic influence on Tigris-Euphrates streamflow. International Journal of Climatology 20, 853–863.

Cullen, H.M., deMenocal, P.B., Hemming, S., Hemming, G., Brown, F.H., Guilderson, T., Sirocko, F., 2000. Climate change and the collapse of the Akkadian empire: Evidence from the deep sea. Geology 28, 4, 379.

Cunningham, W. D., Mann, P., 2007. Tectonics of strike-slip restraining and releasing bends. Geological Society, London, Special Publications 290, 1-12.

Cushman, J.A. 1933. Foraminifera their classification and economic use. Cushman Laboratory for Foraminiferal Research, Special Publication 4, 349.

Cushman, J.A., 1922. The Foraminifera of the Atlantic Ocean: Part 3 Textulariidae. Washington Government Printing Office. Smithsonian Institute United States National Museum, Bulletin 104.

Dansgaard, W., Johnsen, S.J., Clausen, H.B., Langway, C.C., 1971. Climatic record revealed by the Camp Century ice core. In: Turekian, K. (Ed.), The Late Cenozoic Glacial Ages. Yale Univ. Press, New Haven, 37.

Denton, G.H., Karle´n, W., 1973. Holocene climatic variations: their pattern and possible cause. Quaternary Research 3, 155.

deMenocal, P.B., 2001. Cultural Responses to Climate Change During the Late Holocene. Science 292, 667.

d'Orbiny, A.D., 1839. Foraminiferes. In: Ramon de la Sagra, Histoire physique, politique et natiaturelle de l'Ile de Cuba, 1- 224. Arthus Bertrand, Paris.

Edelman-Furstenberg, Y., Almogi-Labin, A., Hemleben, C., 2009. Palaeoceanographic evolution of the central Red Sea during the late Holocence. The Holocene 19, 1, 117-127.

Enzel, Y., Bookman, R., Sharon, D., Gvirtzman, H., Dayan, U., Ziv, B., Stein, M., 2003. Late Holocene climates of the Near East deduced from Dead Sea level variations and regional winter rainfall. Quaternary Research 60, 263–273.

Fichtel, L. and Moll, J. P. C., 1798, Shellacea microscopica aliaqueminuta ex generibus Argonauta et Nautilus ad naturam picta et descripta: Pichler, Vienna.

Fleitmann, D., Burns, S.J., Mudelsee, M., Neff, U., Kramers, J., Mangini, A., Matter, A., 2003. Holocene forcing of the Indian monsoon recorded in a stalagmite from Southern Oman. Science 300, 1737–1739.

Fleitmann, D., Burns, S.J., Mangini, A., Mudelsee, M., Kramers, J., Villa, I., Neff, U., Al-Subbarye, A.A., Buettner, A., Hippler, D., Matter. A., 2007. Holocene ITCZ and Indian monsoon dynamics recorded in stalagmites from Oman and Yemen (Socotra). Quaternary Science Reviews 26, 170–188.

Freund, R., Zak, I., Garfunkel, Z., Goldberg, M., Weissbrod, T., Derin, B., 1970. The shear along the Dead Sea right. Philos, Trans. Roy Soc. London 267, 105-127.

Frumpkin, A. 2009. Stable isotopes of a subfossil Tamarix tree from the Dead Sea region, Israel, and their implications for the Intermediate Bronze Age environmental crisis. Quaternary Research 71, 319.

Gasse, F., 2000. Hydrological changes in the African tropics since the Last Glacial Maximum. Quaternary Science Reviews 19, 189–211.

Garfunkel, Z., 1988. The pre-Quaternary geology of Israel. The zoogeography of Israel. Dr W. Junk Publishers, Dordrecht. Netherlands

Garfunkel, Z., 1981. Internal structure of the Dead Sea leaky transform (rift) in relation to plate kinematics. Tectonophysics 80, 81 – 108.

Garfunkel, Z., 1970. The tectonics of the western margins of the southern Arava: a contribution to the understanding of rifting. Hebrew University.

Goldstein, S.T., 1999. Foraminifera: A Biological Overview, 37-56, in B.K. Sen Gupta (Ed.) Modern Foraminifera; Kluwer, Dordrecht, The Netherlands.

Goodman, B., 2007. Tsunami Study in Caesarea. Second expedition. http://www.ecoocean.com/en/scientists/research/ViewResearch.aspx?rid=6&lang=2

Goodman-Tchernov, B.N., Dey, H.W., Reinhardt, E.G., McCoy, F., Mart, Y., 2009. Tsunami waves generated by the Santorini eruption reached Eastern Mediterranean shores. Geology 37, 10, 943-946.

Goodman, B., Reinhardt, E., Dey, H., Boyce, J., Schwarcz, H., Sahoflu, V., Erkanal, H., Artzy, M., 2008. Evidence for Holocene Marine Transgression and Shoreline Progradation Due to Barrier Development in Iskele, Bay of Izmir, Turkey. Journal of Coastal Research 24, 5, 1269-1280.

Googlemaps, 2011. http://www.googlemaps.com. 2011.

Gupta, A.K., Anderson, D.M., Overpeck, J.T., 2003. Abrupt changes in the Asian southwest monsoon during the Holocene and their links to the North Atlantic Ocean. Nature 421, 354–357.

Hammer, Ѳ., Harper, D.A.T., Ryan, P.D. 2009. PAST: Palaeontological Statistics software pakage for education and data analysis. Palaeontologia Electronica 4, 1, 9.

Harpez, Y. 1960. Hydrological Investigations in the Southern Desert of Israel. Water Planning for Israel Ltd. Tel-Aviv, 124-131.

Hartman, G., Ben-Avraham, Z., Tibor, G., Niemi, T.M., Al-Zoubi, A., Sade, R.A., Hall, J.K., Akawi, E., Abueladas, A., Makovsky, Y., 2010. Sequences of generation and mortality of fringing reefs in changing sedimentary environments along the northern shelf of the Gulf of Eilat/Aqaba. Conference proceedings. Haifa University, Haifa, Israel.

Hartman, G., 2011. Quaternary Evolution of a Transform Basin: The northern Gulf of Eilat/Aqaba. Unpublished Ph.D. dissertation, Tel-Aviv University, Tel-Aviv, Israel.

Ibrahim, K.M., McCourt, W.J., 1995. Neoproterozoic granitic magmatism and tectonic evolution of the northern Arabian Shield: evidence from southwest Jordan. Journal of African Earth Sciences 20, 2, 103-118.

Israeli Meteorological Service. 2011. http://www.ims.gov.il/IMSEng/CLIMATE.

Jarrar, G., Stern, R.J., Saffarini, G., Al-Zubi, H., 2003. Late- and post-orogenic Neoproterozoic intrusions of Jordan: implications for crustal growth in the northernmost segment of the East African Orogen. Precambrian Research 123, 295–319.

Johnsen, S.J., Dansgaard, W., Clausen, H.B., 1972. Oxygen isotope profiles through the Antarctic and Greenland Ice Sheets. Nature 235, 429.

Khalil, M.T., .Abd El-Rahman, N.S., 1997. Abundance and diversity of surface zooplankton in the Gulf of Aqaba, Red Sea, Egypt. Journal of Plankton Research 19, 7, 927-936.

Khalil, L., Schmidt, K., 2009. Prehistoric 'Aqaba I. Orient-Archaologia Band 23. Rahden/Westfalen, Germany: Verlag Marie Leidorf.

Klinger, Y., Avouac, J.P., Abou Karaki, N., Dorbath, L., Bourles, D., and Reyss, J.L., 2000. Slip rate on the Dead Sea transform fault in Northern Araba valley (Jordan). Geophysical Journal International. 142. 755-768.

Lamy, F., Arz, H.W., Bond, G.C., Bahr, A., Patzold, J., 2006. Multicentennial-scale hydrological changes in the Black Sea and northern Red Sea during the Holocene and the Arctic/North Atlantic Oscillation. Paleoceanography 21, 1008.

Le Béon M., Klinger, Y., Al-Qaryouti, M., Mériaux, A.-S., Finkel, R.C., Elias, A., Mayyas, O., Ryerson, F.J., and Tapponnier, P., 2010, Holocene and Late Pleistocene slip rate of the southern Dead Sea Transform determined from ^{10}Be cosmogenic dating of offset alluvial fans. Journal of Geophysical Research. 115, B11414, doi:10.1029/2009JB007198

Legge, H.L., Mutterlose, J., Arzs, H.W., 2006. Climatic changes in the northern Red Sea during the last 22,000 years as recorded by calcareous nonnofossils. Paleoceanography 21, 1003.

Linné, C., 1758. Systema Naturae per Regna Tria Naturae, Secundum Classes, Ordines, Genera, Species, cum Characteribus, Differentiis, Synonymis, Locis, 1, 10th ed., Lipsiae (G. Engelmann), 1-824.

Makovsky, Y., Wunch, A., Areily, R., Shaked, Y., Rivline, A., Shemesh, A., Ben-Avrahm, Z., and Agnon, A., 2008, Quaternary transform kinematics constrained by sequence

stratigraphy and submerged features: The Gulf of Aqaba: Earth and Planetary Science Letters, 271, 109-122.

Mayewski, P.A., Meeker, L.D., Twickler, M.S., Whitlow, S., Yang, Q., Lyons, W.B., Prentice, M., 1997. Major features and forcing of high- latitude northern hemisphere atmospheric circulation using a 110,000- year long glaciochemical series. Journal of Geophysical Research 102,26345.

Mayewski, P.A, Rohling, E.E., Stager, J.C., Karle´n, W., Maasch, K.A., Meeker, L.D., Meyerson, E.A., Gasse, F., van Kreveld, S., Holmgren, K., Lee-Thorp, J., Rosqvist, G., Rack, F., Staubwasser, M., Schneider, R.R., Steig, E.J. 2004. Holocene climate variability. Quaternary Research 62, 243.

Moustafa, Y.A., Patzold, J., Loya, Y., Wefer, G. 2000. Mid-Holocene stable isotope record of corals from the northern Red Sea. International Journal of Earth Sciences 88, 742-751.

Naidu, P.D., Malmgren, B., 1996. A high-resolution record of late Quaternary upwelling along the Oman margin, Arabian Sea based on planktonic foraminifera. Paleoceanography 11, 129.

Niemi, T.M., Smith, A.M. II., 1999. Initial results of the southeastern Wadi Araba, Jordan geoarchaeological study: Implications for shifts in later Quaternary aridity. Geoarchaeology, 14, 791-820.

Noren, A.J., Bierman, P.R., Steig, E.J., Lini, A., Southon, J.A., 2002. Millennial-scale storminess variability in the northeastern United States during the Holocene. Nature 419, 821.

O'Brien, S.R., Mayewski, P.A., Meeker, L.D., Meese, D.A., Twickler, M.S., Whitlow, S.I., 1995. Complexity of Holocene climate as reconstructed from a Greenland ice core. Science 270, 1962.

Parker, S.T., 1997. Preliminary report on the 1994 season of the Roman 'Aqaba Project. Bulletin of the American Schools of Oriental Research, 305, 19-44.

Paytan Biogeochemistry Lab, 2011. Nutrient Dynamics and Ecosystem structure in the Gulf of Aqaba Physical Forcing and External Nutrient Sources.

Peters, R., Jaffe, B., 2010. Identification of tsunami deposits in the geologic record; developing criteria using recent tsunami deposits: U.S. Geological Survey Open-File Report 2010-1239, 39.

Pisias, N., Dauphin, J.P., Sancetta, C., 1973. Spectral analysis of late Pleistocene–Holocene sediments. Quaternary Research 3, 3.

Pratico, G.D., 1993. Nelson Glueck's 1938-1940 excavations of Tell el-Kheleifeh: A reappraisal. American Schools of Oriental Research, Archaeological Reports 3. Atlanta : Scholars Press.

Prothero, D.R., 2004. Bringing Fossils to Life; An Introduction to Paleobiology second edition. McGraw-Hill, New York.

Quennell, A.M., 1959. Tectonics of the Dead Sea rift. Int. Geol. Congr. 20 (Mexico), Assos. Serv. Geol. Afr. 385-405.

Reimer, P.J., Baillie, M.G.L., Bard, E., Bayliss, A., Beck, J.W., Blackwell, P.G. Bronk Ramsey, C., Buck, C.E., Burr, G.S., Edwards, R.L., Friedrich, M., Grootes, P.M., Guilderson, T.P., Hajdas, I., Heaton, T.J., Hogg, A.G, Hughen, K.A., Kaiser, K.F., Kromer, B., McCormac, F.G., Manning, S.W., Reimer, R.W., Richards, D.A., Southon, J.R., Talamo, S., Turney, C.S.M., van der Plicht, J., Weyhenmeyer, C.E., (2009) Radiocarbon 51:1111-1150.

Reinhardt, E.G., Goodman, B.N., Boyce, J.I., Lopez, G., Hengstum, P., Rink, W.J., Mart, Y., Raban, A., 2006. The tsunami of 13 December A.D. 115 and the destruction of Herod the Great's harbor at Caesarea Maritima, Israel. Geology 34, 12, 1061-1064.

Reiss, Z., Luz, B., Almogi-Labin, A., Halicz, E., Winter, A., Wolf, M., Ross, D.A.1980. Late Quaternary paleoceanography of the Gulf of Aqaba (Eilat), Red Sea. Quaternary Research 14. 294-308.

Reiss, Z., Hottinger, L., 1984. The Gulf of Aqaba *Ecological Micropaleontology*. Springer-Verlag, Berlin, Heidelberg, New York, Tokyo.

Sedimentologist, 2011. http://sedimentologist-liu.blogspot.com/2010/11/itcz-intertropical-convergence-zone.html.

Shaked, Y., Agnon, A., Lazar, B., Marco, S., Avner, U., Stein, M., 2004. Large earthquakes kill coral reefs at the north-west Gulf of Aqaba. Terra Nova 16, 133.

Sonett, C.P., Finney, S.A., 1990. The spectrum of radiocarbon. Philosophical Transactions of the Royal Society of London A 330, 413.

Stager, C.J., Cumming, B., Meeker, L.D., 1997. A high-resolution 11,400- yr diatom record from Lake Victoria, East Africa. Quaternary Research 47, 8.

StatSoft, Inc. 2011. Electronic Statistics Textbook. Tulsa, OK: StatSoft. WEB: http://www.statsoft.com/textbook/.

Staubwasser, M., Sirocko, F., Grootes, P.M., Segl, M., 2003. Climate change at the 4.2 ka BP termination of the Indus valley civilization and Holocene south Asian monsoon variability. Geophysical Research Letters 30, 7–1–7–4.

Stuiver, M., Braziunas, T.F., 1989. Atmospheric 14C and century-scale solar oscillations. Nature 388, 405.

Stuiver, M., Braziunas, T.F., 1993. Sun, ocean, climate and atmospheric 14CO2: an evaluation of causal and spectral relationships. Holocene 3, 289.

Sylvester, A.G., 1988. Strike-slip faults. Geological Society of America Bulletin 100, 11, 1666-1703.

ten Brink, U.S., Ben-Avraham, Z. 1989. The anatomy of a pull-apart basin: Seismic reflection observations of the Dead Sea basin. Tectonics 7, 2, 333-350.

Tibor, G., Niemi, T.M., Ben-Avraham, Z., Al-Zoubi, A., Hartman, G., Sade, R.A., Hall, J.K., Akawi, E., Abueladas, A., Al-Ruzouq, R., 2010. Active tectonic morphology and submarine deformation of the northern Gulf of Eilat/Aqaba from analyses of multibeam data. Conference, Haifa Israel.

Weiss, H., Courty, M.A.,Wetterstrom,W., Guichard, F., Senior, L., Meadow, R., Curnow, A., 1993. The genesis and collapse of third millennium North Mesopotamian civilization. Science 261, 995–1004.

Whitcomb, D., 1994, Ayla: Art and industry in the Islamic port of Aqaba: University of Chicago, IL.: Special Publications, Oriental Institute.

World Meteorological Organization, 2011. http://worldweather.wmo.int/069/c00591.htm. 2011.

Wright, H.E., Kutzbach, J.E., Webb, T., Ruddiman, W.F., Street-Perrott, F.A., Bartlein, P.J., 1993. Global Climates since the Last Glacial Maximum. University of Minnesota Press, Minneapolis, London.

VITA

Julie Louise Galloway was born in Butte, Montana on September 26th 1983. She moved with her family to Kansas City, Missouri in 1989 where she spent the remainder of her childhood. Julie received a home-based education and graduated in the spring of 2002.

After spending time living in Alaska, Montana, and Oregon, Miss Galloway returned to Kansas City to earn an Associates of Arts from Longview Community College in Lee's Summit, Missouri. She spent the next two years living in Utah and traveling. In the fall of 2007, she enrolled in the University of Missouri-Kansas City and graduated with a B.S. in Geology in 2009.

Julie continued her education and the University of Missouri-Kansas City and began pursuing her M.S. degree in January 2010. Over the course of the M.S. project, she made three trips overseas to Jordan and Israel to collect data, collaborate with geoscientists, and assist in ongoing research projects.

During her studies, she has completed two undergraduate research projects in Baja, Mexico and in the Bahamas, received numerous research grants and scholarships, and presented her research at two international professional society meetings. She received the Association for Engineering Geologists-American Society Civil Engineers Scholarship and the UMKC Women's Council Graduate Assistance Fund Award. Miss Galloway is a member of Geological Society of America and the Association for Engineering Geologists.